NUREG/CR-6609

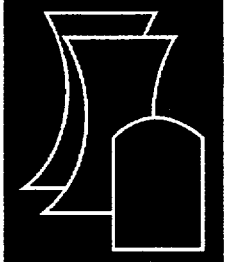

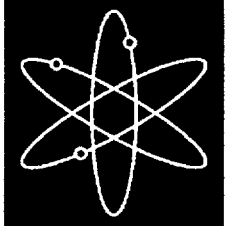

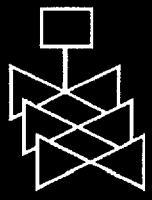

Comparison of Irradiation-Induced Shifts of K_{Jc} and Charpy Impact Toughness for Reactor Pressure Vessel Steels

Oak Ridge National Laboratory

U.S. Nuclear Regulatory Commission
Office of Nuclear Regulatory Research
Washington, DC 20555-0001

AVAILABILITY OF REFERENCE MATERIALS IN NRC PUBLICATIONS

NRC Reference Material

As of November 1999, you may electronically access NUREG-series publications and other NRC records at NRC's Public Electronic Reading Room at www.nrc.gov/NRC/ADAMS/index.html. Publicly released records include, to name a few, NUREG-series publications; *Federal Register* notices; applicant, licensee, and vendor documents and correspondence; NRC correspondence and internal memoranda; bulletins and information notices; inspection and investigative reports; licensee event reports; and Commission papers and their attachments.

NRC publications in the NUREG series, NRC regulations, and *Title 10, Energy*, in the Code of *Federal Regulations* may also be purchased from one of these two sources.

1. The Superintendent of Documents
   U.S. Government Printing Office
   P. O. Box 37082
   Washington, DC 20402–9328
   www.access.gpo.gov/su_docs
   202–512–1800
2. The National Technical Information Service
   Springfield, VA 22161–0002
   www.ntis.gov
   1–800–533–6847 or, locally, 703–805–6000

A single copy of each NRC draft report for comment is available free, to the extent of supply, upon written request as follows:

Address: Office of the Chief Information Officer,
Reproduction and Distribution
Services Section
U.S. Nuclear Regulatory Commission
Washington, DC 20555-0001
E-mail: DISTRIBUTION@nrc.gov
Facsimile: 301–415–2289

Some publications in the NUREG series that are posted at NRC's Web site address www.nrc.gov/NRC/NUREGS/indexnum.html are updated periodically and may differ from the last printed version. Although references to material found on a Web site bear the date the material was accessed, the material available on the date cited may subsequently be removed from the site.

Non-NRC Reference Material

Documents available from public and special technical libraries include all open literature items, such as books, journal articles, and transactions, *Federal Register* notices, Federal and State legislation, and congressional reports. Such documents as theses, dissertations, foreign reports and translations, and non-NRC conference proceedings may be purchased from their sponsoring organization.

Copies of industry codes and standards used in a substantive manner in the NRC regulatory process are maintained at—

The NRC Technical Library
Two White Flint North
11545 Rockville Pike
Rockville, MD 20852–2738

These standards are available in the library for reference use by the public. Codes and standards are usually copyrighted and may be purchased from the originating organization or, if they are American National Standards, from—

American National Standards Institute
11 West 42nd Street
New York, NY 10036–8002
www.ansi.org
212–642–4900

The NUREG series comprises (1) technical and administrative reports and books prepared by the staff (NUREG–XXXX) or agency contractors (NUREG/CR–XXXX), (2) proceedings of conferences (NUREG/CP–XXXX), (3) reports resulting from international agreements (NUREG/IA–XXXX), (4) brochures (NUREG/BR–XXXX), and (5) compilations of legal decisions and orders of the Commission and Atomic and Safety Licensing Boards and of Directors' decisions under Section 2.206 of NRC's regulations (NUREG–0750).

NUREG/CR-6609

Comparison of Irradiation-Induced Shifts of K_{Jc} and Charpy Impact Toughness for Reactor Pressure Vessel Steels

Manuscript Completed: February 1999
Date Published: November 2000

Prepared by
M. A. Sokolov, R. K. Nanstad

Oak Ridge National Laboratory
Managed by Lockheed Martin Energy Research Corp.
Oak Ridge, TN 37831-6151

C. J. Fairbanks, NRC Project Manager

Prepared for
Division of Engineering Technology
Office of Nuclear Regulatory Research
U.S. Nuclear Regulatory Commission
Washington, DC 20555-0001
NRC Job Code W6953

ABSTRACT

The current provisions for determination of the upward temperature shift of the lower-bound static fracture toughness curve due to irradiation of reactor pressure vessel steels are based on the assumption that they are the same as for the Charpy 41-J shifts as a consequence of irradiation. The objective of this report by the Heavy-Section Steel Irradiation Program is to evaluate this assumption relative to data reported in open literature. Depending on the specific source, different sizes of fracture toughness specimens, procedures for the determination of K_{Jc}, and fitting functions were used. It was anticipated that data scatter might be reduced by using a consistent approach to analyze the published data. A method employing Weibull statistics was applied to analyze original fracture toughness data of unirradiated and irradiated pressure vessel steels. The master curve concept was used to determine shifts of fracture toughness transition curves. A hyperbolic tangent function was used to fit Charpy absorbed-energy data. The fracture toughness shifts were compared with Charpy impact shifts evaluated with various criteria. Linear regression analysis showed that for weld metals, on average, the fracture toughness shift is the same as the Charpy 41-J temperature shift, while for base metals, on average, the fracture toughness shift at 41 J is 16% greater than the shift of the Charpy 41-J transition temperature, with both correlations having relatively large (95%) confidence intervals of ±26°C and ±36°C, respectively.

CONTENTS

ABSTRACT iii

LIST OF FIGURES vii

LIST OF TABLES xi

ACKNOWLEDGMENTS xiii

FOREWORD xv

1. INTRODUCTION 1

2. ANALYSIS PROCEDURE 1

3. THE WEIBULL STATISTIC/MASTER CURVE APPROACH AND THE ASME K_{Ic} DATABASE 4

4. RESULTS OF ANALYSIS 16

5. THE MASTER CURVE SHAPE 19

6. CORRELATIONS BETWEEN STATIC FRACTURE TOUGHNESS AND CHARPY IMPACT CURVE SHIFTS 29

7. FRACTURE TOUGHNESS, NIL-DUCTILITY TRANSITION-TEMPERATURE SHIFTS, AND RADIATION HARDENING; SEARCHING FOR A CORRELATION 47

8. MEASURED FRACTURE TOUGHNESS SHIFT VS PREDICTIONS OF EMBRITTLEMENT 56

9. SUMMARY AND CONCLUSIONS 63

10. REFERENCES 64

APPENDIX A: WEIBULL STATISTICS AND THE MASTER CURVE A-1

APPENDIX B: SUMMARY TABLES B-1

LIST OF FIGURES

1 K_{Ic} reference toughness curve with supporting data as presented in EPRI NP-719-SR 6

2 Linear-elastic K_{Ic} data of the HSST Plate 02 statistically adjusted to 1T size with the corresponding master curve and tolerance bounds 7

3 The ASME K_{Ic} data statistically adjusted to 1T size equivalence and described by the master curve and corresponding upper and lower tolerance bounds 8

4 Comparison of RT_{NDT} and T_{100} for materials in the ASME database 10

5 The ASME K_{Ic} database vs temperature normalized by (a) RT_{NDT} and (b) T_{100} 11

6 Statistically based size effect on median and upper and lower tolerance bounds at $T = T_{100}$ 12

7 Comparison of lower tolerance bounds with the ASME K_{Ic} lower-bound curve for HSST Plate 02 13

8 Comparison of lower tolerance bounds with the ASME K_{Ic} lower-bound curve for A508 Class 2 forging 14

9 Comparison of lower tolerance bounds with the ASME K_{Ic} lower-bound curve for A533 grade B class 1 submerged-arc weld 15

10 Plot of Charpy energy at temperature $T = T_{100}$ as a function of yield strength 17

11 Plot of Charpy energy at temperature $T = T_{100}$ as a function of the reference fracture toughness temperature 18

12 Relationship between T_{100} and T_{41J} for both base and weld metals in the unirradiated and irradiated conditions 20

13 The unirradiated fracture toughness data size-adjusted to 1T equivalence and normalized to T_{100} with the master curve and 3 and 97% tolerance bounds 22

14 The irradiated fracture toughness data size-adjusted to 1T equivalence and normalized to T_{100} with the master curve and 3 and 97% tolerance bounds 23

15 Fracture toughness data for highly embrittled materials with the best-fit equations 25

16 Fracture toughness data for materials with T_{41J} above 100°C with the best-fit equations 26

17 Fracture toughness data for materials with Charpy USE below 100 J with the best-fit equations 27

18 Unirradiated (valid and unvalid) fracture toughness data as measured, normalized to T_{100} with the 3% tolerance bound to the master curve 30

19 Irradiated (valid and unvalid) fracture toughness data as measured, normalized to T_{100} with the 3% tolerance bound to the master curve 31

20 Correlation between fracture toughness T_{100} and Charpy T_{41J} shifts for (a) weld and (b) base metal 33

21 Correlation between fracture toughness T_{100} and Charpy T_{41J} shifts for base metal data in (a) L-T orientation and (b) T-L orientation 35

22 Power law fit to fracture toughness and Charpy shifts for (a) weld and (b) base metals 36

23 Linear (a) and power law (b) fit to all the data 38

24 Correlation between fracture toughness T_{100} and Charpy T_{68J} shifts for (a) weld and (b) base metals 39

25 Correlation between fracture toughness T_{100} and Charpy T_{MT} shifts for (a) weld and (b) base metals 40

26 Correlation between fracture toughness T_{100} and Charpy $T_{28^{\circ}J}$ shifts for (a) weld and (b) base metals 41

27 Correlation between fracture toughness T_{100} and Charpy $T_{0.9mm}$ shifts for (a) weld and (b) base metals 42

28 Correlation between fracture toughness T_{100} and Charpy $T_{50\%}$ shifts for (a) weld and (b) base metals 43

29 Correlation of the HSSI data only with (a) linear and (b) power law fits to all data from Fig. 23 45

30 Difference between fracture toughness and Charpy shifts as a function of Charpy upper-shelf energy in the irradiated condition 46

31 Difference between fracture toughness and Charpy shifts as a function of the ratio of USE_{UNIRR} to USE_{IRR} 46

32 Difference between fracture toughness and Charpy shifts as a function of yield strength of materials in the irradiated condition 48

33 Difference between fracture toughness and Charpy shifts as a function of yield strength increase 48

34 Difference between fracture toughness and Charpy shifts as a function of Charpy T_{41J} in the irradiated condition 49

35 Difference between fracture toughness and Charpy shifts as a function of Charpy T_{41J} in the unirradiated condition 49

36 Difference between fracture toughness and Charpy shifts as a function of Charpy T_{41J} shift 50

37 Difference between fracture toughness and Charpy shifts as a function of neutron fluence 51

38 Correlation between fracture toughness shift and yield strength increase for (a) weld and (b) base metals 53

39 Correlation between fracture toughness shift and yield strength increase for both weld and base metals 54

40 Correlation between transition temperature shift and yield-strength increase for all fracture toughness data in the present study and Charpy data in the PR-EDB 54

41 Comparison of (a) fracture toughness T_{100} and drop-weight NDT temperatures and (b) corresponding radiation-induced shifts 55

42 Comparison of fracture toughness shifts with prediction of embrittlement based on Regulatory Guide 1.99 Rev. 2 for (a) weld metals and (b) base metals 59

43 Comparison of fracture toughness shifts with prediction of embrittlement based on Regulatory Guide 1.99 Rev. 1 60

44 Comparison of fracture toughness shifts with prediction of embrittlement based on French predictive equation FIM 60

45 Comparison of fracture toughness shifts with prediction of embrittlement based on proposed equations in NUREG/CR-6551 for (a) weld metals and (b) plate and forging metals 61

46 Comparison of fracture toughness shifts with prediction of embrittlement based on JEPE predictive equation for (a) weld metal and (b) base metal 62

LIST OF TABLES

Table		Page
1	Fitting coefficients of Eq. (10) with α fixed to 30	21
2	Fitting coefficients of Eq. (10) with α fixed to 30 and β to 70	24
3	Fitting coefficient γ with 95% confidence intervals for different groups of materials	28

ACKNOWLEDGMENTS

This research is sponsored by the Office of Nuclear Regulatory Research, U.S. Nuclear Regulatory Commission, under Interagency Agreement DOE 1886-N695-3W with the U.S. Department of Energy under Contract DE-AC05-96OR22464 with Lockheed Martin Energy Research Corporation.

The authors would like to thank Julia Bishop for her contributions in the preparation of the draft manuscript of this report. The authors would also like to thank Donald McCabe, John Merkle, and Roger Stoller for reviewing the report.

FOREWORD

The work reported here was performed at the Oak Ridge National Laboratory (ORNL) under the Heavy-Section Steel Irradiation (HSSI) Program, T. M. Rosseel, Program Manager. The program is sponsored by the Office of Nuclear Regulatory Research of the U.S. Nuclear Regulatory Commission (NRC). The technical monitor for the NRC is C. J. Fairbanks.

This report is designated HSSI Report 21. Reports in this series are listed below:

1. F. M. Haggag, W. R. Corwin, and R. K. Nanstad, Martin Marietta Energy Systems, Inc., Oak Ridge Natl. Lab., Oak Ridge, Tenn., *Irradiation Effects on Strength and Toughness of Three-Wire Series-Arc Stainless Steel Weld Overlay Cladding*, USNRC Report NUREG/CR-5511 (ORNL/TM-11439), February 1990.

2. L. F. Miller, C. A. Baldwin, F. W. Stallman, and F. B. K. Kam, Martin Marietta Energy Systems, Inc., Oak Ridge Natl. Lab., Oak Ridge, Tenn., *Neutron Exposure Parameters for the Metallurgical Test Specimens in the Sixth Heavy-Section Steel Irradiation Series*, USNRC Report NUREG/CR-5409 (ORNL/TM-11267), March 1990.

3. S. K. Iskander, W. R. Corwin, and R. K. Nanstad, Martin Marietta Energy Systems, Inc., Oak Ridge Natl. Lab., Oak Ridge, Tenn., *Results of Crack-Arrest Tests on Two Irradiated High-Copper Welds*, USNRC Report NUREG/CR-5584 (ORNL/TM-11575), December 1990.

4. R. K. Nanstad and R. G. Berggren, Martin Marietta Energy Systems, Inc., Oak Ridge Natl. Lab., Oak Ridge, Tenn., *Irradiation Effects on Charpy Impact and Tensile Properties of Low Upper-Shelf Welds, HSSI Series 2 and 3*, USNRC Report NUREG/CR-5696 (ORNL/TM-11804), August 1991.

5. R. E. Stoller, Martin Marietta Energy Systems, Inc., Oak Ridge Natl. Lab., Oak Ridge, Tenn., *Modeling the Influence of Irradiation Temperature and Displacement Rate on Radiation-Induced Hardening in Ferritic Steels*, USNRC Report NUREG/CR5859 (ORNL/TM-12073), August 1992.

6. R. K. Nanstad, D. E. McCabe, and R. L. Swain, Martin Marietta Energy Systems, Inc., Oak Ridge Natl. Lab., Oak Ridge, Tenn., *Chemical Composition RT_{NDT} Determinations for Midland Weld WF-70*, USNRC Report NUREG/CR-5914 (ORNL-6740), December 1992.

7. R. K. Nanstad, F. M. Haggag, D. E. McCabe, S. K. Iskander, K. O. Bowman, and B. H. Menke, Martin Marietta Energy Systems, Inc., Oak Ridge Natl. Lab., Oak Ridge, Tenn., *Irradiation Effects on Fracture Toughness of Two High-Copper Submerged-Arc Welds*, USNRC Report NUREG/CR-5913 (ORNL/TM-12156/V1), October 1992.

8. S. K. Iskander, W. R. Corwin, and R. K. Nanstad, Martin Marietta Energy Systems, Inc., Oak Ridge Natl. Lab., Oak Ridge, Tenn., *Crack-Arrest Tests on Two Irradiated High-Copper Welds*, USNRC Report NUREG/CR-6139 (ORNL/TM-12513), March 1994.

9. R. E. Stoller, Martin Marietta Energy Systems, Inc., Oak Ridge Natl. Lab., Oak Ridge, Tenn., *A Comparison of the Relative Importance of Copper Precipitates and Point Defects in Reactor Pressure Vessel Embrittlement*, USNRC Report NUREG/CR-6231 (ORNL/TM-6811), December 1994.

10. D. E. McCabe, R. K. Nanstad, S. K. Iskander, and R. L. Swain, Martin Marietta Energy Systems, Inc., Oak Ridge Natl. Lab., Oak Ridge, Tenn., *Unirradiated Material Properties of Midland Weld WF-70*, USNRC Report NUREG/CR-6249 (ORNL/TM-12777), October 1994.

11. P. M. Rice and R. E. Stoller, Lockheed Martin Energy Systems, Oak Ridge Natl. Lab., Oak Ridge, Tenn., *Microstructural Characterization of Selected AEA/UCSB Model FeCuMn Alloys*, USNRC Report NUREG/CR-6332 (ORNL/TM-12980), June 1996.

12. J. H. Giovanola and J. E. Crocker, *SRI International, Fracture Toughness Testing with Cracked Round Bars: Feasibility Study*, USNRC Report NUREG/CR-6342 (ORNL/SUB/94-DHK60), to be published.

13. F. M. Haggag and R. K. Nanstad, Lockheed Martin Energy Systems, Oak Ridge Natl. Lab., Oak Ridge, Tenn., *Effects of Thermal Aging and Neutron Irradiation on the Mechanical Properties of Three-Wire Stainless Steel Weld Overlay Cladding*, USNRC Report NUREG/CR-6363 (ORNL/TM-13047), May 1997.

14. M. A. Sokolov and D. J. Alexander, Lockheed Martin Energy Systems, Oak Ridge Natl. Lab., Oak Ridge, Tenn., *An Improved Correlation Procedure for Subsize and Full-Size Charpy Impact Specimen Data*, USNRC Report NUREG/CR-6379 (ORNL/TM-13088), March 1997.

15. S. K. Iskander and R. E. Stoller, Lockheed Martin Energy Research Corporation, Oak Ridge Natl. Lab., Oak Ridge, Tenn., *Results of Charpy V-Notch Impact Testing of Structural Steel Specimens Irradiated at ~30 °C to 1 x 10^6 Neutrons/cm2 in a Commercial Reactor Cavity*, USNRC Report NUREG/CR-6399. (ORNL-6886), April 1997.

16. S. K. Iskander, P. P. Milella, and A. Pini, Lockheed Martin Energy Research Corporation, Oak Ridge Natl. Lab., Oak Ridge, Tenn., *Results of Crack-Arrest Tests on Irradiated A 503 Class 3 Steel*, USNRC Report NUREG/CR-6447 (ORNL-6894), February 1998.

17. P. Pareige, K. F. Russell, R. E. Stoller, and M. K. Miller, Lockheed Martin Energy Research Corporation, Oak Ridge Natl. Lab., Oak Ridge, Tenn., *Influence of Long-Term Thermal Aging on the Microstructural Evolution of Nuclear Reactor Pressure Vessel Materials: An Atom Probe Study*, USNRC Report NUREG/CR-6537 (ORNL-13406), March 1998.

18. I. Remec, C. A. Baldwin, and K. B. K. Kam, Lockheed Martin Energy Research Corporation, Oak Ridge Natl. Lab., Oak Ridge, Tenn., *Neutron Exposure Parameters for Capsule 10.05 in the Heavy-Section Steel Irradiation Program Tenth Irradiation Series*, USNRC Report NUREG/CR-6600 (ORNL/TM-13548), October 1998.

19. I. Remes, C. A. Baldwin, and F. B. K. Kam, Lockheed Martin Energy Research Corporation, Oak Ridge Natl. Lab., Oak Ridge, Tenn., *Neutron Exposure Parameters for the Dosimetry Capsule in the Heavy-Section Steel Irradiation Program Tenth Irradiation Series*, USNRC Report NUREG/CR-6601 (ORNL/TM-13549), October 1998.

20. D. E. McCabe, R. K. Nanstad, S. K. Iskander, D. W. Heatherly, and R. L. Swain, Lockheed Martin Energy Research Corporation, Oak Ridge Natl. Lab., Oak Ridge, Tenn., *Evaluation of WF-70 Weld Metal from the Midland Unit 1 Reactor Vessel-Final Report*, USNRC Report NUREG/CR-5736 (ORNL/TM-13748), to be published.

21. This report.

The HSSI Program includes both follow-on and the direct continuation of work that was performed under the Heavy-Section Steel Technology (HSST) Program. Previous HSST reports related to irradiation effects in pressure vessel materials and those containing unirradiated properties of materials used in HSSI and HSST irradiation programs are tabulated below as a convenience to the reader.

C. E. Childress, Union Carbide Corp. Nuclear Div., Oak Ridge Natl. Lab., Oak Ridge, Tenn., *Fabrication History of the First Two 12-in.-Thick A-533 Grade B, Class 1 Steel Plates of the Heavy-Section Steel Technology Program*, ORNL-4313, February 1969.

T. R. Mager and F. O. Thomas, Westinghouse Electric Corporation, PWR Systems Division, Pittsburgh, Pa., *Evaluation by Linear Elastic Fracture Mechanics of Radiation Damage to Pressure Vessel Steels*, WCAP-7328 (Rev.), October 1969.

P. N. Randall, TRW Systems Group, Redondo Beach, Calif., *Gross Strain Measure of Fracture Toughness of Steels*, HSSTP-TR-3, Nov. 1, 1969.

L. W. Loechel, Martin Marietta Corporation, Denver, Colo., *The Effect of Testing Variables on the Transition Temperature in Steel*, MCR-69-189, Nov. 20, 1969.

W. O. Shabbits, W. H. Pryle, and E. T. Wessel, Westinghouse Electric Corporation, PWR Systems Division, Pittsburgh, Pa., *Heavy-Section Fracture Toughness Properties of A533 Grade B Class 1 Steel Plate and Submerged Arc Weldment*, WCAP-7414, December 1969.

C. E. Childress, Union Carbide Corp. Nuclear Div., Oak Ridge Natl. Lab., Oak Ridge, Tenn., *Fabrication History of the Third and Fourth ASTM A-533 Steel Plates of the Heavy-Section Steel Technology Program*, ORNL-4313-2, February 1970.

P. B. Crosley and E. J. Ripling, Materials Research Laboratory, Inc., Glenwood, Ill., *Crack Arrest Fracture Toughness of A533 Grade B Class 1 Pressure Vessel Steel*, HSSTP-TR-8, March 1970.

F. J. Loss, Naval Research Laboratory, Washington, D.C., *Dynamic Tear Test Investigations of the Fracture Toughness of Thick-Section Steel*, NRL-7056, May 14, 1970.

T. R. Mager, Westinghouse Electric Corporation, PWR Systems Division, Pittsburgh, Pa., *Post-Irradiation Testing of 2T Compact Tension Specimens*, WCAP-7561, August 1970.

F. J. Witt and R. G. Berggren, Union Carbide Corp. Nuclear Div., Oak Ridge Natl. Lab., Oak Ridge, Tenn., *Size Effects and Energy Disposition in Impact Specimen Testing of ASTM A533 Grade B Steel*, ORNL/TM-3030, August 1970.

D. A. Canonico, Union Carbide Corp. Nuclear Div., Oak Ridge Natl. Lab., Oak Ridge, Tenn., *Transition Temperature Considerations for Thick-Wall Nuclear Pressure Vessels*, ORNL/TM-3114, October 1970.

T. R. Mager, Westinghouse Electric Corporation, PWR Systems Division, Pittsburgh, Pa., *Fracture Toughness Characterization Study of A533, Grade B, Class 1 Steel*, WCAP-7578, October 1970.

W. O. Shabbits, Westinghouse Electric Corporation, PWR Systems Division, Pittsburgh, Pa., *Dynamic Fracture Toughness Properties of Heavy-Section A533 Grade B Class 1 Steel Plate*, WCAP-7623, December 1970.

C. E. Childress, Union Carbide Corp. Nuclear Div., Oak Ridge Natl. Lab., Oak Ridge, Tenn., *Fabrication Procedures and Acceptance Data for ASTM A-533 Welds and a 10-in.-Thick ASTM A-543 Plate of the Heavy Section Steel Technology Program*, ORNL-TM-4313-3, January 1971.

D. A. Canonico and R. G. Berggren, Union Carbide Corp. Nuclear Div., Oak Ridge Natl. Lab., Oak Ridge, Tenn., *Tensile and Impact Properties of Thick-Section Plate and Weldments*, ORNL/TM-3211, January 1971.

C. W. Hunter and J. A. Williams, Hanford Eng. Dev. Lab., Richland, Wash., *Fracture and Tensile Behavior of Neutron-Irradiated A533-B Pressure Vessel Steel*, HEDL-TME-71-76, Feb. 6, 1971.

C. E. Childress, Union Carbide Corp. Nuclear Div., Oak Ridge Natl. Lab., Oak Ridge, Tenn., *Manual for ASTM A533 Grade B Class 1 Steel (HSST Plate 03) Provided to the International Atomic Energy Agency*, ORNL/TM-3193, March 1971.

P. N. Randall, TRW Systems Group, Redondo Beach, Calif., *Gross Strain Crack Tolerance of A533-B Steel*, HSSTP-TR-14, May 1, 1971.

C. L. Segaser, Union Carbide Corp. Nuclear Div., Oak Ridge Natl. Lab., Oak Ridge, Tenn., *Feasibility Study, Irradiation of Heavy-Section Steel Specimens in the South Test Facility of the Oak Ridge Research Reactor*, ORNL/TM-3234, May 1971.

H. T. Corten and R. H. Sailors, University of Illinois, Urbana, Ill., *Relationship Between Material Fracture Toughness Using Fracture Mechanics and Transition Temperature Tests*, T&AM Report 346, Aug. 1, 1971.

L. A. James and J. A. Williams, Hanford Eng. Dev. Lab., Richland, Wash., *Heavy Section Steel Technology Program Technical Report No. 21, The Effect of Temperature and Neutron Irradiation Upon the Fatigue-Crack Propagation Behavior of ASTM A533 Grade B, Class 1 Steel*, HEDL-TME 72-132, September 1972.

P. B. Crosley and E. J. Ripling, Materials Research Laboratory, Inc., Glenwood, Ill., *Crack Arrest in an Increasing K-Field*, HSSTP-TR-27, January 1973.

W. J. Stelzman and R. G. Berggren, Union Carbide Corp. Nuclear Div., Oak Ridge Natl. Lab., Oak Ridge, Tenn., *Radiation Strengthening and Embrittlement in Heavy-Section Steel Plates and Welds*, ORNL-4871, June 1973.

J. M. Steichen and J. A. Williams, Hanford Eng. Dev. Lab., Richland, Wash., *High Strain Rate Tensile Properties of Irradiated ASTM A533 Grade B Class 1 Pressure Vessel Steel*, HEDL-TME 73-74, July 1973.

J. A. Williams, Hanford Eng. Dev. Lab., Richland, Wash., *The Irradiation and Temperature Dependence of Tensile and Fracture Properties of ASTM A533, Grade B, Class 1 Steel Plate and Weldment*, HEDL-TME 73-75, August 1973.

J. A. Williams, Hanford Eng. Dev. Lab., Richland, Wash., *Some Comments Related to the Effect of Rate on the Fracture Toughness of Irradiated ASTM A553-B Steel Based on Yield Strength Behavior*, HEDL-SA 797, December 1974.

J. A. Williams, Hanford Eng. Dev. Lab., Richland, Wash., *The Irradiated Fracture Toughness of ASTM A533, Grade B, Class 1 Steel Measured with a Four-Inch-Thick Compact Tension Specimen*, HEDL-TME 75-10, January 1975.

J. G. Merkle, G. D. Whitman, and R. H. Bryan, Union Carbide Corp. Nuclear Div., Oak Ridge Natl. Lab., Oak Ridge, Tenn., *An Evaluation of the HSST Program Intermediate Pressure Vessel Tests in Terms of Light-Water-Reactor Pressure Vessel Safety*, ORNL/TM-5090, November 1975.

J. A. Davidson, L. J. Ceschini, R. P. Shogan, and G. V. Rao, Westinghouse Electric Corporation, Pittsburgh, Pa., *The Irradiated Dynamic Fracture Toughness of ASTM A533, Grade B, Class 1 Steel Plate and Submerged Arc Weldment*, WCAP-8775, October 1976.

J. A. Williams, Hanford Eng. Dev. Lab., Richland, Wash., *Tensile Properties of Irradiated and Unirradiated Welds of A533 Steel Plate and A508 Forgings*, NUREG/CR-1158 (ORNL/SUB-79/50917/2), July 1979.

J. A. Williams, Hanford Eng. Dev. Lab., Richland, Wash., *The Ductile Fracture Toughness of Heavy-Section Steel Plate*, NUREG/CR-0859, September 1979.

K. W. Carlson and J. A. Williams, Hanford Eng. Dev. Lab., Richland, Wash., *The Effect of Crack Length and Side Grooves on the Ductile Fracture Toughness Properties of ASTM A533 Steel*, NUREG/CR-1171 (ORNL/SUB-79/50917/3), October 1979.

G. A. Clarke, Westinghouse Electric Corp., Pittsburgh, Pa., *An Evaluation of the Unloading Compliance Procedure for J-Integral Testing in the Hot Cell, Final Report*, NUREG/CR-1070 (ORNL/SUB-7394/1), October 1979.

P. B. Crosley and E. J. Ripling, Materials Research Laboratory, Inc., Glenwood, Ill., *Development of a Standard Test for Measuring KIa with a Modified Compact Specimen*, NUREG/CR-2294 (ORNL/SUB-81/7755/1), August 1981.

H. A. Domian, Babcock and Wilcox Company, Alliance, Ohio, *Vessel V-8 Repair and Preparation of Low Upper-Shelf Weldment*, NUREG/CR-2676 (ORNL/SUB/81-85813/1), June 1982.

R. D. Cheverton, S. K. Iskander, and D. G. Ball, Union Carbide Corp. Nuclear Div., Oak Ridge Natl. Lab., Oak Ridge, Tenn., *PWR Pressure Vessel Integrity During Overcooling Accidents: A Parametric Analysis*, NUREG/CR-2895 (ORNL/TM-7931), February 1983.

J. G. Merkle, Union Carbide Corp. Nuclear Div., Oak Ridge Natl. Lab., Oak Ridge, Tenn., *An Examination of the Size Effects and Data Scatter Observed in Small Specimen Cleavage Fracture Toughness Testing*, NUREG/CR-3672 (ORNL/TM-9088), April 1984.

W. R. Corwin, Martin Marietta Energy Systems, Inc., Oak Ridge Natl. Lab., Oak Ridge, Tenn., *Assessment of Radiation Effects Relating to Reactor Pressure Vessel Cladding*, NUREG/CR-3671 (ORNL-6047), July 1984.

W. R. Corwin, R. G. Berggren, and R. K. Nanstad, Martin Marietta Energy Systems, Inc., Oak Ridge Natl. Lab., Oak Ridge, Tenn., *Charpy Toughness and Tensile Properties of a Neutron Irradiated Stainless Steel Submerged-Arc Weld Cladding Overlay*, NUREG/CR-3927 (ORNL/TM-9709), September 1984.

J. J. McGowan, Martin Marietta Energy Systems, Inc., Oak Ridge Natl. Lab., Oak Ridge, Tenn., *Tensile Properties of Irradiated Nuclear Grade Pressure Vessel Plate and Welds for the Fourth HSST Irradiation Series*, NUREG/CR-3978 (ORNL/TM-9516), January 1985.

J. J. McGowan, Martin Marietta Energy Systems, Inc., Oak Ridge Natl. Lab., Oak Ridge, Tenn., *Tensile Properties of Irradiated Nuclear Grade Pressure Vessel Welds for the Third HSST Irradiation Series*, NUREG/CR-4086 (ORNL/TM-9477), March 1985.

W. R. Corwin, G. C. Robinson, R. K. Nanstad, J. G. Merkle, R. G. Berggren, G. M. Goodwin, R. L. Swain, and T. D. Owings, Martin Marietta Energy Systems, Inc., Oak Ridge Natl. Lab., Oak Ridge, Tenn., *Effects of Stainless Steel Weld Overlay Cladding on the Structural Integrity of Flawed Steel Plates in Bending, Series 1*, NUREG/CR-4015 (ORNL/TM-9390), April 1985.

W. J. Stelzman, R. G. Berggren, and T. N. Jones, Martin Marietta Energy Systems, Inc., Oak Ridge Natl. Lab., Oak Ridge, Tenn., *ORNL Characterization of Heavy-Section Steel Technology Program Plates 01, 02, and 03*, NUREG/CR-4092 (ORNL/TM-9491), April 1985.

G. D. Whitman, Martin Marietta Energy Systems, Inc., Oak Ridge Natl. Lab., Oak Ridge, Tenn., *Historical Summary of the Heavy-Section Steel Technology Program and Some Related Activities in Light-Water Reactor Pressure Vessel Safety Research*, NUREG/CR-4489 (ORNL-6259), March 1986.

R. H. Bryan, B. R. Bass, S. E. Bolt, J. W. Bryson, J. G. Merkle, R. K. Nanstad, and G. C. Robinson, Martin Marietta Energy Systems, Inc., Oak Ridge Natl. Lab., Oak Ridge, Tenn., *Test of 6-in.-Thick Pressure Vessels. Series 3: Intermediate Test Vessel V-8A - Tearing Behavior of Low Upper-Shelf Material*, NUREG-CR-4760 (ORNL-6187), May 1987.

D. B. Barker, R. Chona, W. L. Fourney, and G. R. Irwin, University of Maryland, College Park, Md., *A Report on the Round Robin Program Conducted to Evaluate the Proposed ASTM Standard Test Method for Determining the Plane Strain Crack Arrest Fracture Toughness, Kla, of Ferritic Materials*, NUREG/CR-4966 (ORNL/SUB/79-7778/4), January 1988.

L. F. Miller, C. A. Baldwin, F. W. Stallman, and F. B. K. Kam, Martin Marietta Energy Systems, Inc., Oak Ridge Natl. Lab., Oak Ridge, Tenn., *Neutron Exposure Parameters for the Metallurgical Test Specimens in the Fifth Heavy-Section Steel Technology Irradiation Series Capsules*, NUREG/CR-5019 (ORNL/TM-10582), March 1988.

J. J. McGowan, R. K. Nanstad, and K. R. Thoms, Martin Marietta Energy Systems, Inc., Oak Ridge Natl. Lab., Oak Ridge, Tenn., *Characterization of Irradiated Current-Practice Welds and A533 Grade B Class 1 Plate for Nuclear Pressure Vessel Service*, NUREG/CR-4880 (ORNL-6484/V1 and V2), July 1988.

R. D. Cheverton, W. E. Pennell, G. C. Robinson, and R. K. Nanstad, Martin Marietta Energy Systems, Inc., Oak Ridge Natl. Lab., Oak Ridge, Tenn., *Impact of Radiation Embrittlement on Integrity of Pressure Vessel Supports for Two PWR Plants*, NUREG/CR-5320 (ORNL/TM-10966), February 1989.

J. G. Merkle, Martin Marietta Energy Systems, Inc., Oak Ridge Natl. Lab., Oak Ridge, Tenn., *An Overview of the Low-Upper-Shelf Toughness Safety Margin Issue*, NUREG/CR-5552 (ORNL/TM-11314), August 1990.

R. D. Cheverton, T. L. Dickson, J. G. Merkle, and R. K. Nanstad, Martin Marietta Energy Systems, Inc., Oak Ridge Natl. Lab., Oak Ridge, Tenn., *Review of Reactor Pressure Vessel Evaluation Report for Yankee Rowe Nuclear Power Station (YAEC No. 1735)*, NUREG/CR-5799 (ORNL/TM-11982), March 1992.

1. INTRODUCTION

Prevention of reactor pressure vessel (RPV) failure in light-water-cooled nuclear power reactors depends primarily on maintaining the RPV material fracture toughness at levels that will resist fracture, either brittle or ductile, during plant operation, including both normal and emergency conditions. The basic fracture toughness requirements are contained in Title 10, *Code of Federal Regulations*, Part 50 (10 CFR 50) [1], which references Section XI of the American Society of Mechanical Engineers (ASME) *Boiler and Pressure Vessel Code* [2]. Section XI contains fracture toughness (K_{Ic}) and crack-arrest toughness (K_{Ia}) curves as a function of temperature normalized to a reference nil-ductility temperature (RT_{NDT}), namely, T-RT_{NDT}. 10 CFR 50 includes provisions for the adjustment of RT_{NDT} to account for irradiation embrittlement, while *Regulatory Guide 1.99* (RG 1.99) [3] describes general procedures for calculating such adjustment. The "adjusted reference temperature" (ART) is defined in Appendix G of 10 CFR 50 as "the reference temperature as adjusted for irradiation effects by adding to RT_{NDT} the temperature shift, measured at the 30-ft-lb (41-J) level, in the average Charpy curve for the irradiated material relative to that for the unirradiated material." Code 10 CFR 50 references the American Society for Testing and Materials (ASTM) Standard E-185 [4] for determination of the temperature shift between the unirradiated and irradiated Charpy curves at the 41-J level (ΔT_{41J}) from surveillance test results. The data that formed the basis for the calculative procedures given in RG 1.99 were Charpy 41-J shift values also. Thus, the fracture toughness curves are shifted by virtue of the change in the T_{41J}.

Some of the implicit assumptions with these procedures are that (1) the Charpy 41-J shift is the same as the RT_{NDT} shift, (2) the K_{Ic} fracture toughness and K_{Ia} crack-arrest toughness shifts are the same as the Charpy 41-J shift, and (3) the shapes of the two curves do not change as a consequence of irradiation. This report addresses the last two assumptions regarding the fracture toughness curve relative to the database assembled from different publications [5–25] where both irradiation-induced static fracture toughness and Charpy impact shifts were reported. The first assumption will be only briefly discussed because of a lack of sufficient data.

2. ANALYSIS PROCEDURE

Different sizes of fracture toughness specimens, procedures for K_{Jc} determination, and fitting functions reported in the various publications were used. To minimize variability resulting from different analysis procedures, it was decided that all data should be reanalyzed by the consistent procedures discussed

in this report. Thus, raw data tabulated in a source were the preferred choices for entering into the present database. In some publications, however, data were not available in tabulated form. In such cases, data were digitized from the plots. The validity of the published data was assumed to be unknown.

The ASME K_{Ic} curve was based upon data [26] gained from testing large specimens that satisfy the validity requirements of ASTM Standard E-399 [27]. Practically, it is not possible to accumulate the equivalent linear-elastic K_{Ic} database for irradiated material. In fact, the size of compact specimens for irradiation studies is limited to 4T (101.6 mm thick) because of the through-thickness fluence gradients. As a result, capsules for irradiation studies include fracture toughness specimens having thicknesses that do not satisfy ASTM E-399 requirements at the transition-region temperatures in the majority of cases. With testing of relatively small specimens (relative to ASTM E-399), some amount of local crack-tip plasticity is unavoidable, and fracture toughness up to cleavage instability was calculated, using elastic-plastic fracture mechanics, in terms of the J-integral, J_c. Then J_c was converted to its equivalent in terms of the elastic-plastic stress-intensity factor, K_{Jc}. When it was evident that there must have been a loss of constraint for small specimens at high fracture toughness, special consideration was made for qualifying and censoring data. A recently accepted standard by ASTM Committee E-08 [28] specifies the following limit value:

$$K_{Jc(limit)} = \sqrt{\frac{Eb_o\sigma_y}{30}} \quad , \tag{1}$$

where E is elastic modulus, b_o is the initial remaining ligament dimension, and σ_y is the yield strength. If a K_{Jc} value exceeded this limit, then that value was considered an invalid datum. Only data sets with four or more valid fracture toughness values were included in the present analysis.

The fracture toughness data were analyzed by a procedure based on earlier work described by Wallin [29–31] that incorporates the statistical model of Weibull (see some mathematical details in Appendix A). The analysis procedure is based on fitting fracture toughness data to a three-parameter Weibull cumulative distribution function:

$$P_f = 1 - \exp\left(-\left[\frac{K_{Jc} - K_{min}}{K_o - K_{min}}\right]^b \right) \quad , \tag{2}$$

where P_f is the cumulative fracture probability, K_{min} is the location parameter, K_o is the scale parameter, and b is the shape parameter. It was determined, at least for RPV steels [29], that among these three parameters, the shape parameter (Weibull slope) is equal to 4 when the location parameter, K_{min}, is equal to 20 MPa$\sqrt{m}$.

This procedure is applicable only to fracture toughness data statistically size-adjusted to a common size. The statistical size adjustment is based on the weakest-link theory, and for fracture toughness values it has the following form [30]:

$$K_{Jc}^{1T} = 20 + (K_{Jc}^{xT} - 20) \cdot \left(\frac{B_{xT}}{B_{1T}} \right)^{1/4} , \qquad (3)$$

where B_{xT} is thickness of the tested specimen and B_{1T} is the thickness of a 1T specimen. The master curve concept uses only toughness values size-adjusted to that of 1T specimen equivalence.

Thus, a probabilistic-based estimate of median fracture toughness value, $K_{Jc(med)}$, for a data population at a given test temperature can be made as a value of K_{Jc} at cumulative fracture probability, P_f, equal to 0.5. Finally, the concept of the universal curve shape for $K_{Jc(med)}$ vs temperature for 1T size specimens (the so-called "master curve" [32]) was applied to $K_{Jc(med)}$, to define the temperature dependence of K_{Jc} in the transition region as follows [33]:

$$K_{Jc(med)}^{1T} = 30 + 70 \exp[0.019 (T - T_{100})] , \qquad (4)$$

where T_{100} is the reference fracture toughness temperature at $K_{Jc(med)}$ = 100 MPa$\sqrt{m}$. The concept of the universal master curve assumes a reference temperature based on a level of fracture toughness for the material. Thus, fracture toughness of the material can be described by a fracture toughness-based reference temperature rather than by a temperature derived from a combination of drop-weight and Charpy impact tests. Consequently, the radiation-induced shift of fracture toughness of material can be characterized by the shift of the reference fracture toughness temperature, ΔT_{100}.

The fitting procedure employs the maximum-likelihood concept, regarded as the most accurate method of obtaining T_{100}. The properties of the maximum-likelihood and the moment estimators for Weibull distribution are compared in Appendix A. The following equation [31] is used in the present report

based on the assumption that scatter in data sets is modeled by Eqs. (2) and (3) and that the temperature dependence of $K^{1T}_{Jc(med)}$ obeys Eq. (4):

$$\sum_{i=1}^{n} \frac{\delta_i \exp[0.019(T_i - T_{100})]}{11 + 77\exp[0.019(T_i - T_{100})]} - \sum_{i=1}^{n} \frac{(K_{Jc\,i} - 20)^4 \exp[0.019(T_i - T_{100})]}{(11 + 77\exp[0.019(T_i - T_{100})])^5} = 0 \quad , \tag{5}$$

from which T_{100} estimates were determined iteratively. In Eq. (5) the censoring factor Kronecker's δ_i is unity when K_{Jci} satisfies the constraint limit by Eq. (1), and $\delta_i = 0$ when K_{Jci} exceeds the limit by Eq. (1) or when a test did not terminate in cleavage instability.

Most of the Charpy data were presented in the published sources in the form of absorbed energy vs temperature. Nevertheless, lateral expansion and percentage of shear-fracture data were also reanalyzed when it was feasible. The Charpy impact data for each material condition were fitted with a hyperbolic tangent function:

$$E = \frac{USE + LSE}{2} + \frac{USE - LSE}{2} \tanh\left(\frac{T - T_{MT}}{C}\right) \quad , \tag{6}$$

where E is the absorbed energy (J), lateral expansion (mm), or percent shear fracture (%); T is the test temperature (in degrees Celsius); and USE, LSE, T_{MT}, and C are fitting parameters. The parameters USE and LSE represent the upper and lower values, respectively, for shelf energy, lateral expansion, or percent shear values; T_{MT} is the temperature at the middle of the transition range; C is one-half of the transition-zone temperature width and reflects the slope of the curve in the transition zone. All hyperbolic tangent analyses were conducted with the lower-shelf energy fixed at 2.7 J, and lateral expansion and percent shear at zero. The upper-shelf percent shear was always fixed at 100%.

3. THE WEIBULL STATISTIC/MASTER CURVE APPROACH AND THE ASME K_{Ic} DATABASE

The ASME K_{Ic} curve has been plotted as a function of test temperature (T) normalized to a reference nil-ductility temperature, RT_{NDT}, namely, $T\text{-}RT_{NDT}$, and was constructed as the lower boundary to linear-

elastic K_{Ic} values available at that time in the normalized temperature range from –100 to +100°F (–55.6 to +55.6°C). Later, such graphical representation was replaced by the Electric Power Research Institute (EPRI) equation:

$$K_{Ic} = 33.2 + 20.734 \exp\left[0.02\,(T - RT_{NDT})\right] \quad , \tag{7}$$

where K_{Ic} is in ksi $\sqrt{in.}$, and T and RT_{NDT} are in degrees Fahrenheit. The reference nil-ductility temperature is derived from a combination of drop-weight and Charpy impact test results as specified in Ref. [2].

Being a lower bound to a unique but limited database, the ASME K_{Ic} curve concept does not address probability matters. However, there has been a continuing evolution of fracture mechanics that has led to employment of the Weibull distribution function to model the scatter of fracture toughness values in the transition range. Thus a probabilistic-based estimate of a lower tolerance value for a given data population can be made.

In this section, the Weibull-statistic/master curve analysis procedure [Eqs. (2) through (5)] is applied to the linear-elastic K_{Ic} database [26] that has been used to support the ASME K_{Ic} lower-bound curve (see Fig. 1). Most of this database is represented by the data for an A 533 grade B Class 1 plate designated HSST-02. Initially, the K_{Ic} values for HSST Plate 02 only were adjusted to 1T size specimens by Eq. (3), and T_{100} was equal to –18.4°F (–28°C) by using Eq. (5). The master curve and some upper and lower tolerance bounds were plotted against these size-adjusted data in Fig. 2. Expressions for these upper and lower tolerance bounds are given in the recently approved ASTM standard E-1921 [28]. The scatter of HSST Plate 02 data increases as test temperature increases, but tolerance bounds predict the increased scatter very well. Nevertheless, there are three data points at 50°F (10°C) that raise some concern regarding the shape of the master curve at K_{Ic} values above 150 ksi$\sqrt{in.}$ Of course, those are the only three data points at this temperature; thus, an additional replication is required to make further conclusions. On the other hand, two of these specimens were 10T size and one was an 11T compact specimen. There were two more 10T compact specimens tested; one at 25°F (–3.9°C) and another at 0°F (–17.8°C). All five specimens are on the upper bound of the scatter band, suggesting that application of the statistical size correction by Eq. (3) becomes less applicable at such thicknesses. Cleavage fracture is triggered by the small microstructural defects that are always present in commercially produced heavy-section steels. As specimen thickness increases, the probability of

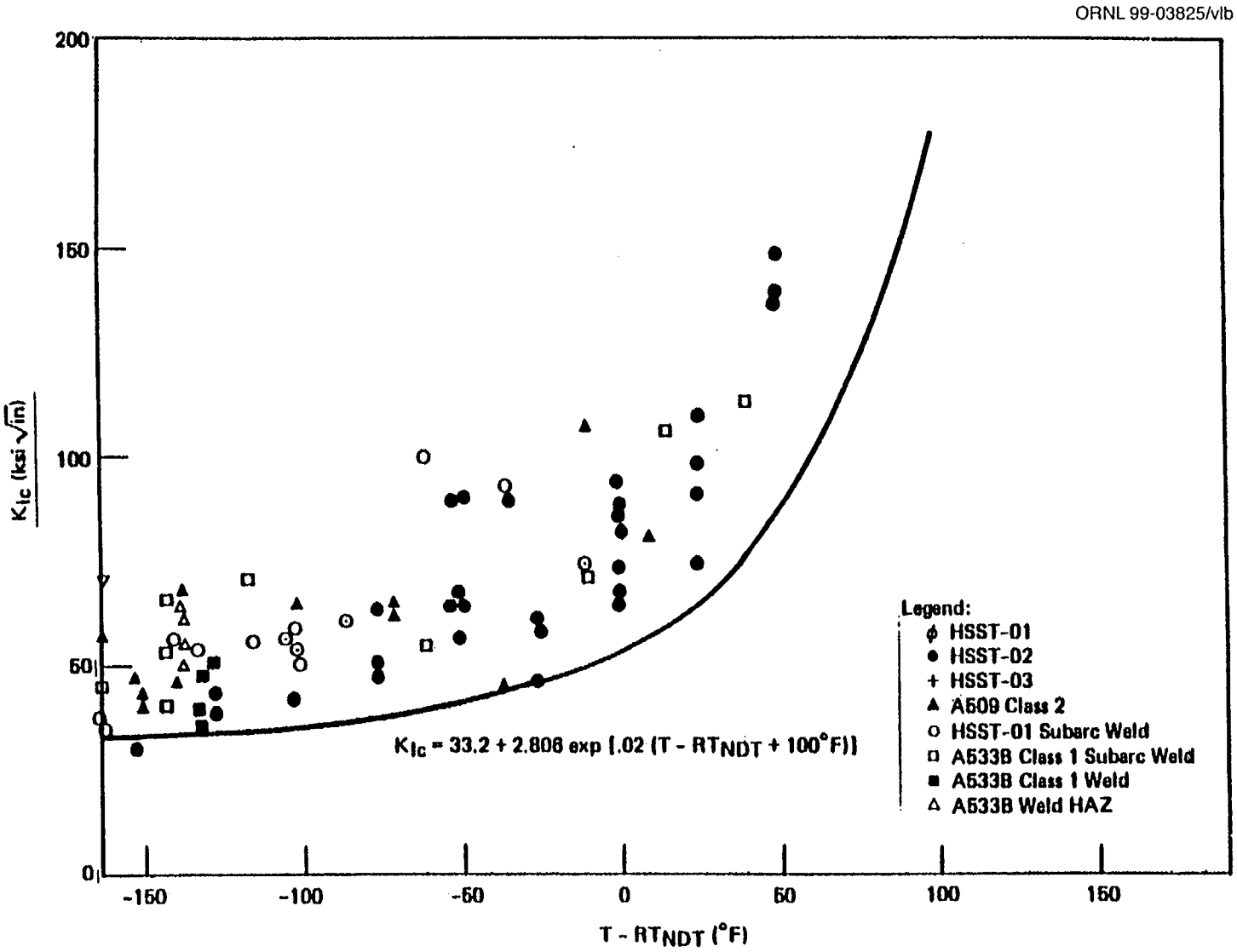

Fig. 1. K_{Ic} reference toughness curve with supporting data as presented in EPRI NP-719-SR.

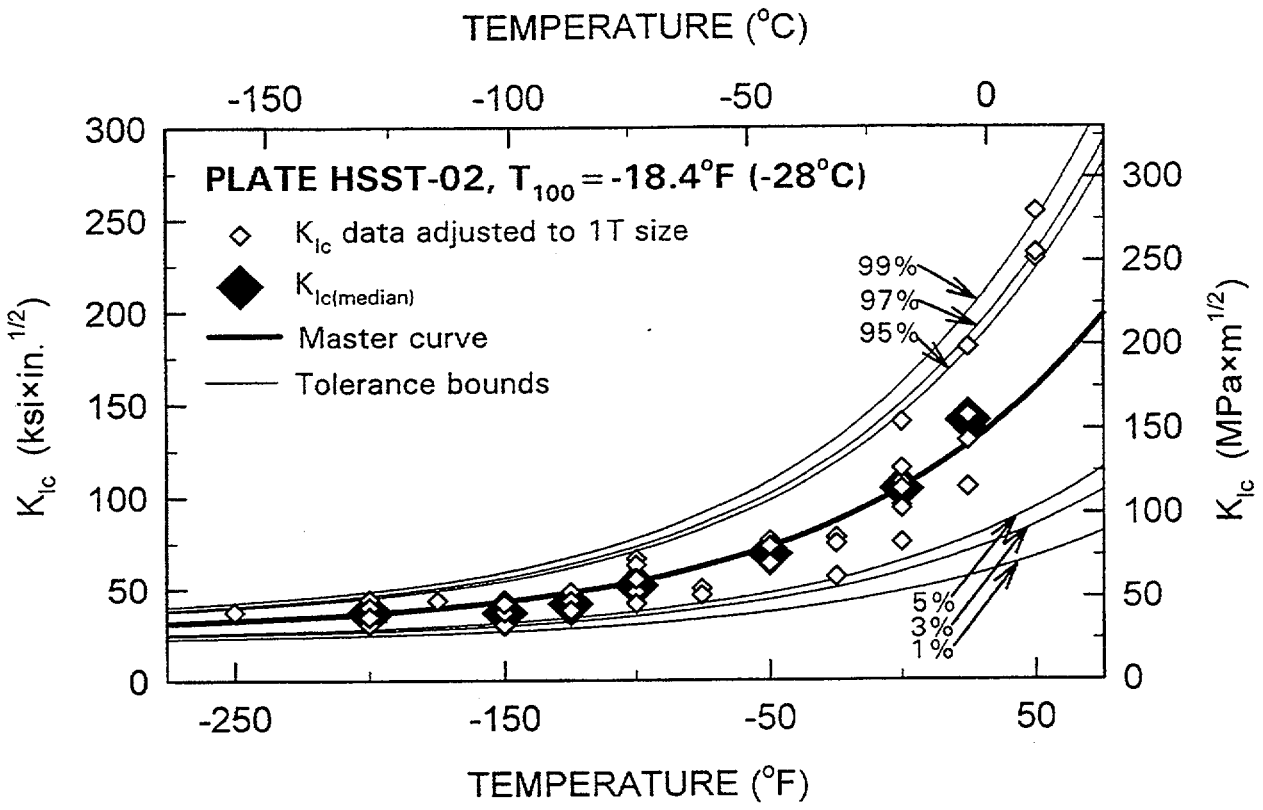

Fig. 2. Linear-elastic K_{Ic} data of the HSST Plate 02 statistically adjusted to 1T size with the corresponding master curve and tolerance bounds.

encountering the trigger point of a critical size on the crack-tip front at a critical stress state also increases. Equation (3) is the mathematical expression for these statistical effects. However, the rate at which the probability of meeting a critical defect increases tends to plateau at some point as the volume of material increases. Specifically, the weakest-link model may become inaccurate for specimen-size-effect calculations when the crack-tip front becomes too long relative to a critical defect size at a given distribution of defects in the volume.

Fortunately, there were several temperatures at which four or more replicated tests were performed. For such replicated tests, values of $K_{Ic(med)}$ were determined (see shaded symbols in Fig. 2). It is a very important observation for this analysis that the master curve fits to these $K_{Ic(med)}$ results very well. Applying the Weibull statistic/master curve approach to describe the HSST-02 data only was successful; therefore, the rest of the K_{Ic} database was analyzed by this procedure.

All 174 K_{Ic} data of eleven materials from the EPRI database [26] were reexamined and checked for accuracy by Nanstad et al. [34], and these data were used in the present analysis. All data were size-

corrected to 1T specimen equivalence, and then T_{100} values for all materials were determined. Figure 3 is the linear-elastic K_{Ic} data in new fracture toughness coordinates [35]. This is a plot of K_{Ic} values adjusted to 1T size equivalence by Eq. (3) vs temperature, T, normalized to the reference fracture toughness temperature, T_{100} (i.e., $T - T_{100}$). The individual T_{100} values for each material are also presented in the Fig. 3 [35]. The master curve by Eq. (4), reformatted to English-unit equivalents, is presented in Fig. 3 as the line designated "50%." For comparison, lower and upper curves that correspond to some lower and upper cumulative probability levels are also presented in Fig. 3.

The following observations can be made based on results in Fig. 3. In Fig. 3, the linear-elastic K_{Ic} data from different materials form a typical fracture toughness data trend, as if it were a large data set from one material. The master curve represents very well the median trend of this database, while the scatter of data is characterized by lower- and upper-bound curves. The present results provide additional support to the statistical nature of brittle fracture and to the importance of using a statistical method to describe probabilities of such events.

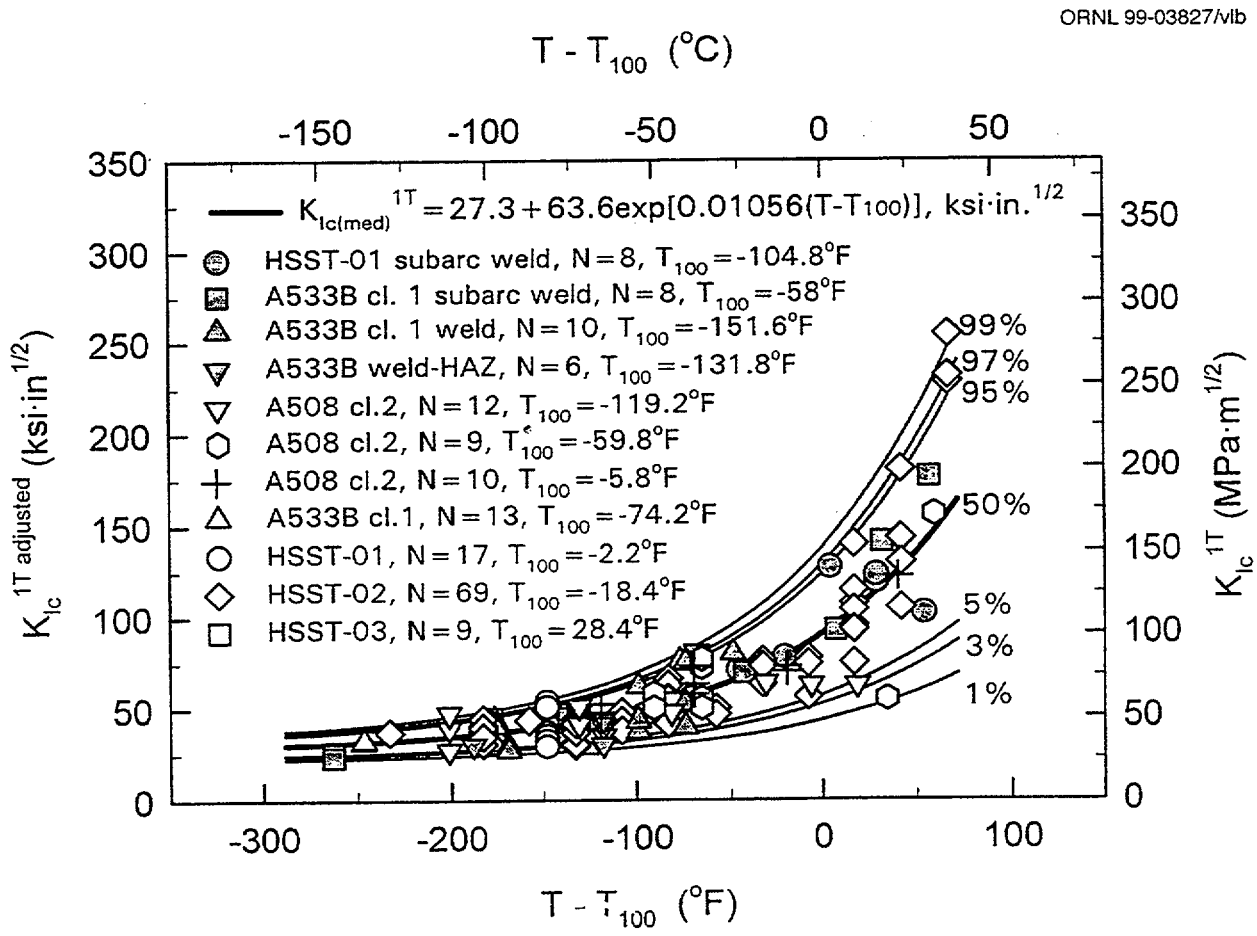

Fig. 3. The ASME K_{Ic} data statistically adjusted to 1T size equivalence and described by the master curve and corresponding upper and lower tolerance bounds.

Thus, different materials can be compared based on fracture toughness level by means of the reference temperature T_{100} rather than RT_{NDT} values. Figure 4 presents a comparison [35] of RT_{NDT} and T_{100} reference temperatures of all materials in the linear-elastic database. There is no obvious correlation between these two reference temperatures for the materials analyzed. The T_{100} temperatures spread evenly among steels in a temperature range from –110 to 0°C (–166 to 32°F). The RT_{NDT} values tend to form two clusters at about 0 and 50°F (-17.8 and 10°C). For 10 of the 11 materials in this database, RT_{NDT} temperature is higher than T_{100}.

The plot in Fig. 5(a) is the current representation of the ASME K_{Ic} database and lower-bound curve by normalizing to RT_{NDT}. The plot in Fig. 5(b) is the same K_{Ic} database (not size-adjusted), but normalized by reference fracture toughness temperature T_{100} from the present work. The ASME K_{Ic} curve is shown with all of the ASME K_{Ic} data, including those below the normalized temperature of –140°F (–77.8°C). The first observation is that the ASME K_{Ic} curve is only a lower bound for the data in the temperature range $-140 \leq T - RT_{NDT} \leq +100$°F; hence it is not a true lower bound to all of the data [34]. Second, in the transition region the shape of this curve is dictated entirely by data from one material, namely HSST Plate 02. As can be seen in Fig. 4, RT_{NDT} and T_{100} values are comparable within about 20°F (–11.1°C) for HSST-02 as well as for HSST-01 and HSST-03. For the rest of the materials, RT_{NDT} is greater than the T_{100} temperature. Hence, having actual fracture toughness values comparable with plate HSST-02, they do not contribute to construction of the transition-region part of the ASME K_{Ic} lower-bound curve because they are shifted too much to the left. In the Fig. 5(b), fracture toughness values of the same materials are compared relative to the median fracture toughness at 100 MPa$\sqrt{m}$ (T_{100}). The master curve is not shown in Fig. 5(b) because data shown are not size-adjusted. However, lower tolerance bounds to the 1T master curve are presented in Fig. 5(b). The statistically based size dependence is very pronounced for the master curve, especially for upper tolerance bounds. At lower probability levels, however, the statistical size effect is not so dominant; hence, as it can be seen in Fig. 5(b), tolerance bounds to the 1T size master curve serve as lower statistical bounds relatively well, even for unadjusted data.

The sensitivity of fracture toughness to various cumulative probabilities for the statistical size correction is illustrated in Fig. 6 for the case $T = T_{100}$. As discussed earlier, relevant to the weakest-link theory, the probability of encountering the weak trigger point for a sample, and, as a result, to obtain a lower toughness value, increases with the thickness of the tested sample. The thickness dependence of median fracture toughness in Fig. 6 illustrates this effect. For the same reason, however, the scatter in fracture toughness values reduces as thickness increases. It makes upper bounds even more size-dependent than the median values, while the lower bounds are less sensitive to statistical size

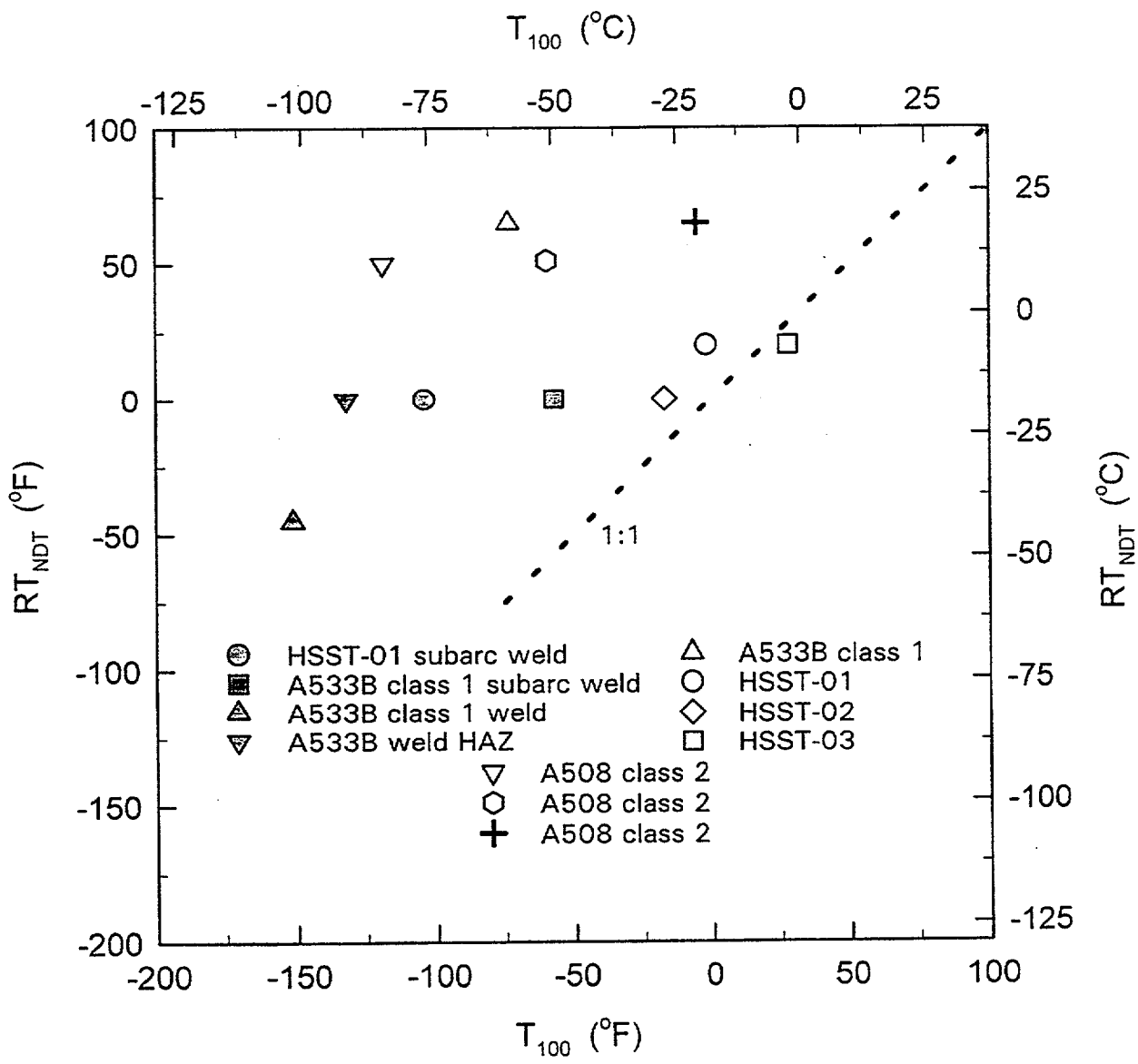

Fig. 4. Comparison of RT_{NDT} and T_{100} for materials in the ASME database.

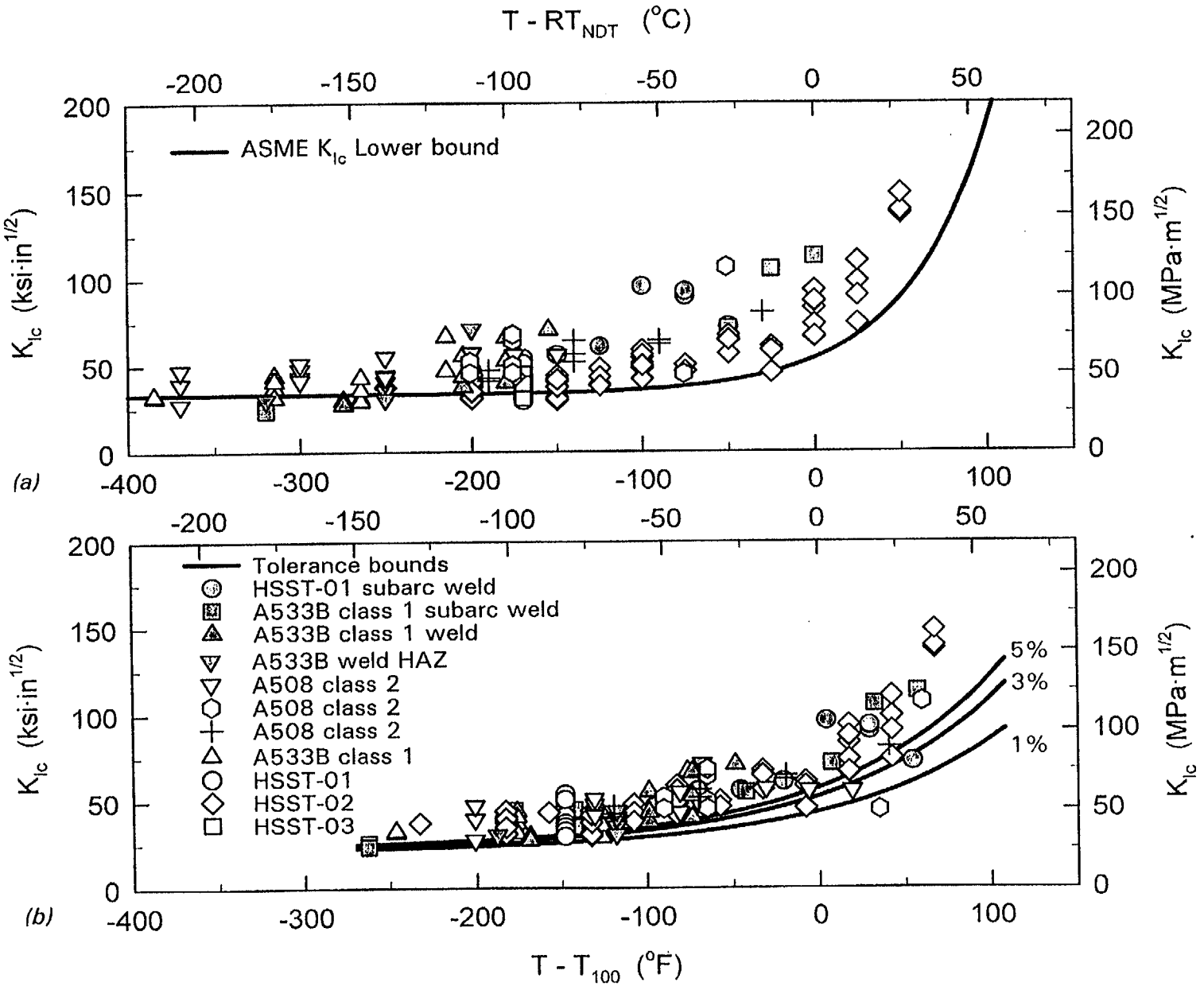

Fig. 5. **The ASME K_{Ic} database vs temperature normalized by (a) RT_{NDT} and (b) T_{100}.** Left and bottom axes are in U.S. custom units, right and top axes are in SI units.

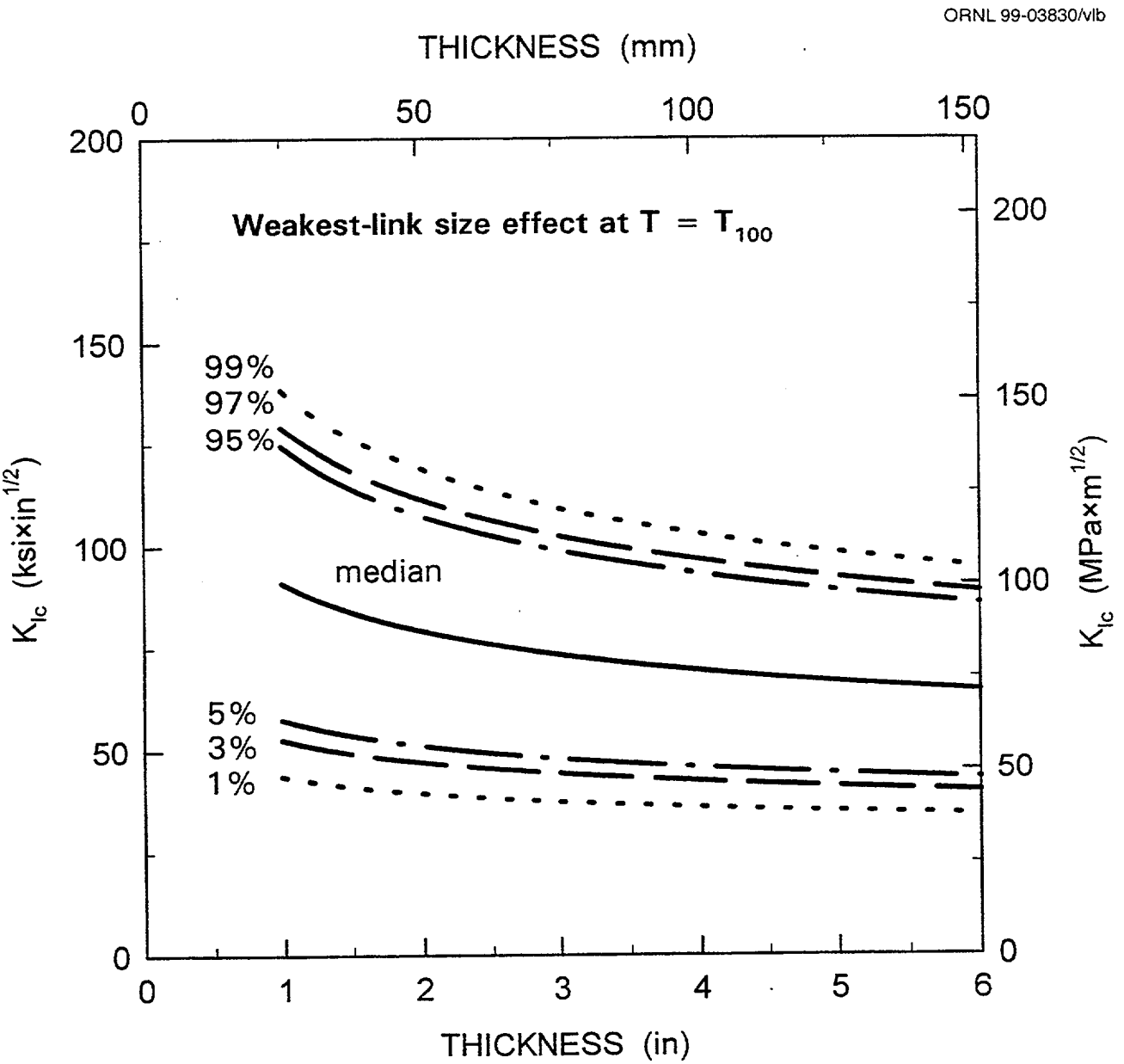

Fig. 6. **Statistically based size effect on median and upper and lower tolerance bounds at $T = T_{100}$.**

adjustment. Thus, being well established for 1T size, these lower tolerance bounds may be considered for engineering applications regardless of the thickness of the structure. The selection of a particular probability level is a matter of engineering judgment.

Based on differences between RT_{NDT} and T_{100}, as in Fig. 4, three materials were selected to compare fracture toughness lower-bound representation by the ASME curve with the tolerance bounds from the present analysis. The first material is HSST Plate 02 (see Fig. 7). For this material RT_{NDT} and T_{100} are more or less comparable. The tolerance bounds provide a good estimation of lower fracture toughness for this data set over the entire temperature range where data are available. The ASME curve works very well in the lower part of the transition range. In the upper part of the transition range the tolerance bounds predict lower fracture toughness than the ASME curve. Figure 8 illustrates the opposite extreme in this database. This A 508 Class 2 forging has the largest difference between RT_{NDT} and T_{100} among the materials analyzed. Available fracture toughness data of this material are considerably underestimated by the ASME curve. It needs to be pointed out that the master curve fitting to a data set like this requires some caution because all data are in the lower part of the transition region. For

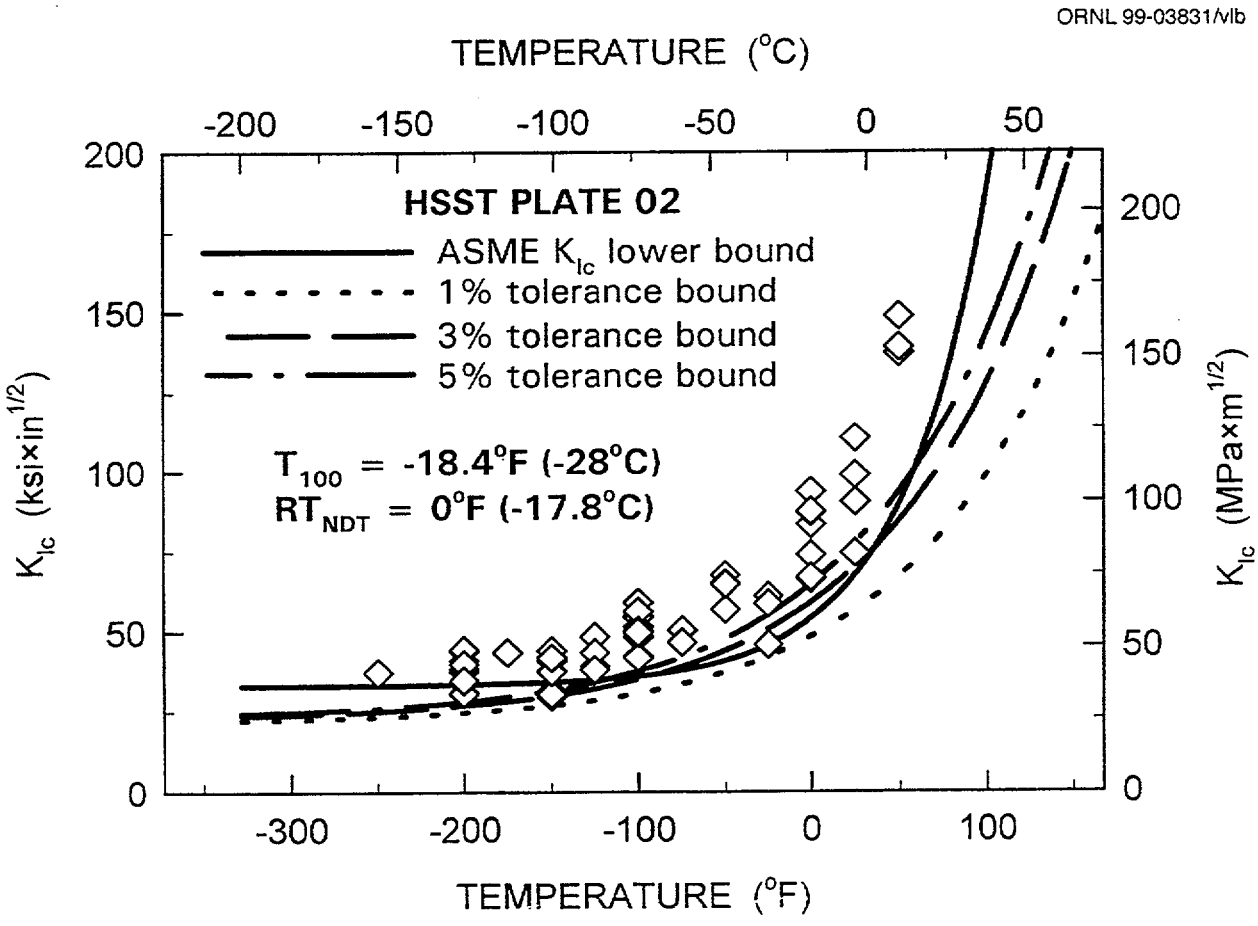

Fig. 7. Comparison of lower tolerance bounds with the ASME K_{Ic} lower-bound curve for HSST Plate 02. Note: fracture toughness data are as-measured.

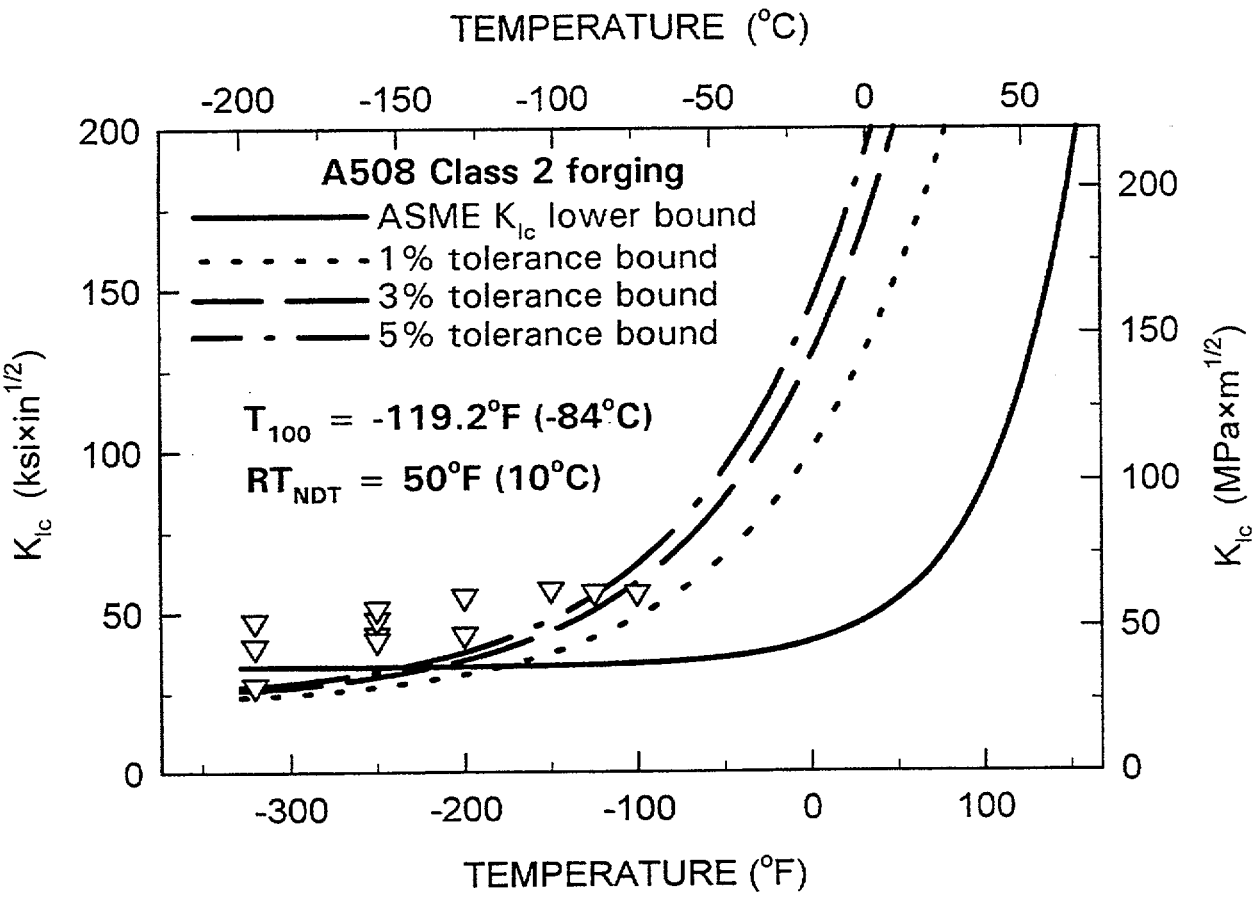

Fig. 8. Comparison of lower tolerance bounds with the ASME K_{Ic} lower-bound curve for A508 Class 2 forging. Note: fracture toughness data are as-measured.

example, ASTM standard E-1921 does not advise the use of the size-adjustment procedure for low fracture toughness values. An A 533 grade B Class 1 submerged-arc weld was selected from the middle of Fig. 4 as the third material (see Fig. 9). For this weld, the RT_{NDT} is 0°F (–17.8°C) and T_{100} is –58.0°F (–50°C). Figure 9 shows that in lower and middle parts of the transition range the ASME curve underestimates the lower bound for fracture toughness values compared with the 5% or 3% tolerance bounds. At –325°F (–198.3°C), fracture toughness data are below the ASME curve. It needs to be pointed out that fracture toughness data in Figs. 7 through 9 are not size-adjusted; i.e., as-measured.

In all cases considered, the tolerance bounds from the present analysis provide reasonable bounding curves to the fracture toughness data. The 5% and 3% tolerance bounds demonstrate a very good prediction of the bounds for the scatter in the fracture toughness. Clearly, the 1% tolerance bound is a more conservative estimate. The ASME K_{Ic} lower-bound curve, however, works very well only for one

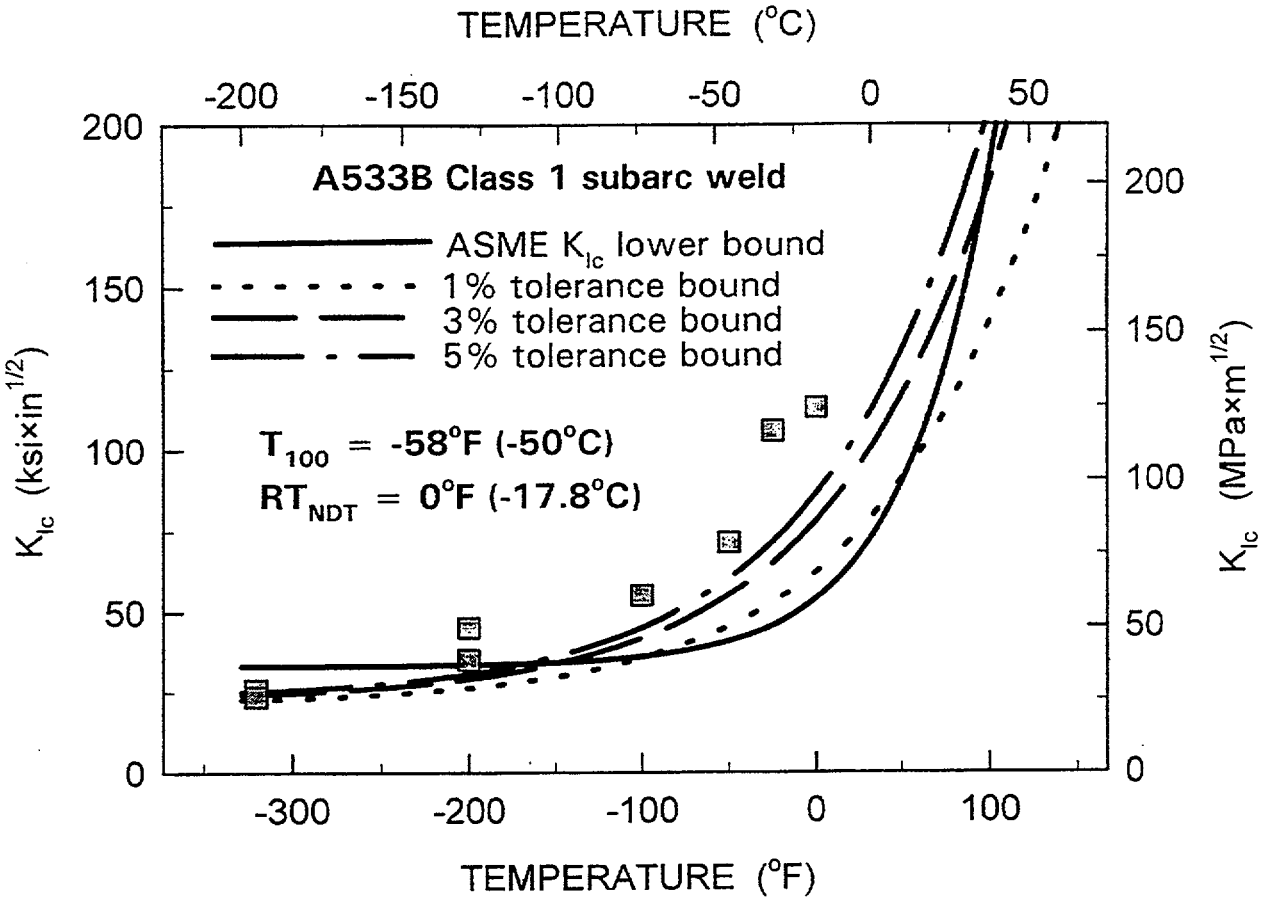

Fig. 9. Comparison of lower tolerance bounds with the ASME K_{Ic} lower-bound curve for A533 grade B class 1 submerged-arc weld. Note: fracture toughness data are as-measured.

material, HSST Plate 02. For HSST Plate 02, the 3% tolerance bound is the closest among the bounds considered compared with the K_{Ic} lower-bound curve (see Fig. 7). Based on that observation, representation of the tolerance bounds in the next sections is limited to 97% and 3% only.

For most of the materials in this database, the ASME lower-bound curve has a tendency to underestimate fracture toughness in the transition range and to overestimate fracture toughness on the lower shelf.

4. RESULTS OF ANALYSIS

The concept of the master curve is compatible with the assumption of an equidistant lateral shift of the fracture toughness temperature dependence as a consequence of irradiation. Thus, a measurement of the radiation-induced shift of the reference fracture toughness temperature is enough to describe completely changes in the transition range. For Charpy curves, this is a more complicated issue because there is usually a drop in upper-shelf energy (USE) and a change in the curve slope. Current practice requires measurement of the Charpy curve shift at the level of 41 J. Because 41 J is an arbitrary index, the ductile-to-brittle transition temperatures at some other indices, including temperatures at 0.9 mm of lateral expansion and 50% shear fracture, are also considered as additional (and sometimes even as alternative) characteristics of the Charpy transition curve. The results of the analyses are summarized in Appendix B, Tables B.1 and B.2. All of the available Charpy data were consistently reanalyzed in the present study, and the transition temperature at some other indices are also reported in Tables B.1 and B.2. Additionally, the USE and lateral expansion (USEXP) are also reported as well as Charpy energy at $T = T_{100}$ (ENERGY), nil-ductility temperature (NDT), yield strength (YIELD), ultimate tensile strength (UTS), and weight percent of some chemical elements.

Figure 10 presents a plot of Charpy energy at $T = T_{100}$ as a function of yield strength for metals in the database. The distribution does not suggest a strong correlation between these parameters. Figure 11 is a plot of Charpy energy at $T = T_{100}$ against T_{100}. For most of the data, the T_{100} temperature corresponds to the lower part of the Charpy curve in the range from 41 J (30 ft-lb) to the lower shelf (with some data as high as 68 J). On average, Charpy energy is equal to 25 J at $T = T_{100}$. However, given the distribution of Charpy energy, it is hard to justify introduction of a new index, T at 25 J in this case, as better than T at 41 J. Although Fig. 11 resembles a shotgun pattern similar to Fig. 10, there is a slight trend to higher Charpy energy at $T = T_{100}$ with increase in the T_{100} value. Assumption of this trend may suggest that the fracture toughness T_{100} shift would be higher than the Charpy T_{41J} shift. It also provides additional support for attempts in some studies [23, 33, 36] to evaluate the DBTT at Charpy-based indexes that would differ for the unirradiated and irradiated materials. In summary, data on Figs. 10 and 11 did not reveal any material-independent-characteristic Charpy energy level that could correlate strongly with the reference fracture toughness temperature T_{100}. This result implies substantial scatter in correlations between transition temperatures derived from Charpy impact energy and static fracture toughness tests.

Having established a database with both the reference fracture toughness and Charpy impact transition temperatures for a wide range of RPV steels in the unirradiated and irradiated conditions, a

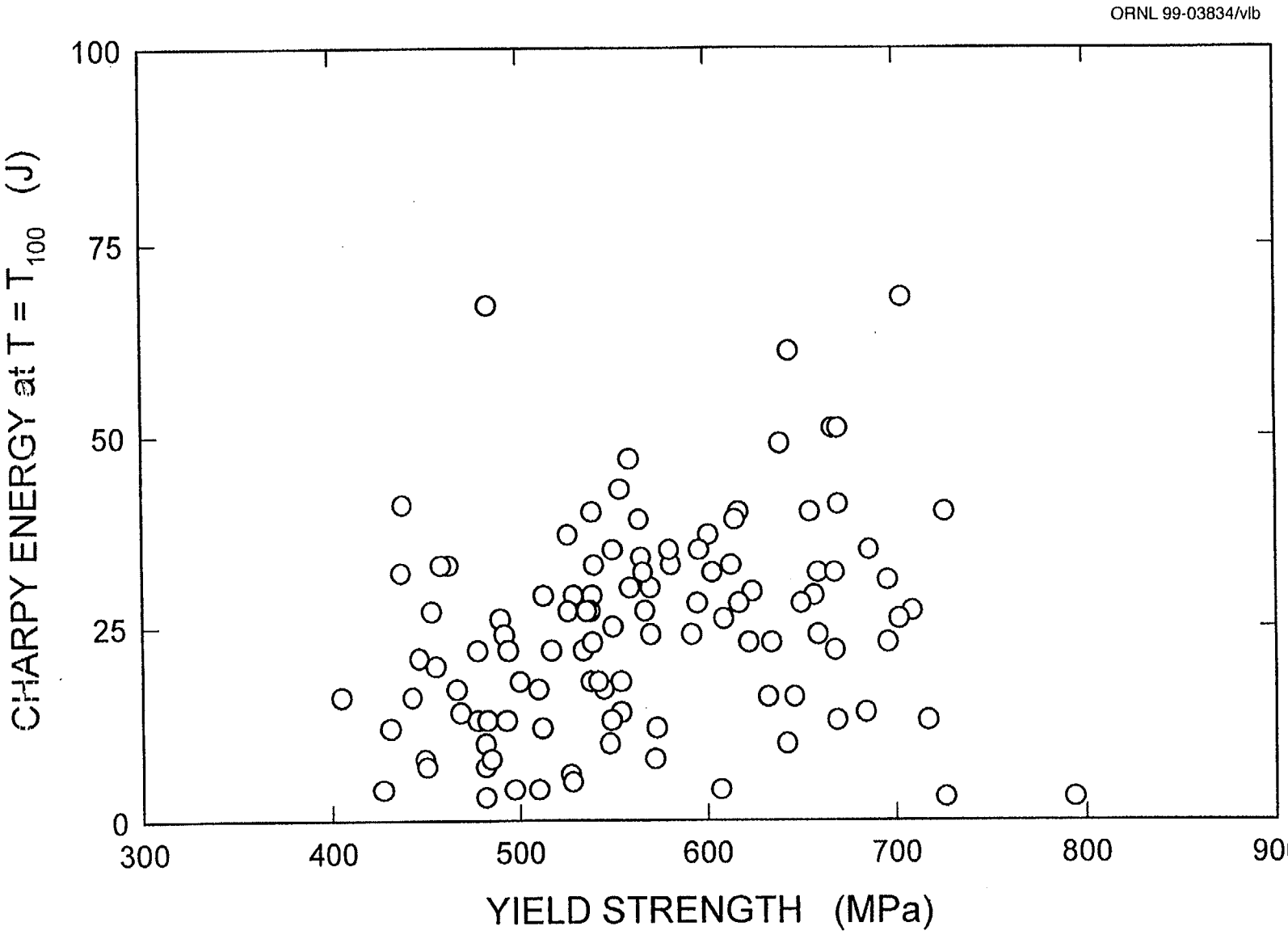

Fig. 10. Plot of Charpy energy at temperature $T = T_{100}$ as a function of yield strength.

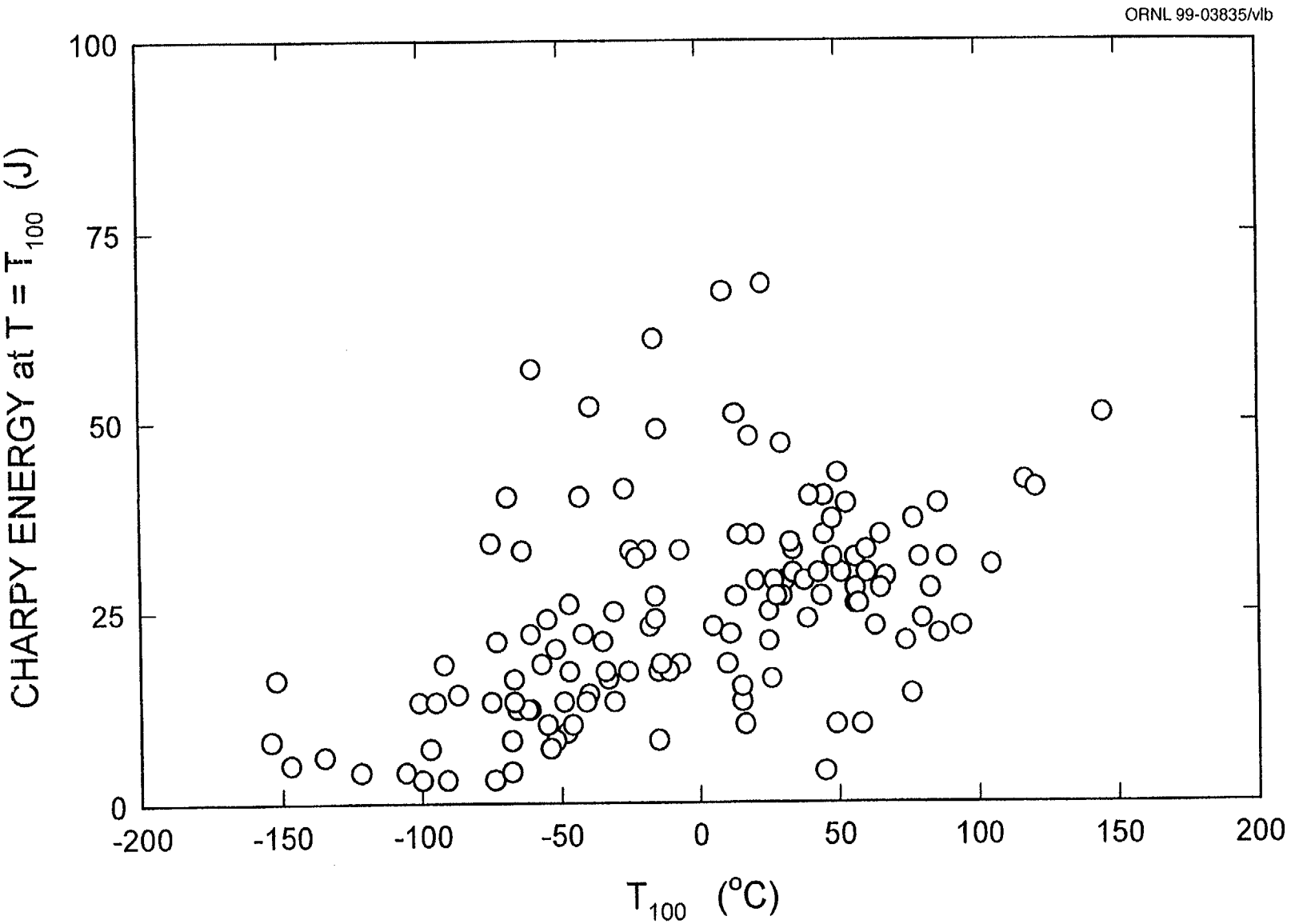

Fig. 11. Plot of Charpy energy at temperature $T = T_{100}$ as a function of the reference fracture toughness temperature.

logical initial step is to evaluate the relationship between the two transition temperatures, T_{100} and T_{41J}. Figure 12 illustrates such a relationship with all the toughness data with companion Charpy data available in the current database, as listed in Tables B.3 and B.4. A linear regression provides the following fit to data:

$$T_{100} = T_{41J} - 24°C \ , \qquad \sigma = 20°C \ , \tag{8}$$

with a relatively high correlation coefficient, $r^2 = 0.90$. The data encompass a very wide range of transition temperatures, providing good means for application of this correlation. For example, the reference fracture toughness temperature varies from about –150 to 150°C. Because many RPV steel Charpy T_{41J} data are available, and because data for irradiated materials are included, Eq. (8) could serve as a first approximation for the static fracture toughness reference temperature, including the irradiated condition; however, it must be noted that data scatter (±2 σ) is about ±40°C.

5. THE MASTER CURVE SHAPE

The shape of the master curve, Eq. (4), was established with both unirradiated and irradiated fracture toughness data [33]. Within the range of materials and exposure conditions examined, this suggests that irradiation does not necessarily alter the shape of the master curve of fracture toughness. Recent analyses [18, 20, 23] of irradiated fracture toughness data by the Weibull statistic/master curve approach supported that assumption, at least for radiation-induced shifts up to 100°C. This issue will be addressed in the following fashion relative to the database established in the present study. Expression for the master curve as in Eq. (4) is a regression fit to the median values of fracture toughness for several low-alloy steels that were thoroughly characterized such that the median K_{Jc} values (or K_o, which is mathematically interchangeable with $K_{Jc(med)}$) could be determined at a given test temperature. In the present study, the data were collected from different sources. In most cases only one or two specimens (especially irradiated ones) had been tested at each test temperature in an attempt to cover the transition region as widely as possible with a limited number of specimens. Consequently, as a post factum in most cases, it is not possible to determine $K^{1T}_{Jc(med)}$ in order to directly examine the fitting coefficients in Eq. (4). The statistical practice used in the present study, namely Eq. (5), already assumes that the data obey Eq. (4). Instead, the temperature for each individual fracture toughness data point has been normalized to the reference fracture toughness

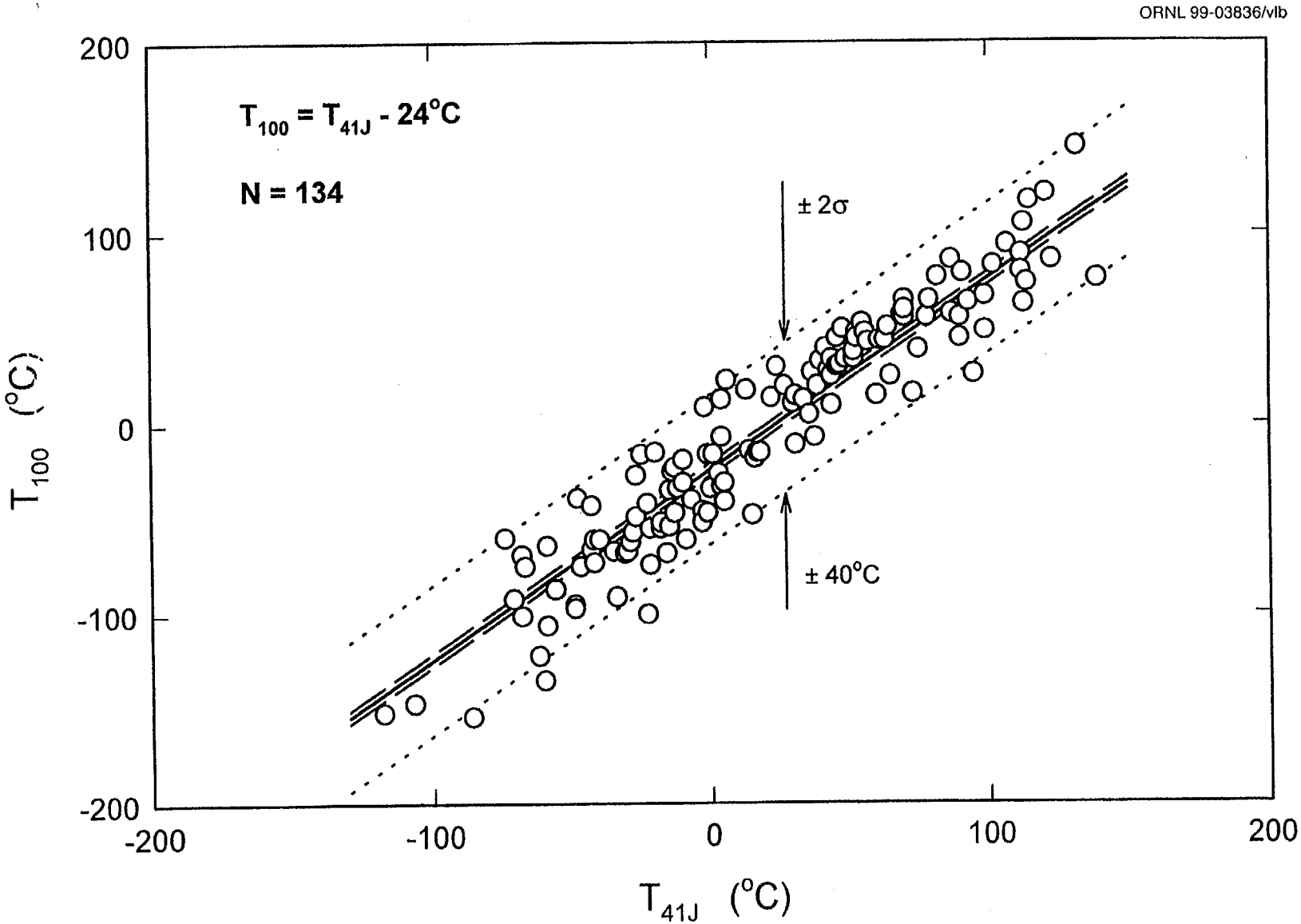

Fig. 12. Relationship between T_{100} and T_{41J} for both base and weld metals in the unirradiated and irradiated conditions.

transition temperature T_{100} for that particular data set, namely $T - T_{100}$, and plotted against the master curve and 3% and 97% tolerance bounds. Expressions for the tolerance bounds are used as given in Ref. [28]:

$$K_{Jc(3\%)} = 24.7 + 33.2 \exp[0.019(T - T_{100})] \ ,$$
$$K_{Jc(97\%)} = 35.3 + 106.8 \exp[0.019(T - T_{100})] \ . \quad (9)$$

Figure 13 summarizes all the unirradiated fracture toughness values in the current database. Each data point has been size-adjusted to its 1T equivalent in fracture toughness value by Eq. (3) and normalized by T_{100} in temperature. Data that do not satisfy the validity limit in Eq. (1) are not included in this plot. There are 653 valid unirradiated data points in the current database. Figure 14 is a similar plot for irradiated data. There are 851 valid irradiated data points in the current database. Visual observation supports an application of the master curve model to describe fracture toughness of RPV steel. Nevertheless, the valid unirradiated and irradiated data were fit to the following function:

$$K_{Jc} = \alpha + \beta \exp[\gamma(T - T_{100})] \ , \quad (10)$$

which has the same form as the master curve in Eq. (4) with α, β, and γ as fitting coefficients. The coefficient α represents the lower shelf in fracture toughness. However, for the present database, fracture toughness data have been mostly generated in the transition range rather than on the lower shelf. Because the purpose of this exercise was to examine the stability of the shape of the master curve in the transition region, it was decided to fix the coefficient α at 30 as it is in Eq. (4). The results are summarized in Table 1.

Table 1. Fitting coefficients of Eq. (10) with α fixed to 30

Condition		β		γ		r^2
Unirradiated	Fit	72.89		0.01669		0.797
	±95% CI	69.98	75.80	0.0160	0.0174	
Irradiated	Fit	68.13		0.01737		0.761
	±95% CI	65.98	70.28	0.0166	0.0181	

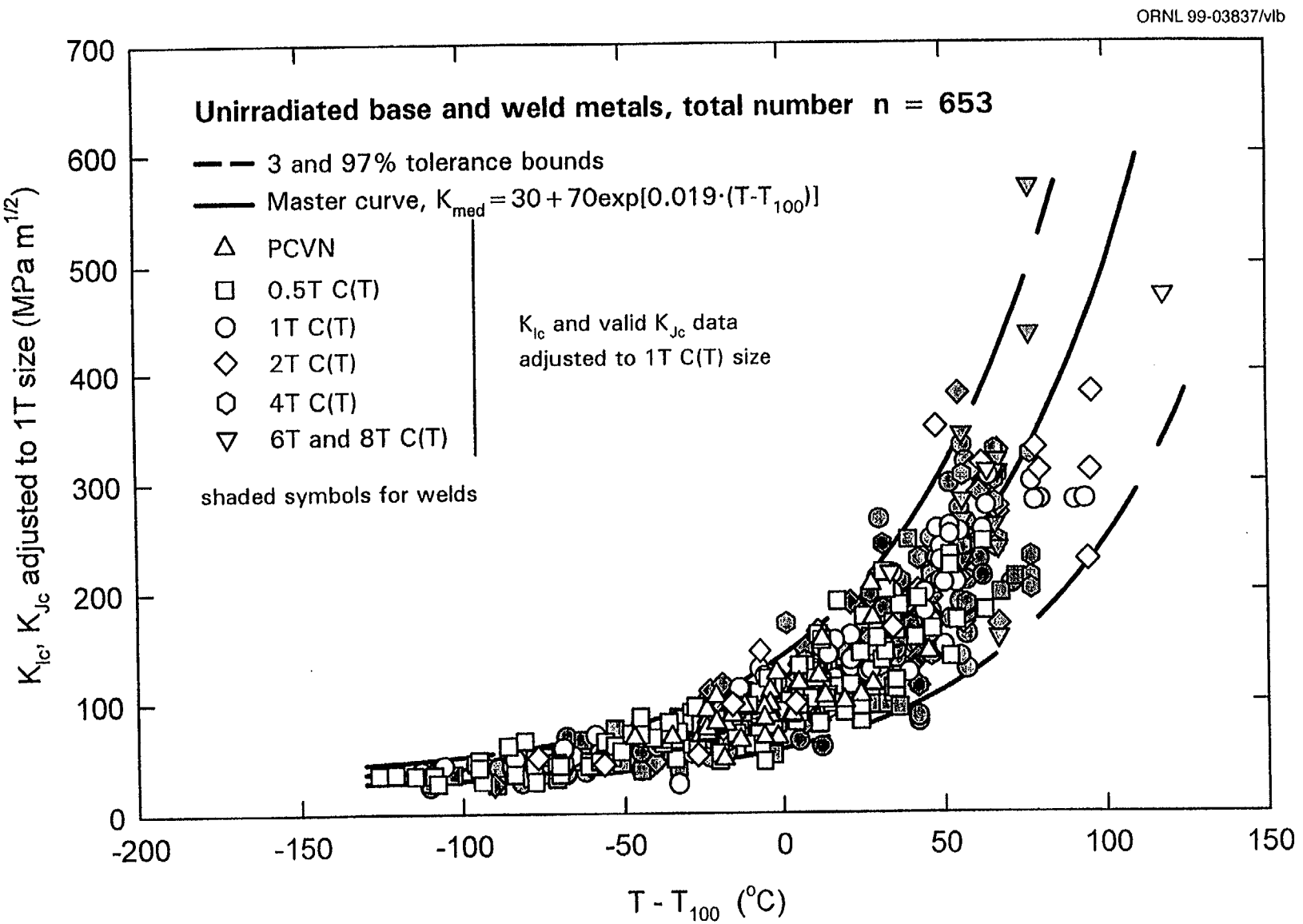

Fig. 13. The unirradiated fracture toughness data size-adjusted to 1T equivalence and normalized to T_{100} with the master curve and 3 and 97% tolerance bounds. Valid data only.

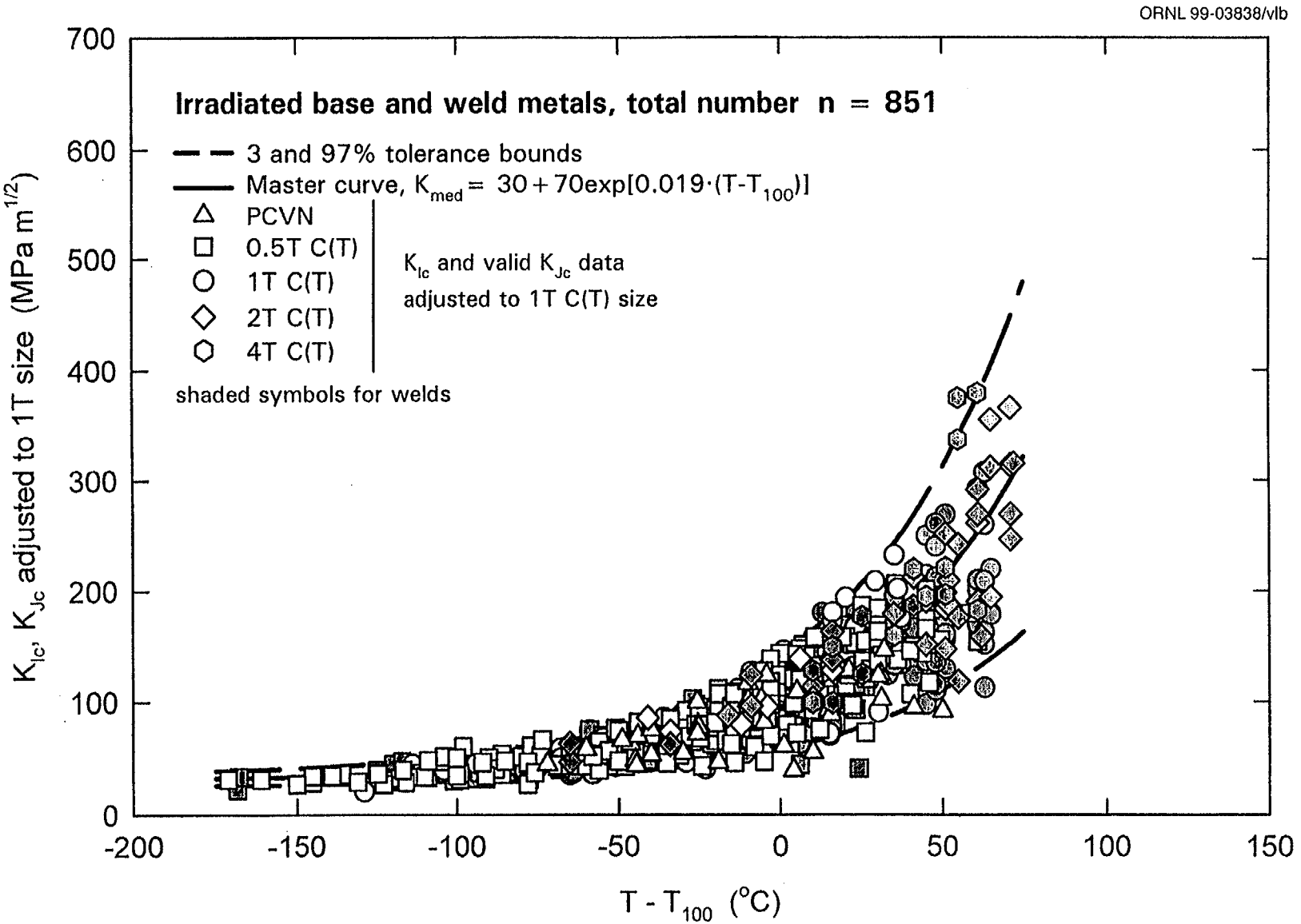

Fig. 14. The irradiated fracture toughness data size-adjusted to 1T equivalence and normalized to T_{100} with the master curve and 3 and 97% tolerance bounds. Valid data only.

As expected, data fit very well to the exponential function (see r^2 column). The coefficients β and γ of the unirradiated and irradiated data are very close to each other with some overlap in 95% confidence intervals for both coefficients. Because the value of 70 from the master curve expression is within the 95% confidence interval for both the unirradiated and irradiated data, it was decided to fix the coefficient β to 70 and perform the fit by γ only. That method linearizes the fitting procedure and simplifies observations of possible curve-shape changes. The result of that analysis is presented in Table 2.

Table 2. Fitting coefficients of Eq. (10) with α fixed to 30 and β to 70

Condition		γ		r^2
Unirradiated	Fit	0.01725		0.795
	±95% CI	0.0169	0.0176	
Irradiated	Fit	0.01691		0.760
	±95% CI	0.0164	0.0174	

Analysis shows that with 95% confidence both the unirradiated and irradiated fracture toughness data have the same temperature dependence in the transition range. For both conditions γ is equal to 0.017. The value of γ in Table 2 is given with additional digits for illustration purposes only. It illustrates that, although with 95% confidence both conditions provide about the same fitting coefficient, the value of γ coefficient for the irradiated condition is slightly lower than the value for unirradiated data. That observation leads to consideration of some special cases in addition to the overall database. Based on these concerns, data were separated in somewhat smaller subgroups. Selection of the materials has been based on the following criteria.

- Highly embrittled materials. For this group, the criterion for data selection was that either the Charpy shift was greater than 100°C or increase of yield strength was higher than 100 MPa (see Fig. 15).
- High Charpy 41-J transition temperature. Any material with absolute value of T_{41J} above 100°C was included in this group (see Fig. 16).
- Low upper-shelf materials. Any material with USE below 100 J was included in this group (see Fig. 17).

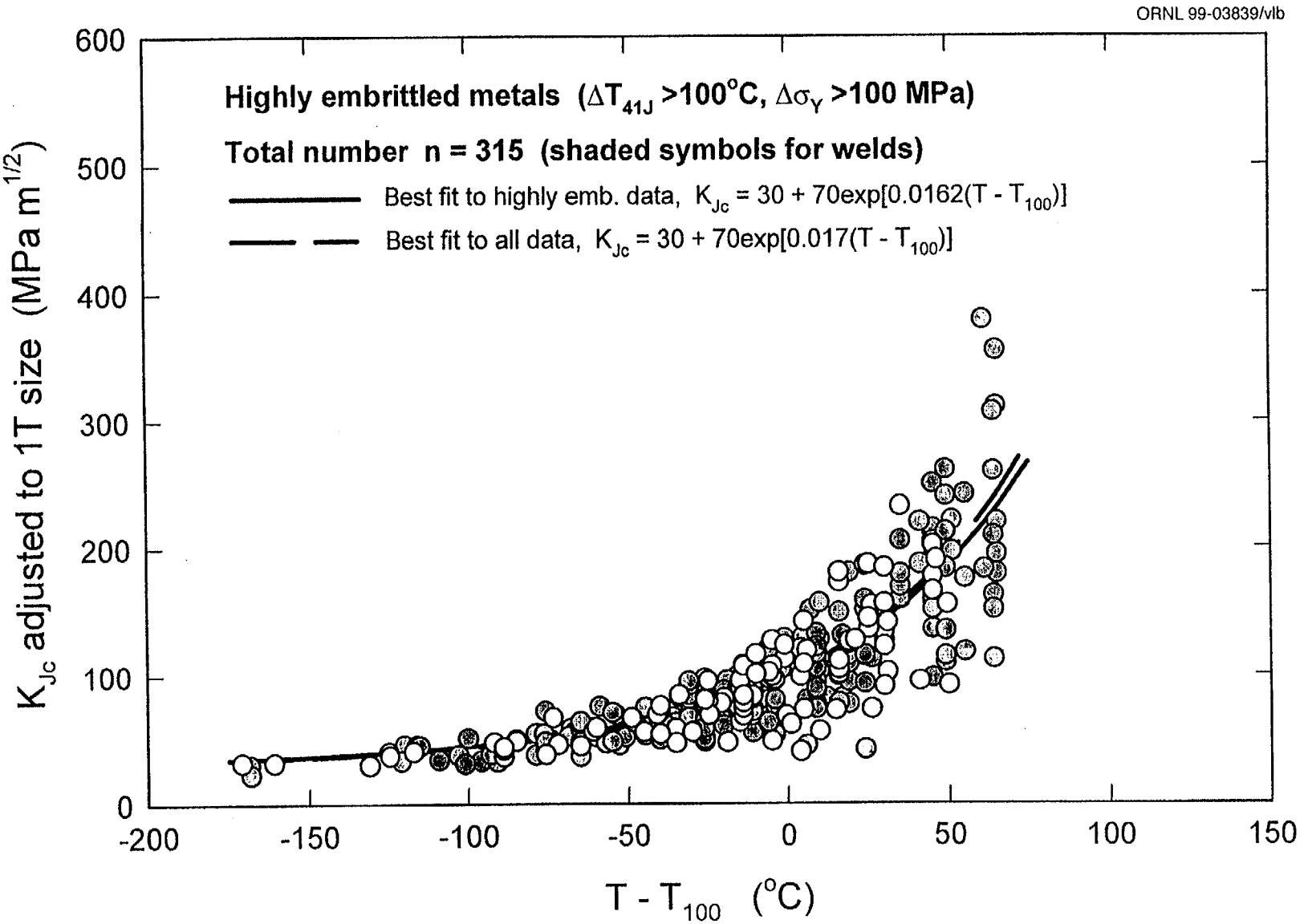

Fig. 15. Fracture toughness data for highly embrittled materials with the best-fit equations.

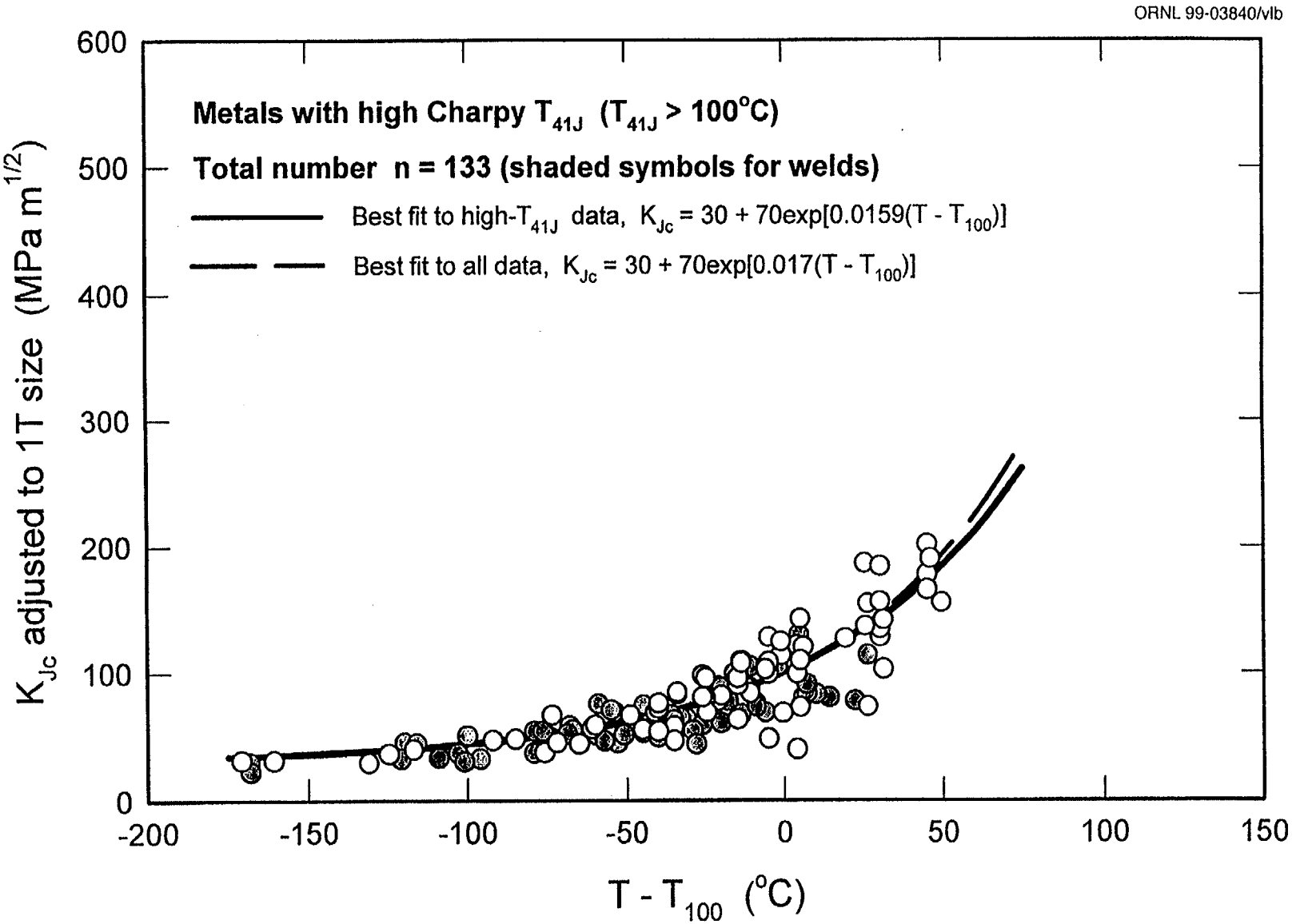

Fig. 16. Fracture toughness data for materials with T_{41J} above 100°C with the best-fit equations.

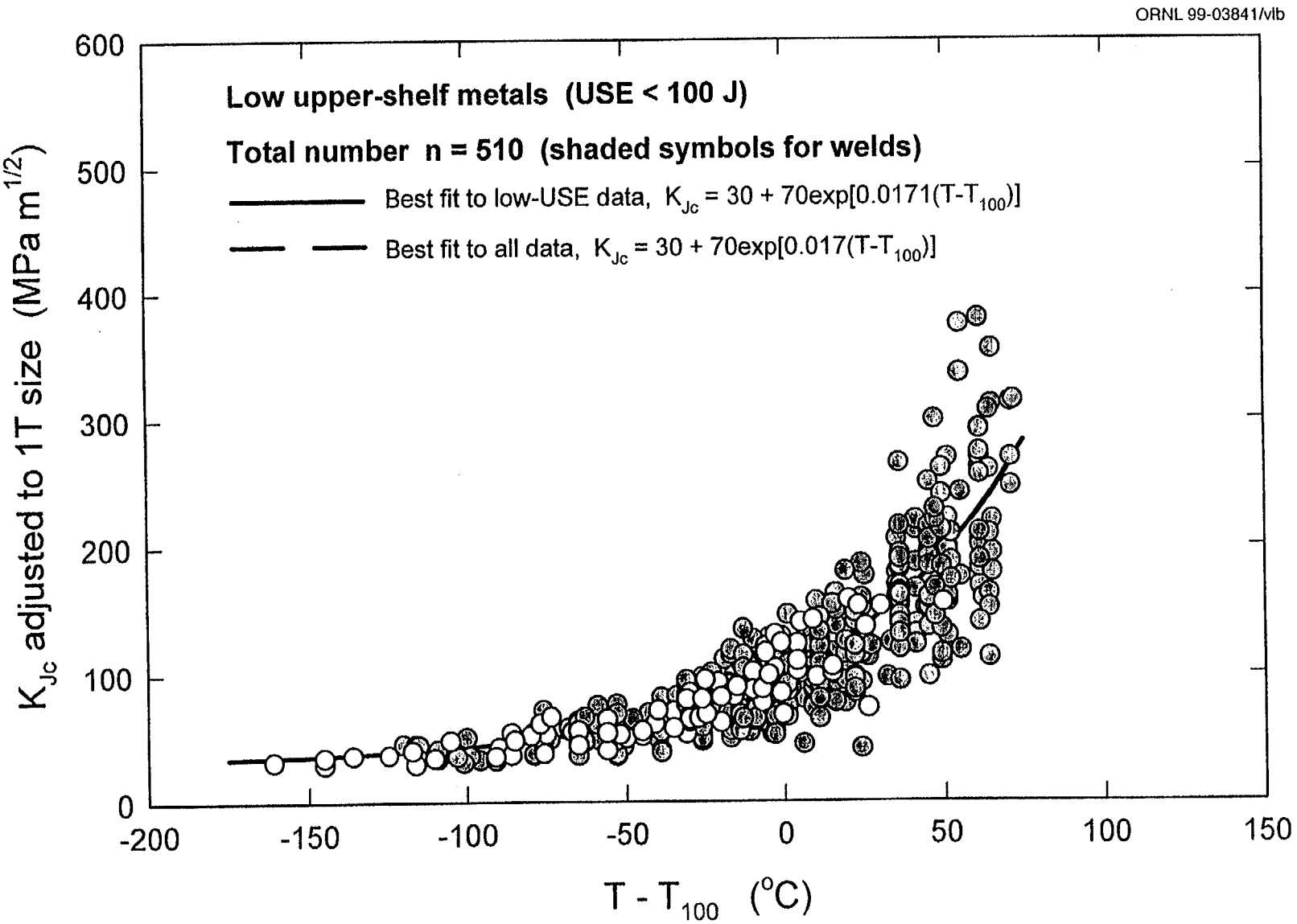

Fig. 17. **Fracture toughness data for materials with Charpy USE below 100 J with the best-fit equations.**

Each group was fitted separately; the fitting coefficient γ and 95% confidence intervals for each group are summarized in Table 3.

Table 3. Fitting coefficient γ with 95% confidence intervals for different groups of materials

Condition		γ		Points	r^2
Irradiated	Fit	0.0169		851	0.76
	±95% CI	0.0164	0.0174		
Highly embrittled	Fit	0.0162		315	0.72
	±95% CI	0.0153	0.0171		
High T_{41J}	Fit	0.0159		133	0.76
	±95% CI	0.0143	0.0175		
Low upper-shelf Charpy energy	Fit	0.0171		510	0.75
	±95% CI	0.0165	0.0177		

The value of 0.017 is within the 95% confidence intervals of all groups considered. However, low values of γ for highly embrittled and, especially, for materials with Charpy T_{41J} above 100°C raise a concern for the fracture toughness curve, maintaining the same shape after a high degree of embrittlement. (All materials with Charpy T_{41J} above 100°C are in the highly embrittled category also.) A simple null-hypothesis test indicates that the γ coefficients (i.e., the curve slope parameter) for the unirradiated and highly embrittled data are different at the 95% confidence level, although a more rigorous statistical evaluation needs to performed. At least, caution needs to be taken in extrapolating the results of analysis of the current database to end-of-life conditions. The materials in the current database with low upper-shelf energy did not reveal any deviation in the master curve shape (by means of γ) compared with the unirradiated and overall irradiated data fits.

A remark is needed regarding the difference between the current fitted value of γ (0.017) and the one in the master curve Eq. (4) (0.019). The master curve expression is a fit to the median fracture toughness values. In the present study the fit has been performed on valid data only. Invalid data cannot be included in such a fit, although they have been included in the determination of the T_{100} values [see Eq. (5)]. In other words, γ in the present study serves as a best-fit coefficient to the valid data only, while the master curve equation is a best fit to the median values only. Thus, the observed small difference does not necessarily challenge the master curve expression.

The present analysis supports the superiority of the master curve methodology for fracture toughness characterization of RPV materials in the transition range. Nevertheless, a few issues remain regarding application of this methodology to the structural integrity of a vessel. One of the issues is size effects. It is clear now that the master curve is a well-established concept, but only for 1T size equivalence. A link to a vessel is not clear right now, and establishment of such a link is outside the scope of this study; however, some discussion of this subject is offered in the light of the obtained results. From a structural-integrity point of view, the master curve itself is not an issue; rather, the lower tolerance bounds from the methodology are the main interest. One way to approach this issue is addressed in Fig. 5(b). Indeed, the lower tolerance bounds from the 1T master curve concept are plotted against the ASME K_{Ic} database (measured data are shown), which is a collection of valid K_{Ic} data obtained by testing very large specimens [up to 11T C(T)]. It is shown in Fig. 5(b) that the tolerance bounds to the 1T size master curve serve as lower tolerance bounds relatively well, even for unadjusted data. The low sensitivity of lower tolerance bounds to statistical size effects is illustrated in Fig. 6. The same approach is used to plot all the unirradiated (Fig. 18) and irradiated (Fig. 19) unadjusted data against the 3% tolerance bound from the 1T master curve methodology. Selection of 3% for the lower tolerance bound is, to some degree, an arbitrary decision, but the following discussion suggests a basis for that choice. As it was shown in Sect. 3, the ASME K_{Ic} curve is indeed the lower bound to fracture toughness data of one material: HSST Plate 02. As it can be seen in Fig. 7, the 3% tolerance bound for HSST Plate 02 comes closer to representing the ASME K_{Ic} curve than does the 5% or 1% tolerance bound.

As in the case with the ASME K_{Ic} database, the 3% tolerance bound provides a very reasonable statistical bound representation of a large database, even of size-unadjusted fracture toughness data for RPV steels in the unirradiated (Fig. 18) and irradiated (Fig. 19) conditions.

6. CORRELATIONS BETWEEN STATIC FRACTURE TOUGHNESS AND CHARPY IMPACT CURVE SHIFTS

To compare the shifts of fracture toughness and Charpy curves caused by irradiation, data sets of irradiated materials were grouped so that average values of neutron fluence for Charpy and fracture toughness data sets would match each other. Although the values for neutron fluence were not always identical, the differences can be viewed as negligible. This argument is supported by the representation of the fluence factor trend shown in RG 1.99 [3], especially because such differences were mostly where the fluence factor starts to follow a trend toward saturation for neutron fluences greater than 1×10^{19} n/cm^2 (E > 1 MeV).

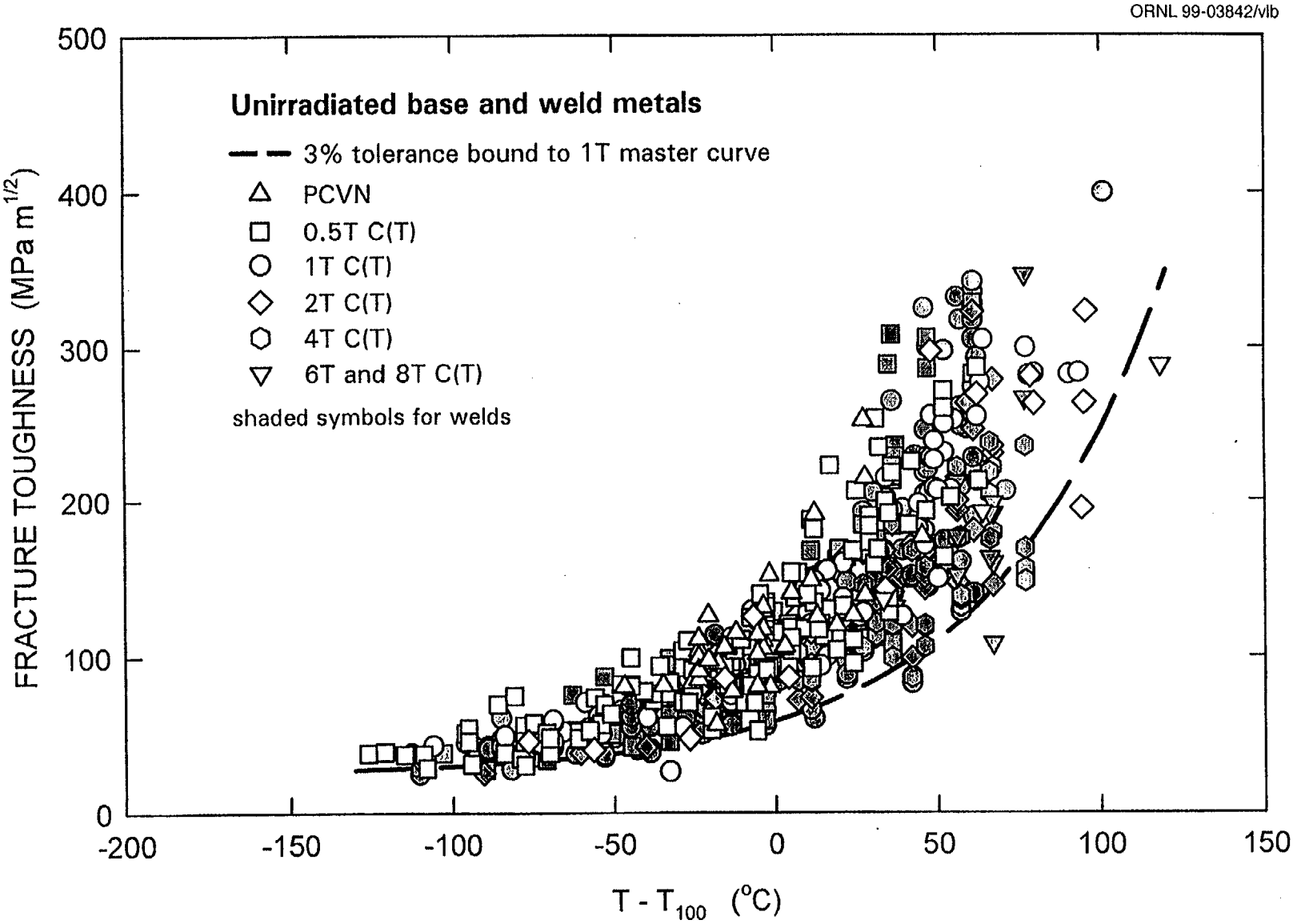

Fig. 18. **Unirradiated (valid and invalid) fracture toughness data as measured, normalized to T_{100} with the 3% tolerance bound to the master curve.**

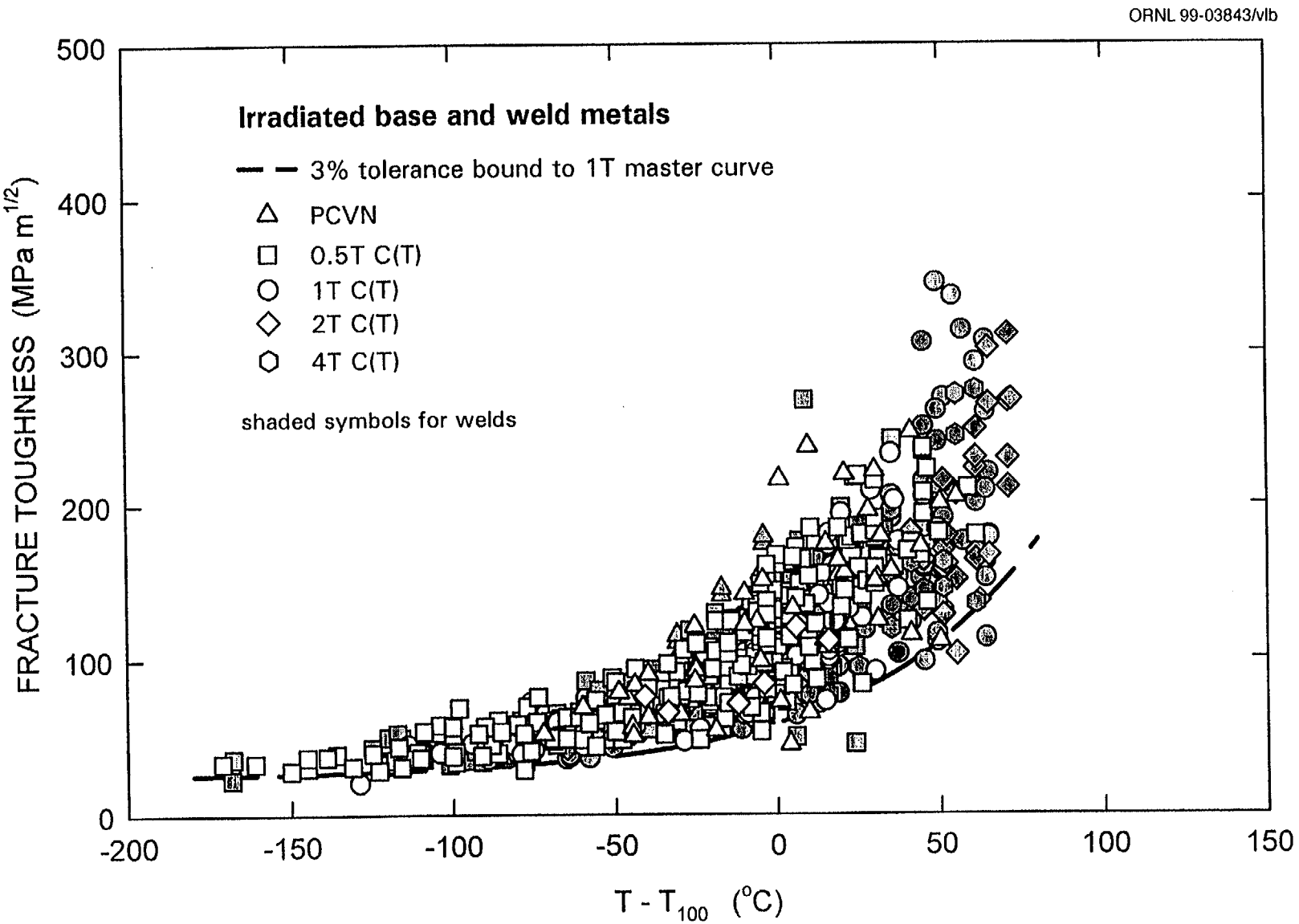

Fig. 19. **Irradiated (valid and invalid) fracture toughness data as measured, normalized to T_{100} with the 3% tolerance bound to the master curve.**

RG 1.99 recognizes that the radiation-induced response for base metals is different from that for weld metals. Therefore, the data were separated in two material groups, base metals and weld metals, based on RG 1.99, in which base and weld metals have different chemistry factor representation. Although it is not a straightforward link to conclude that a relationship between shifts of Charpy impact and static fracture toughness transition temperatures should be different for base metal and weld metal, one may argue the fact that the chemical factor depends on the product form and suggests, therefore, that different properties of RPV steels are likely to respond differently to radiation damage, depending on the product form. Thus, a property derived from the static test of fracture-initiation toughness may respond differently from a property derived from the dynamic impact test in which total absorbed energy at fracture is measured.

Tables B.3 and B.4 in Appendix B summarize shifts of fracture toughness T_{100} and Charpy impact transition temperatures determined at different indices for base metals and weld metals, respectively.

Weld Metal

There are 42 data points for weld metal. Figure 20(a) presents a plot of the fracture toughness T_{100} versus Charpy 41-J shifts. A linear regression (y = ax) gives an exact 1:1 fit:

$$\Delta T_{100} = 1.0 \Delta T_{41J} \quad , \tag{11}$$

where ΔT_{100} is the shift of the reference fracture toughness temperature and ΔT_{41J} is the shift of the Charpy transition temperature at energy level 41 J. The correlation coefficient (r^2) is 0.89, a relatively high value. The dashed and dotted lines are 95% confidence intervals on the mean and predicted values, respectively. The 95% confidence interval on the mean is relatively small. However, the scatter of data reveal an interval on the predicted value of about ±26°C at 95% confidence.

Base Metal

There are 47 data points for the base metal. Most of these data are for plates, A533 grade B and A302 grade B; there are only eight data points for forgings. Figure 20(b) presents a plot of the fracture

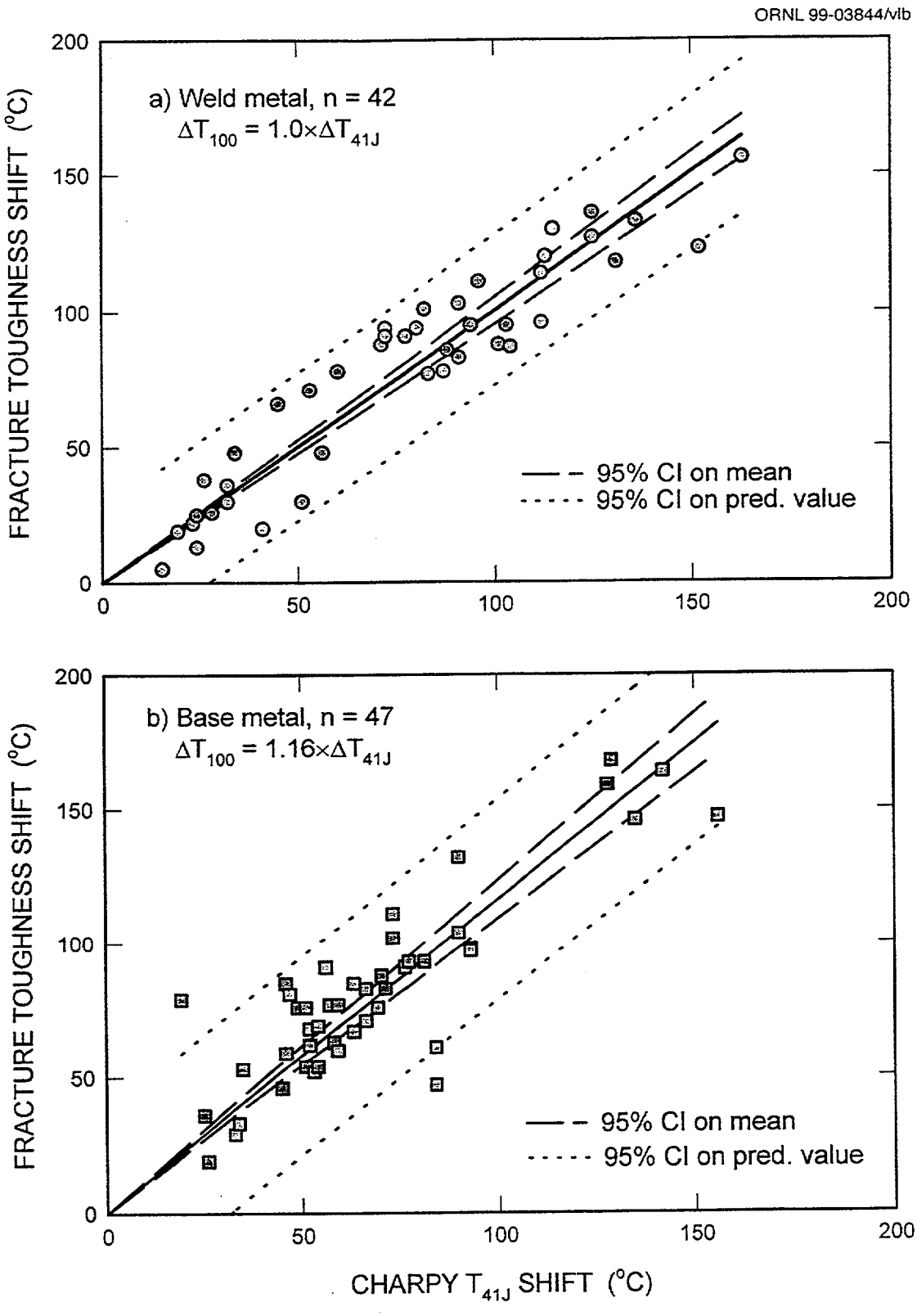

Fig. 20. **Correlation between fracture toughness T_{100} and Charpy T_{41J} shifts for (a) weld and (b) base metal.**

toughness T_{100} vs Charpy 41-J transition temperature shifts for base metal. As in the case with weld metals, a linear regression analysis has been performed and the resulting fit is as follows:

$$\Delta T_{100} = 1.16 \Delta T_{41J} \tag{12}$$

with a correlation coefficient (r^2) of 0.72. Thus, the results of the current analyses show that, on average, the Charpy 41-J shift underestimates the fracture toughness shift for base metal. The scatter of data (±95% confidence interval) is higher for base metal (±36°C) than for weld metal (±26°C). Figure 21 compares the fit to all base metal data (mean and 95% confidence intervals) with data in L-T [Fig. 21(a)] and T-L [Fig. 21(b)] orientations only. A visual comparison does not reveal any significant difference in trend depending on orientation of specimens.

In addition to the linear regression mentioned above, the data were fitted by commercial software, "TableCurve 2D for Windows." TableCurve 2D automatically performs curve-fitting and ranking of up to 3456 preinstalled candidate equations. The routine was set up to rank equations based on the correlation coefficient (r^2) value. Having 3456 equations to compete with, the simple linear equation $y = ax$ was not the highest-ranked equation in the exercise, but it was always in the top 20. All equations but one that provided a better fit to the data than $y = ax$ have very complicated expressions, and it is difficult to justify logically the use of most of them for a correlation between fracture toughness and Charpy shifts. However, one fitting function seems to be logically acceptable and provides a better fit to the data than the linear regression equation. This function, a power law equation, gave the following fit for weld metal:

$$\Delta T_{100} = 1.77 \left(\Delta T_{41J}\right)^{0.88} \quad . \tag{13}$$

It gave the following fit for base metal:

$$\Delta T_{100} = 2.35 \left(\Delta T_{41J}\right)^{0.84} \quad . \tag{14}$$

Such a fit suggests that in the earlier stage of embrittlement (shifts up to about 120°C), on average, the rate of fracture toughness shift is higher than the rate of embrittlement measured by Charpy shift (see Fig. 22). As embrittlement progresses, the Charpy shift would catch up with the fracture

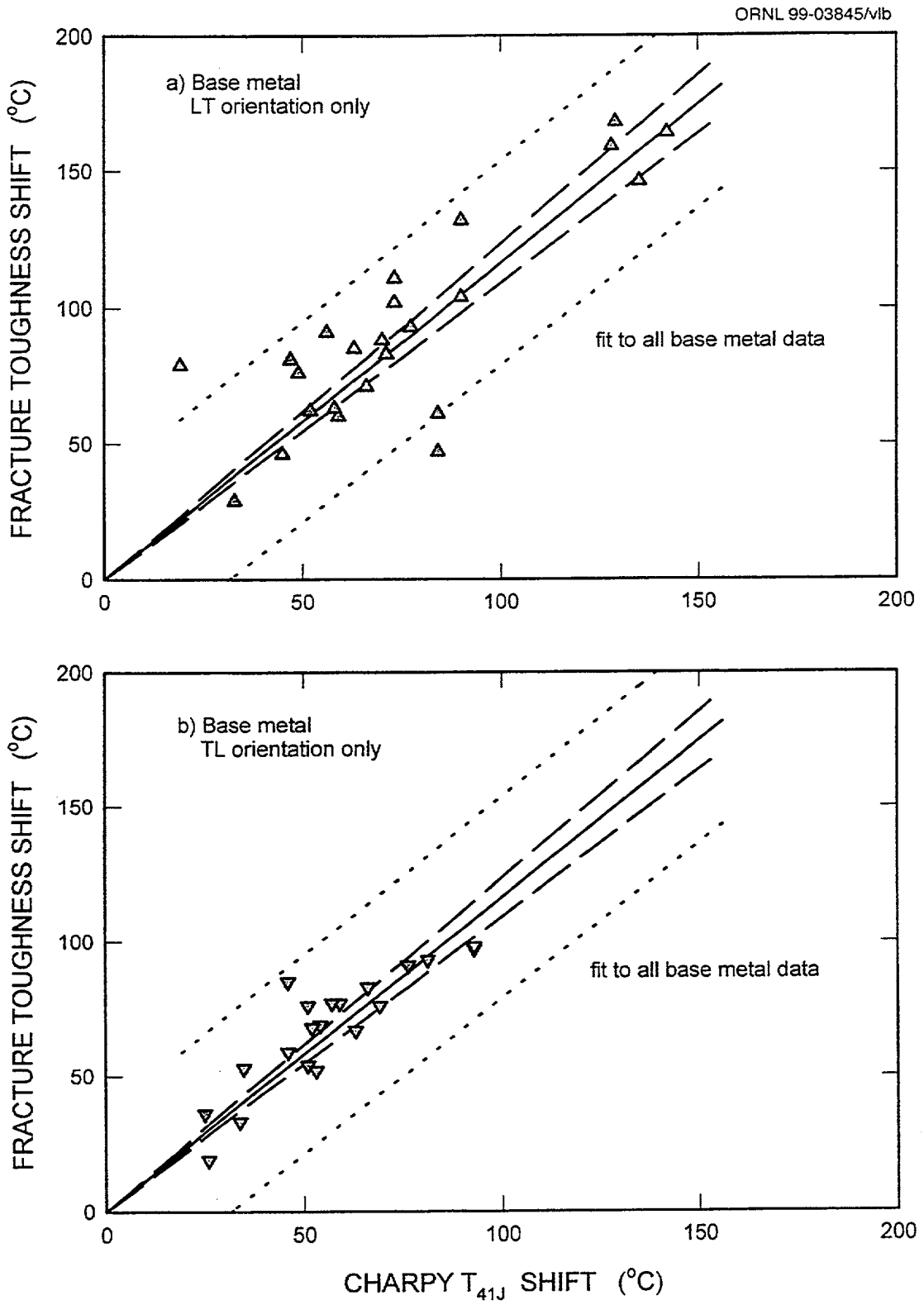

Fig. 21. **Correlation between fracture toughness T_{100} and Charpy T_{41J} shifts for base metal data in (a) L-T orientation and (b) T-L orientation.**

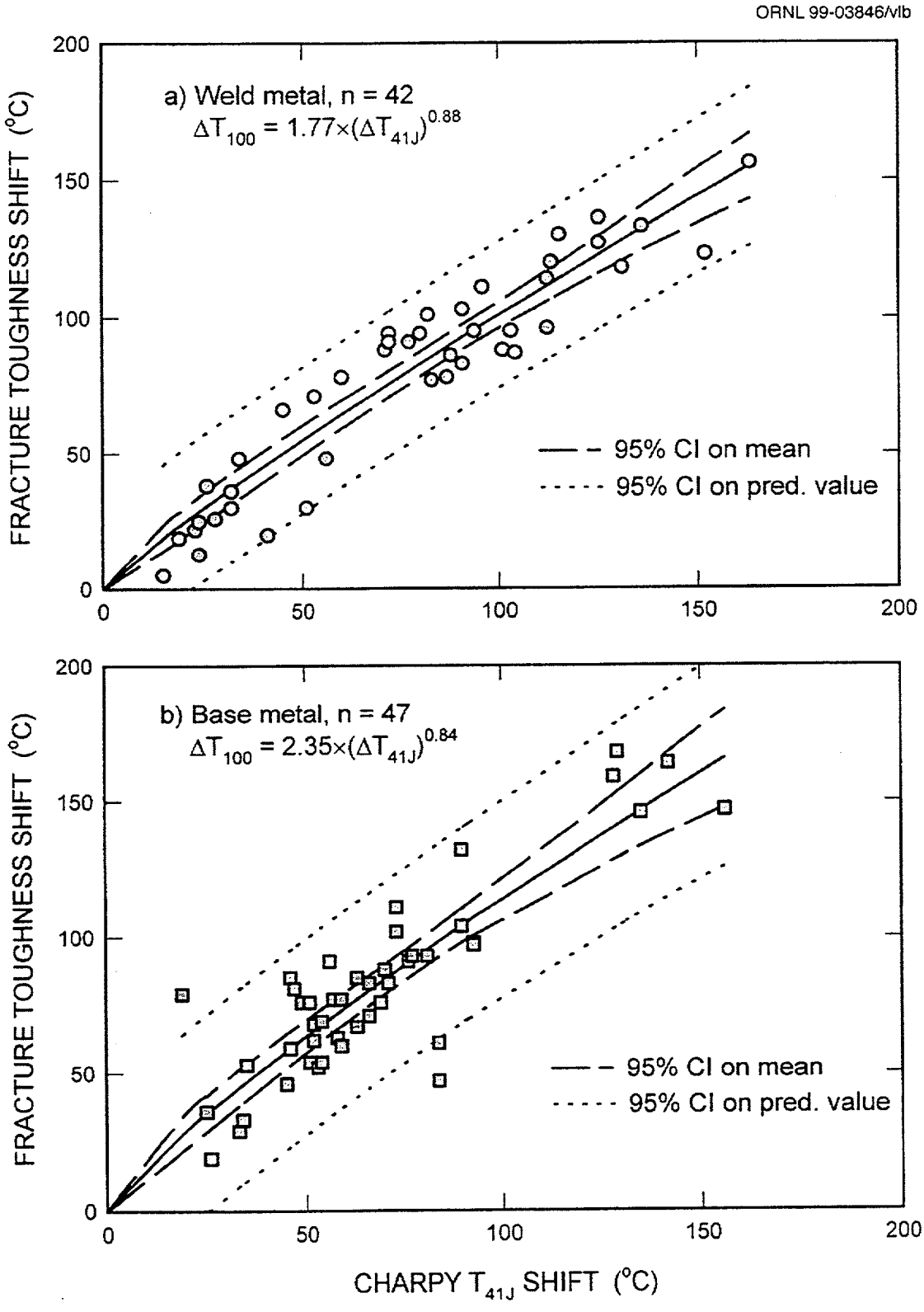

Fig. 22. Power law fit to fracture toughness and Charpy shifts for (a) weld and (b) base metals.

toughness shift and, theoretically, material might degrade to the point where the Charpy USE could decrease below 41 J, making the shift at 41 J infinite.

The weld metal and base metal data were also combined and analyzed as one data set (see Fig. 23). The coefficient of proportionality is equal to 1.08 (the average between weld metal and base metal fits) with $r^2 = 0.78$ [see Fig. 23(a)]. The 95% confidence interval remained about the same as for the fit to the base metal only. The power law equation gave the following fit [see Fig. 23(b)]:

$$\Delta T_{100} = 2.36\left(\Delta T_{41J}\right)^{0.83} \qquad (r^2 = 0.80) \tag{15}$$

with 95% confidence intervals on the predicted value of about ±32°C.

In an effort to find a better correlation (reduced uncertainty) between Charpy impact energy and fracture toughness shifts for prediction of the fracture toughness shift of base metal, other Charpy energy criteria were compared with ΔT_{100}. Charpy transition temperature shifts were determined (1) at 68 J (Fig. 24); (2) at the middle of transition range, T_{MT} from Eq. (6) (Fig. 25); and (3) at adjusted 28 J, 28*J, (Fig. 26). In the third case, an adjustment consists of multiplying the energy level 28 J for determination of irradiated transition temperature by the ratio of unirradiated to irradiated upper-shelf energies and then subtracting the transition temperature for the unirradiated condition at 28 J (see Ref. [33]). Comparisons of ΔT_{100} with Charpy shifts at various energy levels do not show any significant improvements in correlation compared with correlation with ΔT_{41J} in terms of reduced scatter or r^2 value.

In addition to different energy levels, two other commonly used indices were applied to measure shifts of Charpy transition temperature when such data were available for analysis, namely 0.9 mm of lateral expansion ($T_{0.9mm}$) and 50% of shear fracture ($T_{50\%}$). Figures 27 and 28 present correlations between shifts of T_{100} and Charpy lateral expansion and percent shear fracture transition temperatures, respectively. As in the case with different energy criteria, neither the lateral expansion nor percent shear fracture transition temperatures have improved correlation with the fracture toughness shift compared with the Charpy 41 J shift. It should be noted however, that lateral expansion and, especially, percent shear fracture data did not always accompany Charpy energy data.

Thus, the Charpy transition temperature shift measured at 41 J appears to be the best criterion to correlate with the fracture toughness shift based on analysis of the current database in comparison

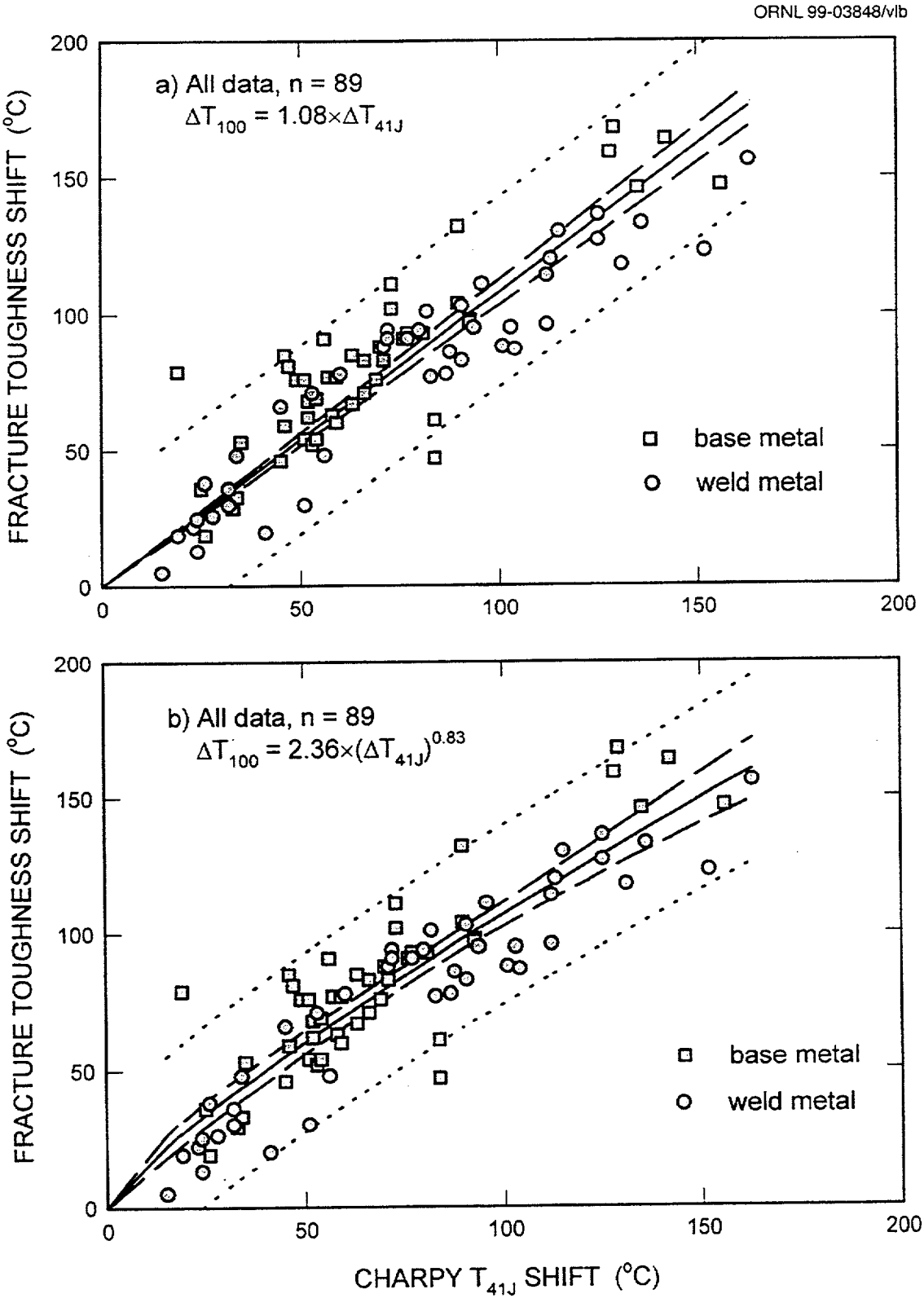

Fig. 23. Linear (a) and power law (b) fit to all the data.

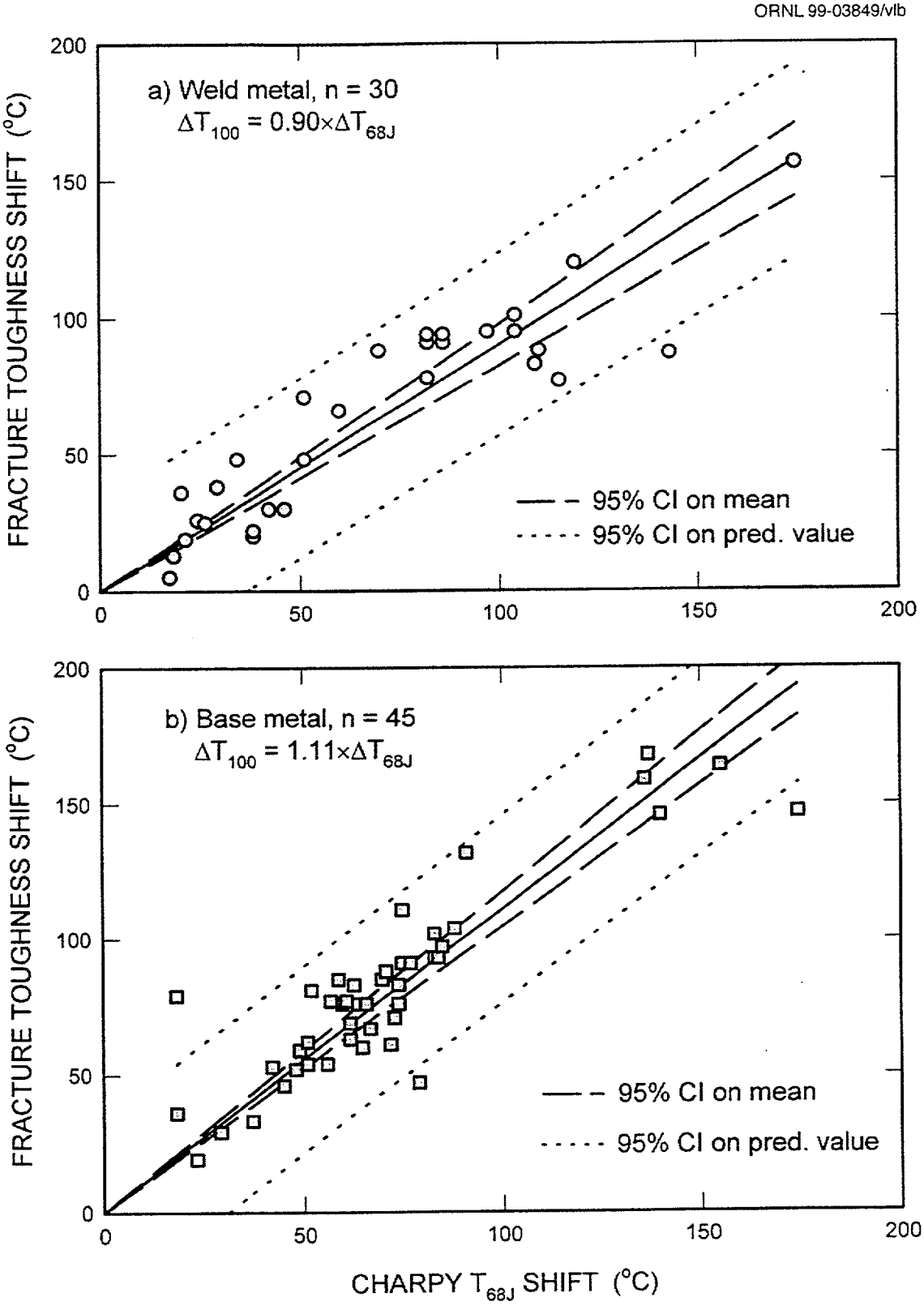

Fig. 24. **Correlation between fracture toughness T_{100} and Charpy T_{68J} shifts for (a) weld and (b) base metals.**

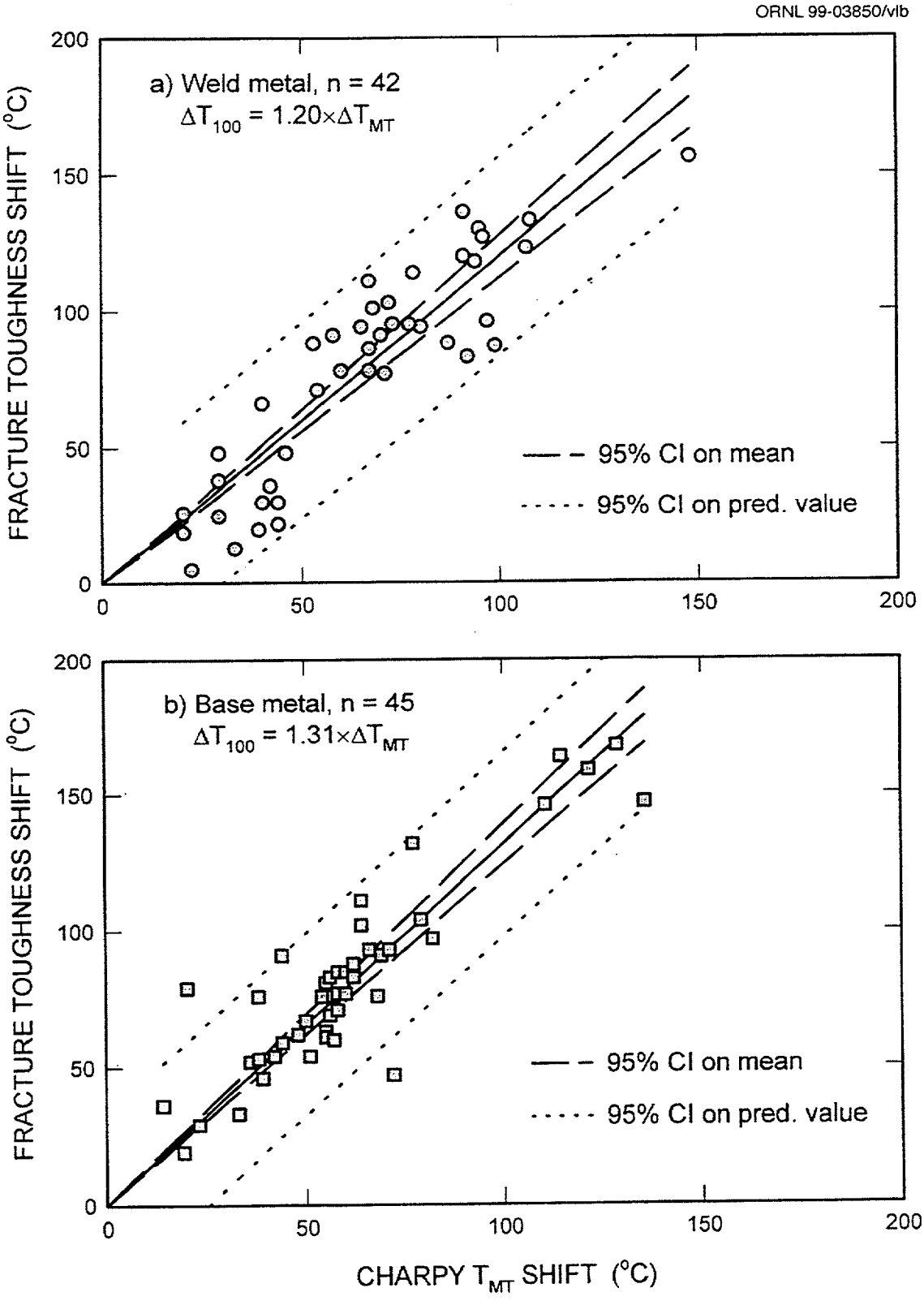

Fig. 25. Correlation between fracture toughness T_{100} and Charpy T_{MT} shifts for (a) weld and (b) base metals.

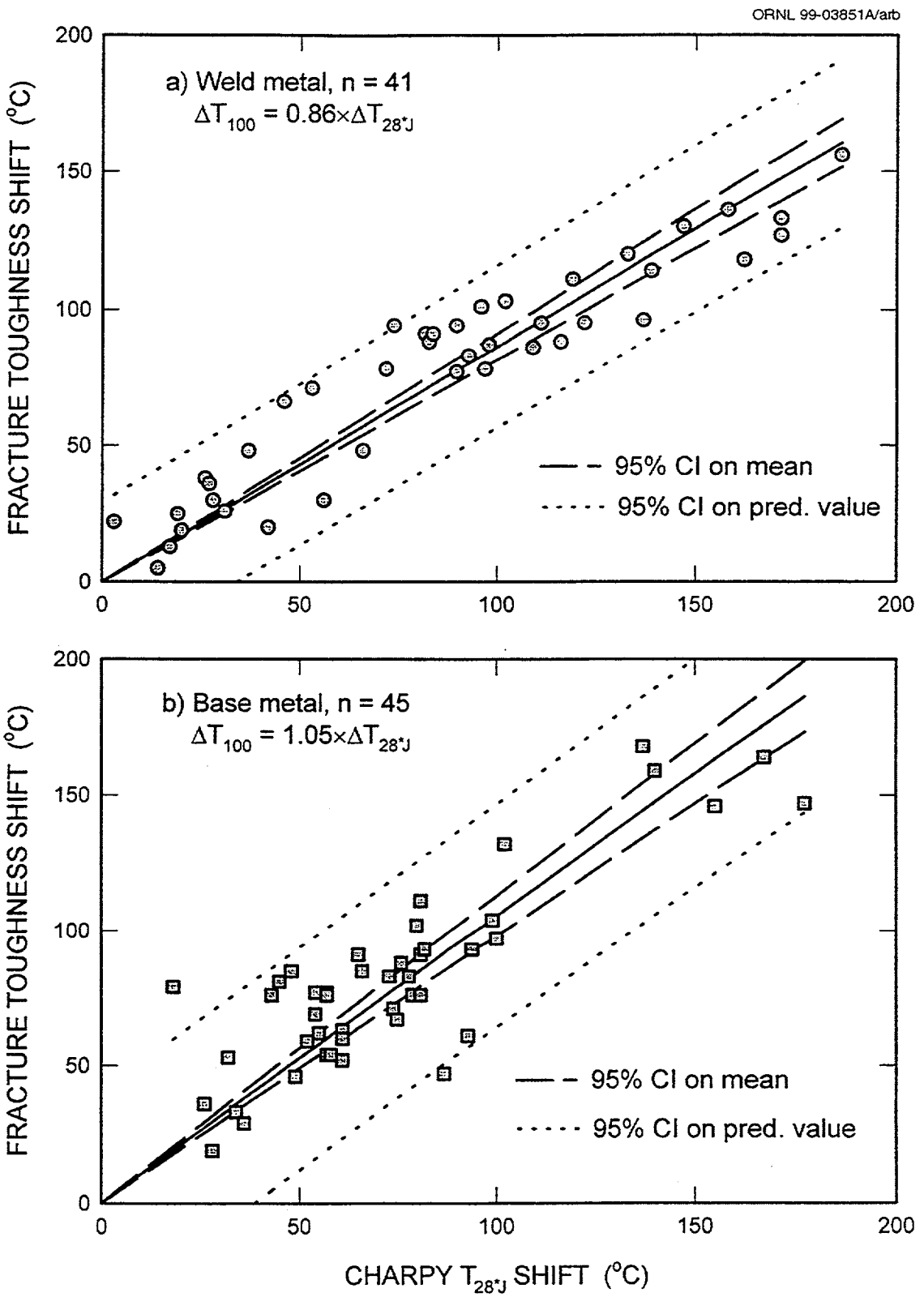

Fig. 26. **Correlation between fracture toughness T_{100} and Charpy $T_{28°J}$ shifts for (a) weld and (b) base metals.**

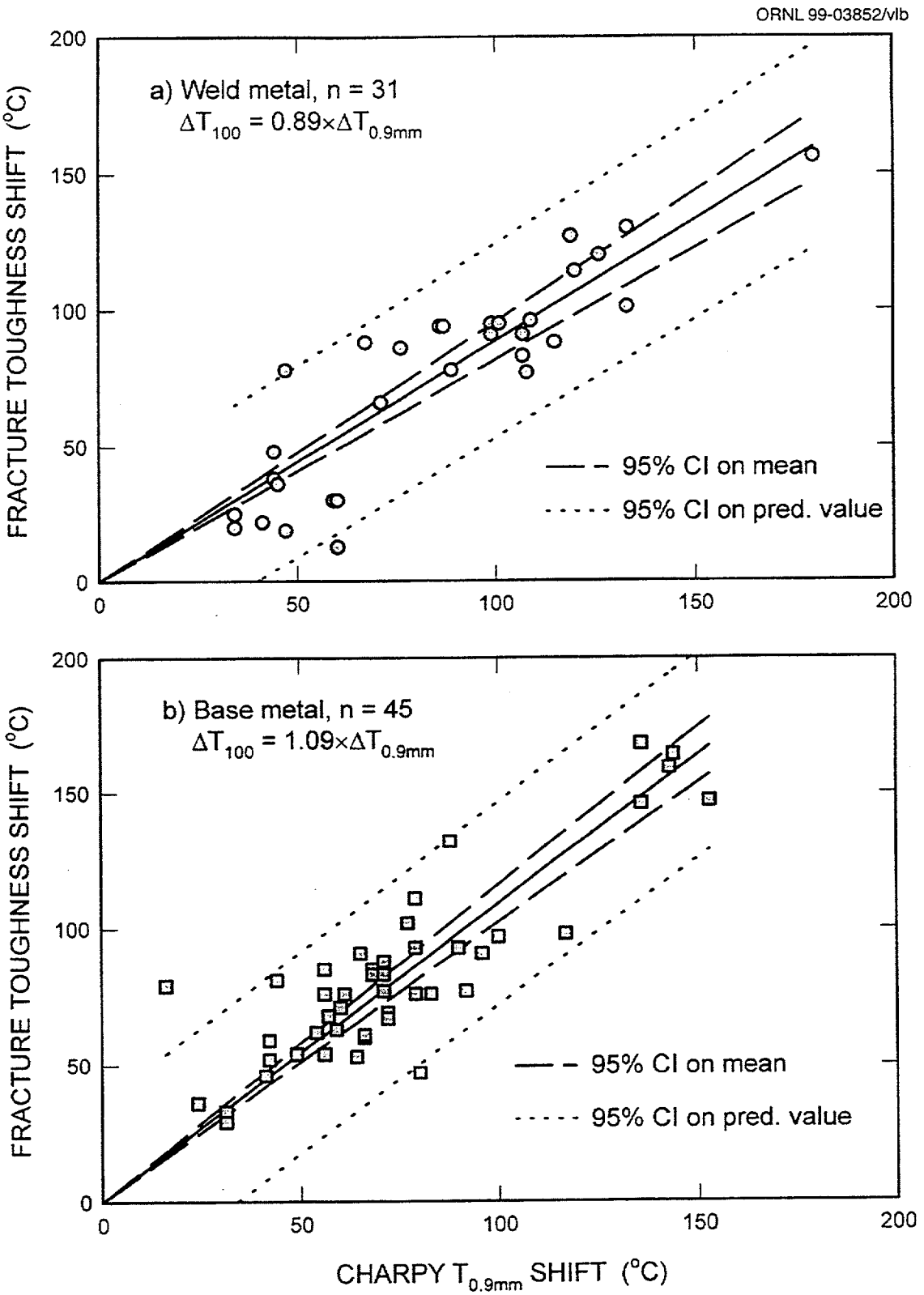

Fig. 27. Correlation between fracture toughness T_{100} and Charpy $T_{0.9mm}$ shifts for (a) weld and (b) base metals.

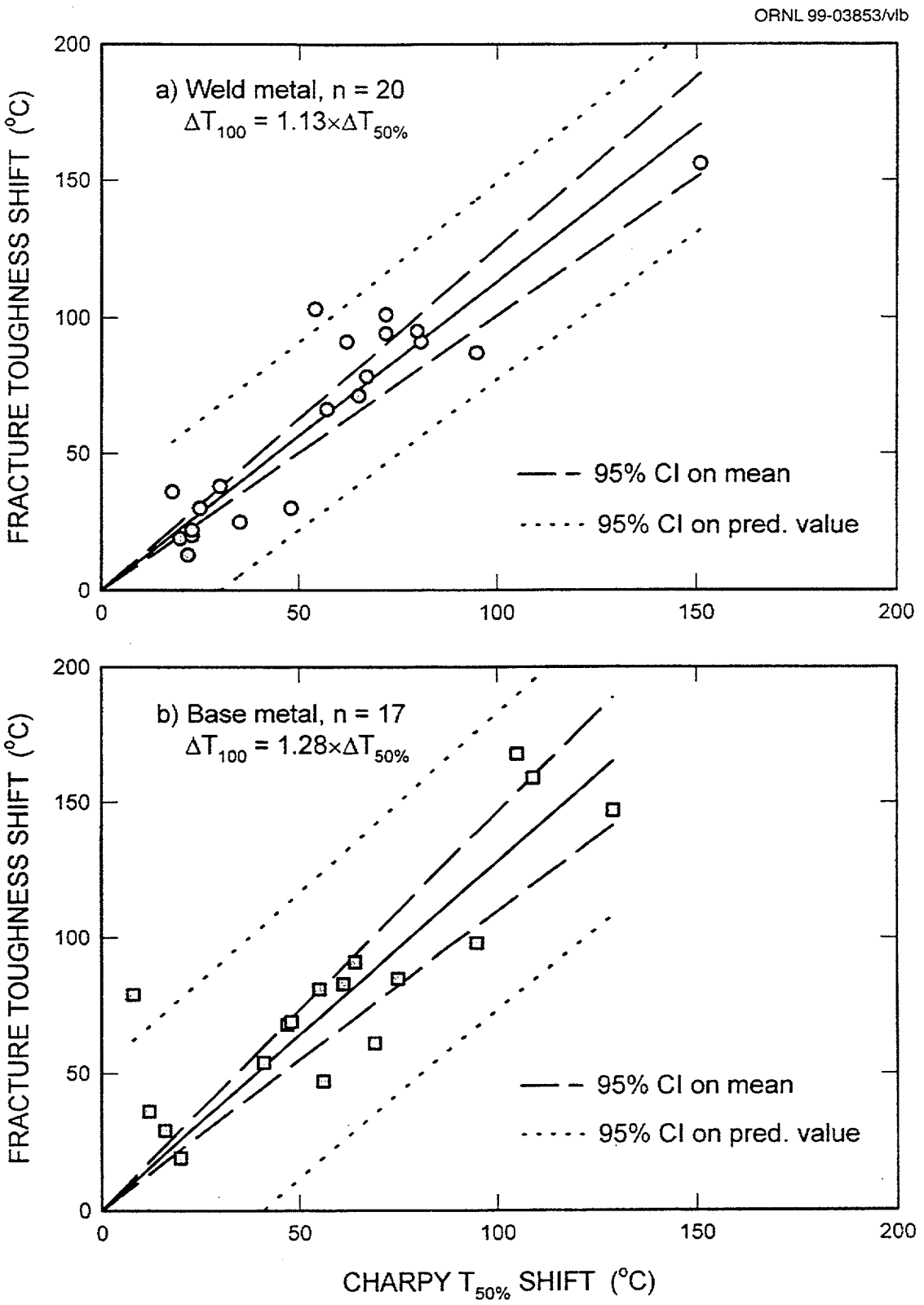

Fig. 28. **Correlation between fracture toughness T_{100} and Charpy $T_{50\%}$ shifts for (a) weld and (b) base metals.**

with other commonly used criteria for measuring transition-temperature shift by the Charpy impact test. However, given the scatter exhibited, the selected correlation is far from perfect.

Among the 89 data points in the database, 21 were generated as a part of the Heavy-Section Steel Irradiation (HSSI) Program, of which 18 points were from weld metals and 3 points were from base metal (HSST Plate 02 at three different fluences only). All HSSI data are plotted against linear and power law fits (with 95% confidence intervals) obtained for all data in the current database in Figs. 29(a) and (b), respectively. Of the 21 HSSI data points, about half (10 points) have shifts less than 40°C. Those are the weld metal data from the HSSI Fourth Irradiation Series [19] as well as the Tenth Irradiation Series Midland beltline and nozzle course welds after irradiation and annealing at 454°C for 168 h [24]. Although each point is used, this low range of shifts is not of the most interest in the current comparison study. The rest of the data points exhibit relatively low scatter (except for one Midland beltline point) with no difference between weld metals and Plate 02 data. These HSSI data tend to give fracture toughness shifts higher than Charpy shifts as the average overall fit predicts. From this point of view, the power law fit from the current database is closer to the HSSI data trend than the linear fit. Again, the HSSI data are limited to shifts up to about 100°C.

The current database is, perhaps, the most comprehensive one to date; nevertheless, some caution still needs to be exercised in the use of these data. For example, all but five base metal data exhibit Charpy shifts below 100°C. The weld metal data are considered to be a better data set because the Charpy shifts are distributed more evenly, but there is a significant amount of low-shift data in the current correlations. Such considerations call for a closer examination of the data in an attempt to search for possible trends in the correlations between Charpy and fracture toughness shifts. Perhaps the fact that the data tend to follow the power law better than the linear fit is one of these trends. Usually, it is better to observe such trends by plotting residuals ($\Delta T_{100} - \Delta T_{41J}$) against various parameters of interest.

Low upper-shelf materials, for example, have for many years been considered as critical materials from a radiation-embrittlement point of view. Figure 30 represents a plot of the residuals vs the value of the irradiated Charpy USE. These data do not reveal any specific trends in the residuals for low upper-shelf materials (for example, below 100 J) compared with the rest of the materials. In this case, an absolute value of the Charpy USE has been used as a critical parameter. Another way to consider the effect of USE is to plot the residuals against the ratio of the unirradiated USE to the irradiated one (see Fig. 31). This way, degradation of the irradiated USE relative to the unirradiated condition rather than

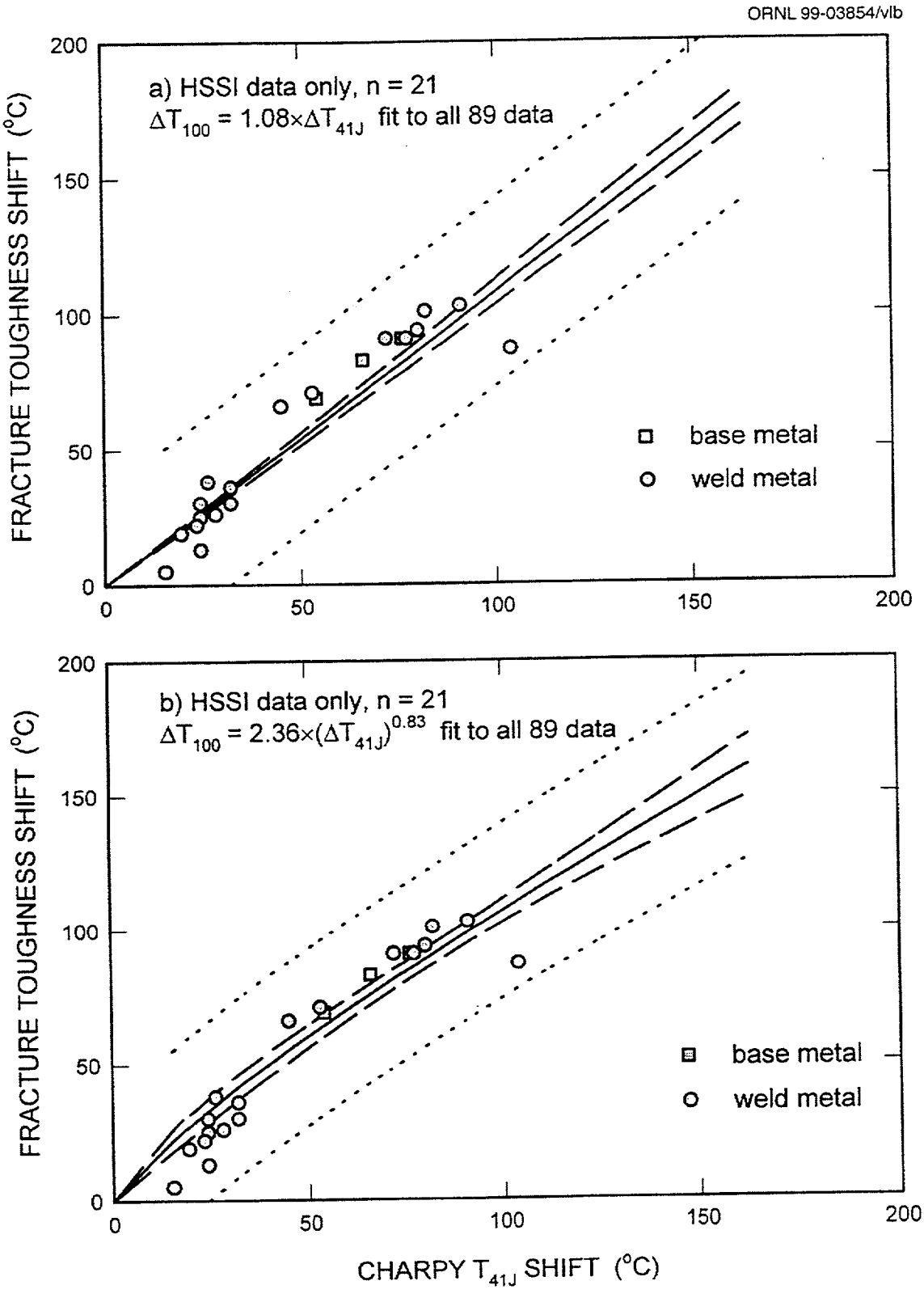

Fig. 29. **Correlation of the HSSI data only with (a) linear and (b) power law fits to all data from Fig. 23.**

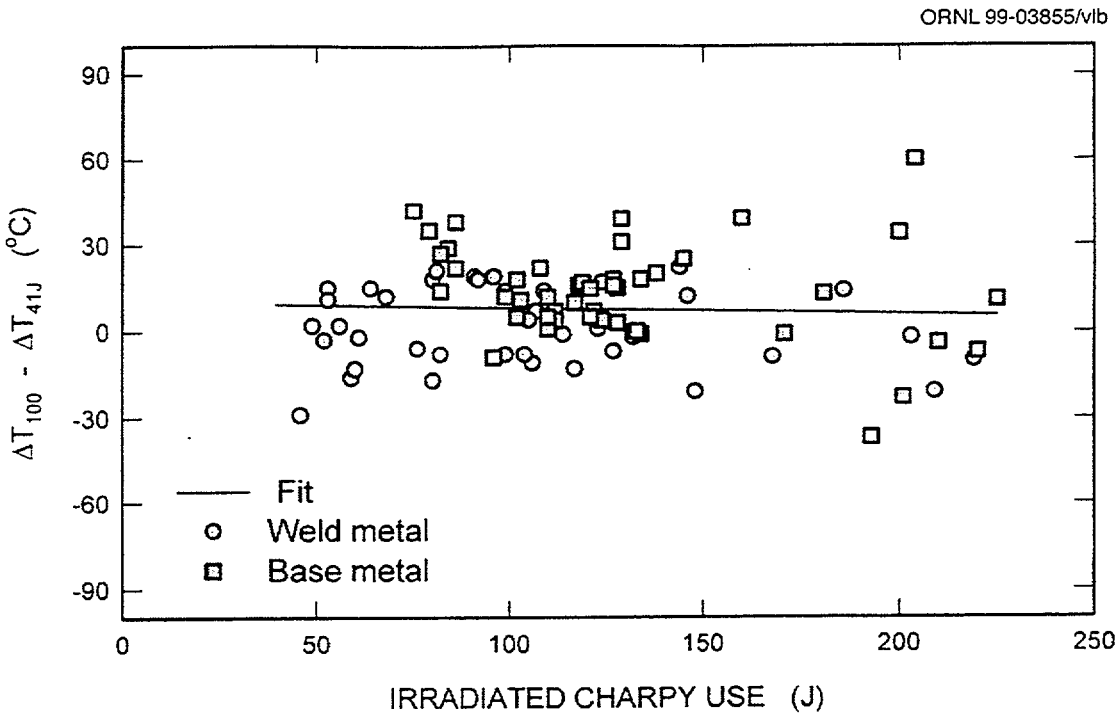

Fig. 30. **Difference between fracture toughness and Charpy shifts as a function of Charpy upper-shelf energy in the irradiated condition.**

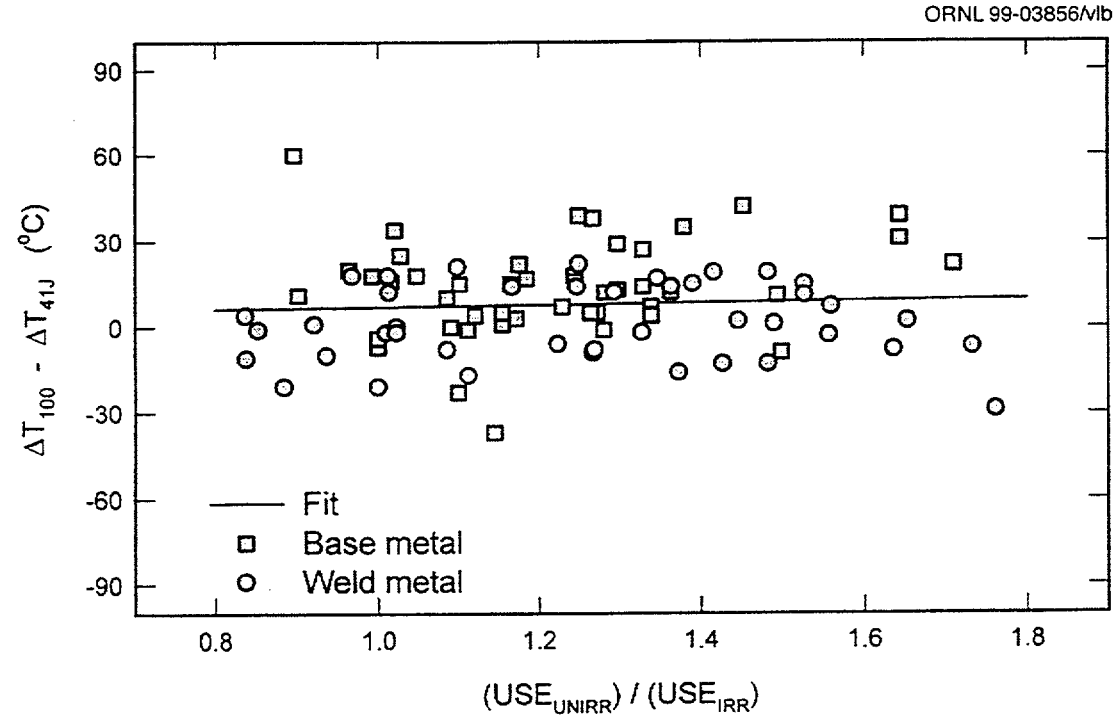

Fig. 31. **Difference between fracture toughness and Charpy shifts as a function of the ratio of USE_{UNIRR} to USE_{IRR}.**

an absolute value of USE is used as a measure of the radiation effect on the USE. Figure 31 shows that for ratios of $(USE_{UNIRR})/(USE_{IRR})$ up to about 1.5 there are no trends in the data.

Figures 32 and 33 are plots of the residuals as a function of the absolute value of the yield strength in the irradiated condition and the yield strength increase, respectively. There is a tendency for materials with a higher absolute value of the yield strength in the irradiated condition to have smaller fracture toughness shifts than Charpy shifts (see Fig. 32), while materials with lower yield strength in the irradiated condition tend to exhibit a greater fracture toughness shift than Charpy shift. At the same time, the degree of hardening, as expressed in terms of yield strength increase, has little effect on the residuals (see Fig. 33).

Figures 34 and 35 are plots of the residuals as a function of the absolute value of T_{41J} in the irradiated and unirradiated conditions, respectively. On average, materials with higher absolute values of Charpy transition temperature tend to have a fracture toughness shift greater than the Charpy shift. Two data points below –100°C on Fig. 35 have a strong effect on the slope of the fit.

Figure 36 is a plot of the residuals as a function of Charpy shift, ΔT_{41J}. Figure 37 is a plot of the residuals as a function of neutron fluence (in the logarithmic scale). There is a trend in the data for the Charpy shift to be smaller than the fracture toughness shift for small Charpy shifts (or low neutron fluence), but it becomes slightly higher than the fracture toughness shift with the increasing degree of embrittlement as measured by Charpy 41J shift (or neutron fluence). To some degree such a trend supports the use of a power law fit to the correlation between the fracture toughness and Charpy shifts. Data generated under the HSSI Program are emphasized by darker color on Fig. 36.

7. FRACTURE TOUGHNESS, NIL-DUCTILITY TRANSITION-TEMPERATURE SHIFTS, AND RADIATION HARDENING; SEARCHING FOR A CORRELATION

In addition to fracture toughness and Charpy data in the unirradiated and irradiated conditions, other useful information has been collected and incorporated into the current database.

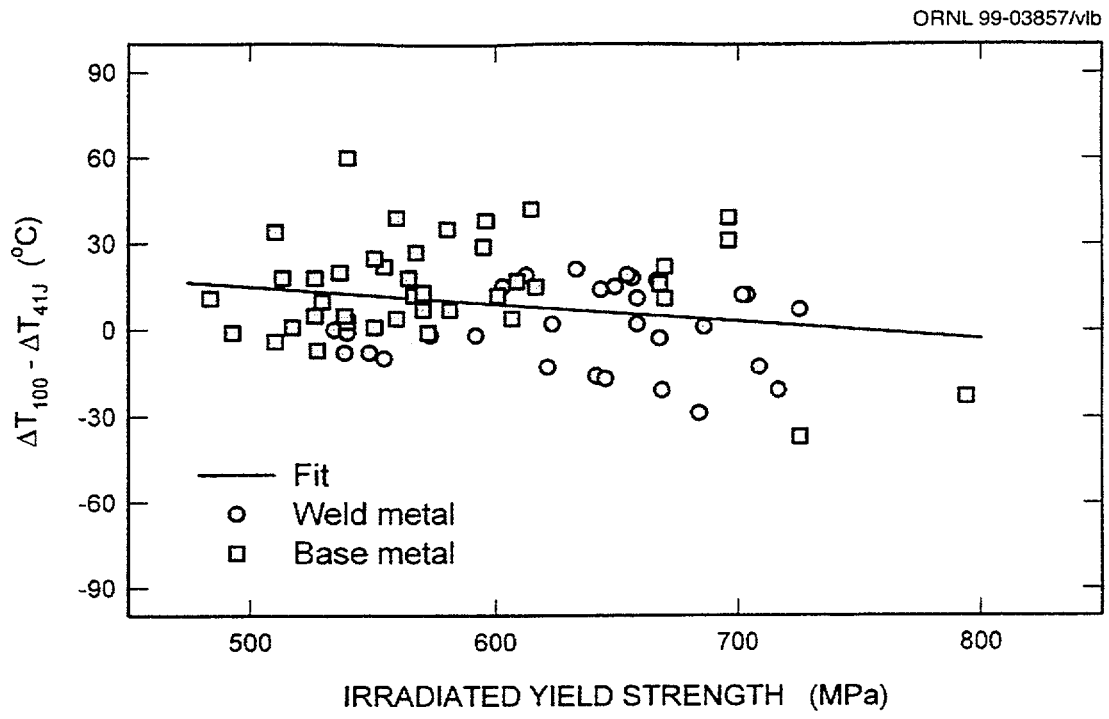

Fig. 32. Difference between fracture toughness and Charpy shifts as a function of yield strength of materials in the irradiated condition.

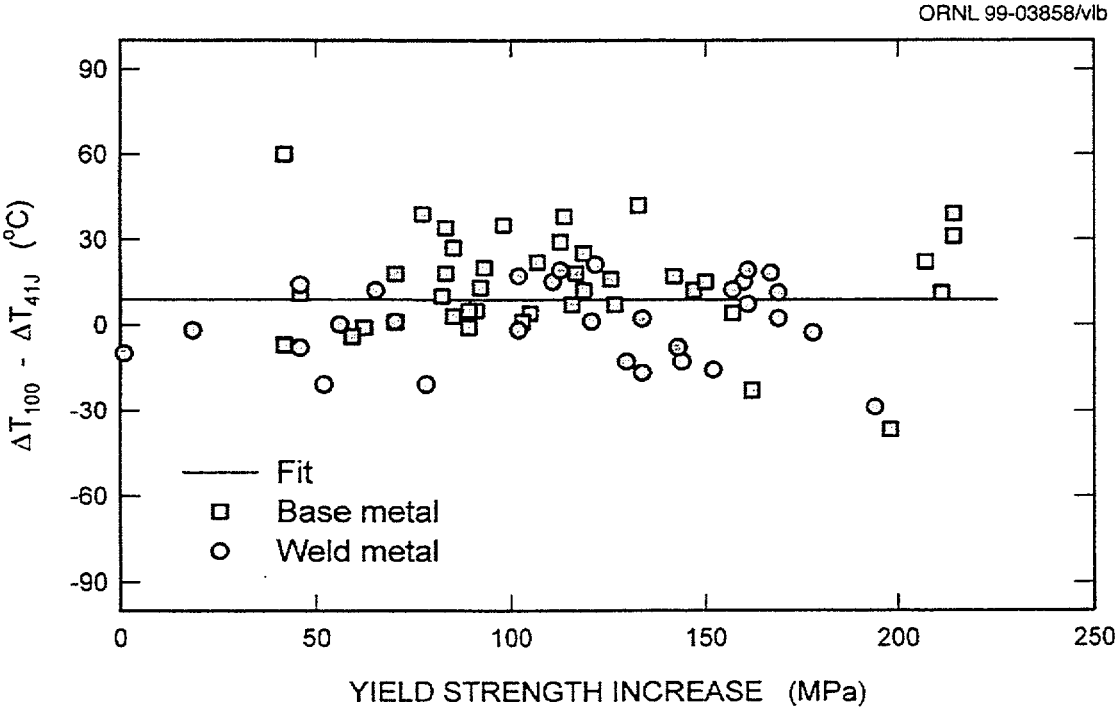

Fig. 33. Difference between fracture toughness and Charpy shifts as a function of yield strength increase.

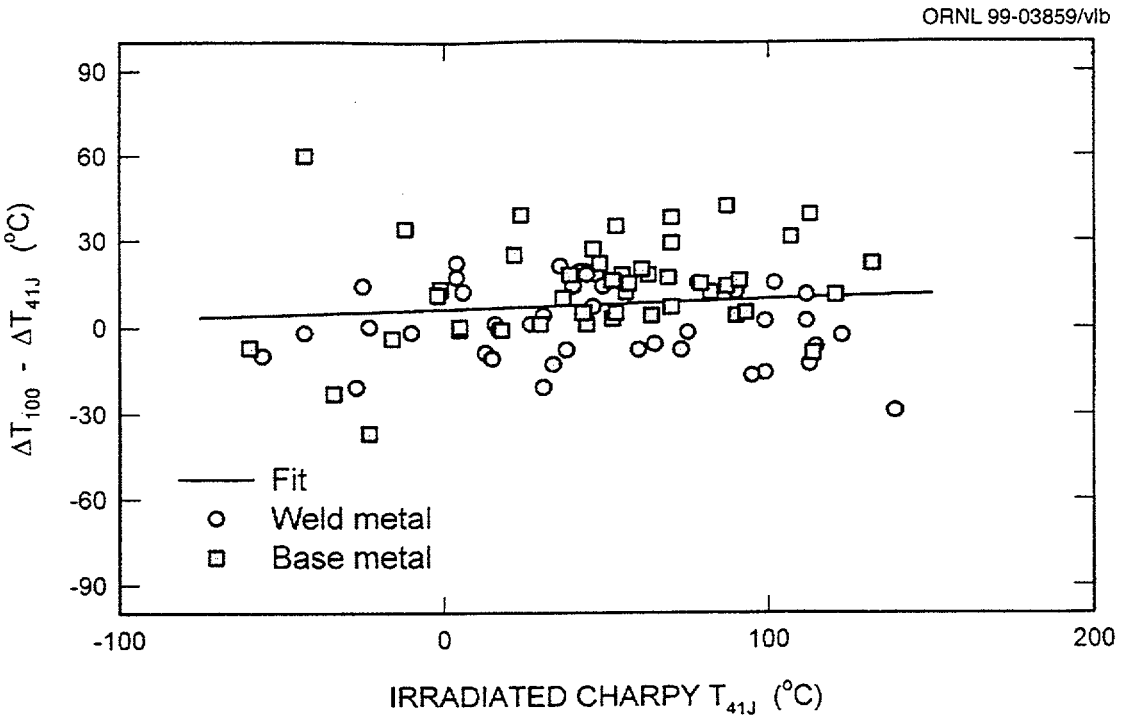

Fig. 34. Difference between fracture toughness and Charpy shifts as a function of Charpy T_{41J} in the irradiated condition.

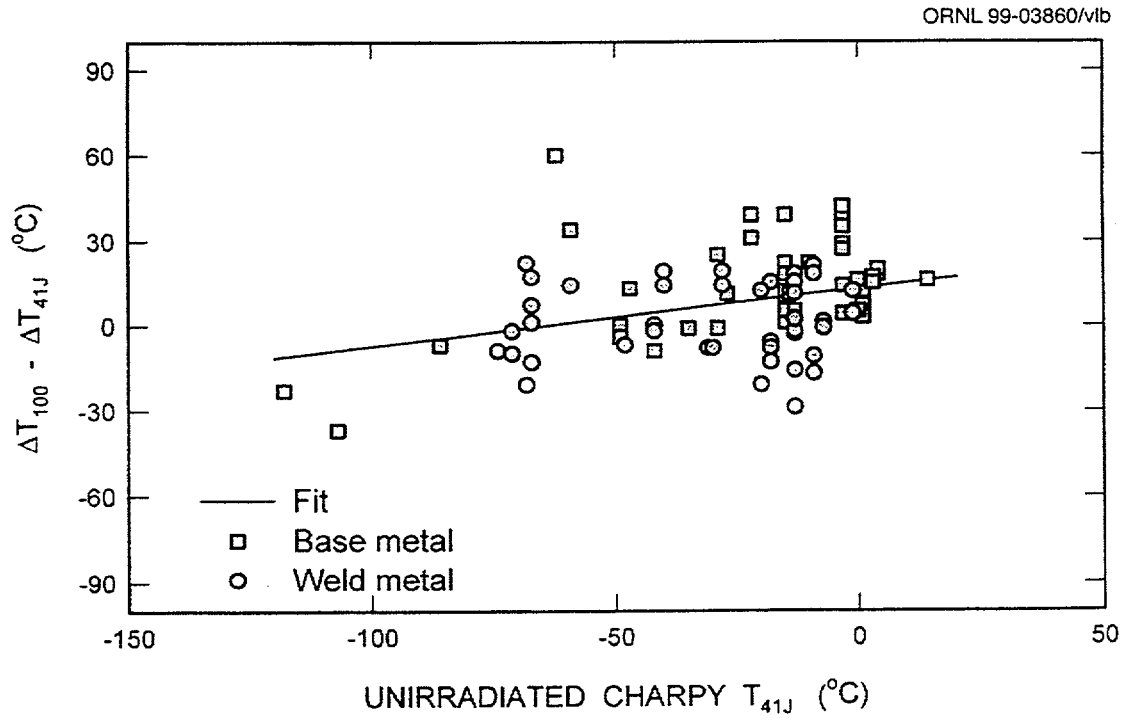

Fig. 35. Difference between fracture toughness and Charpy shifts as a function of Charpy T_{41J} in the unirradiated condition.

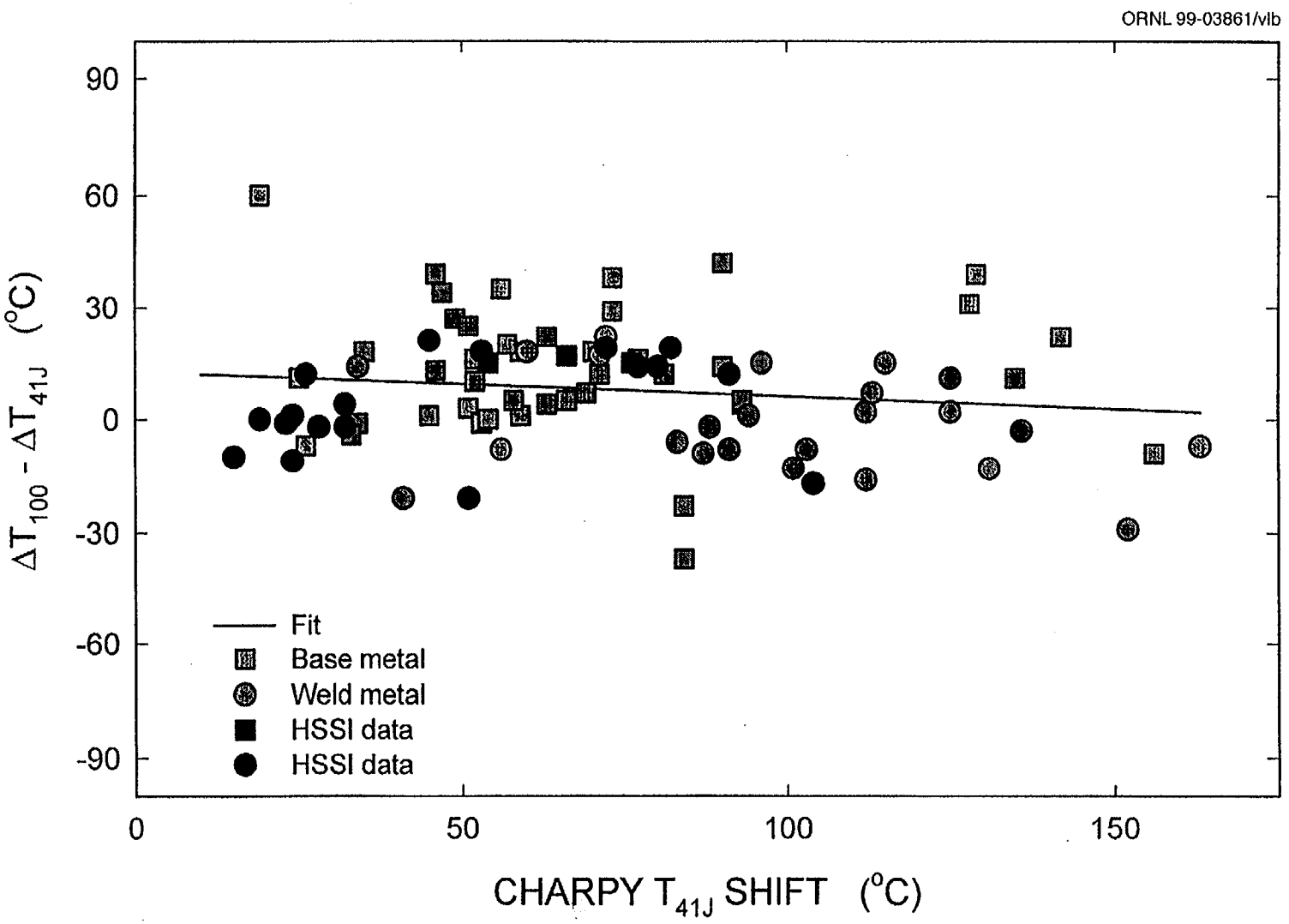

Fig. 36. Difference between fracture toughness and Charpy shifts as a function of Charpy T_{41J} shift.

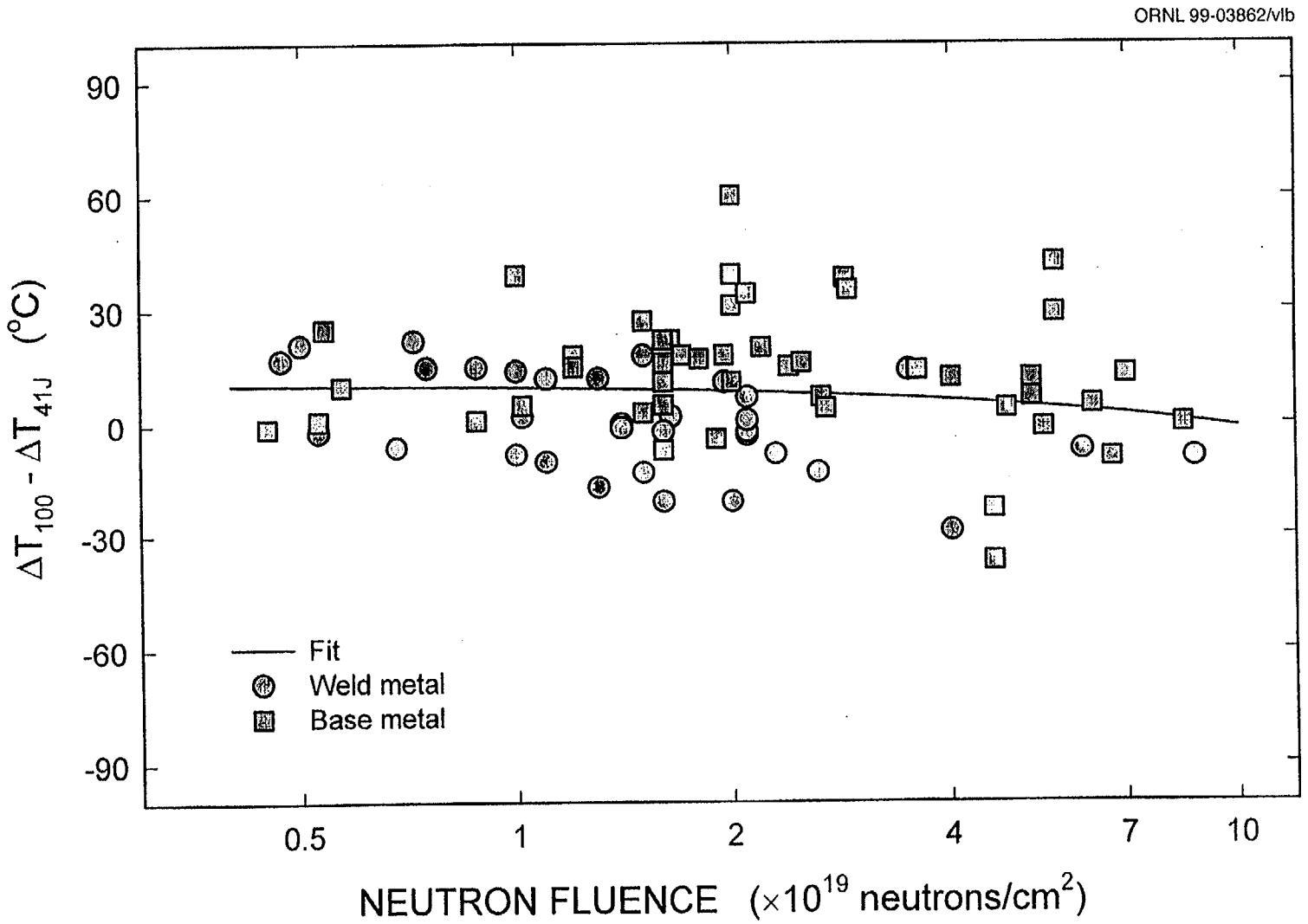

Fig. 37. Difference between fracture toughness and Charpy shifts as a function of neutron fluence.

Figure 38 presents a comparison of radiation hardening ($\Delta\sigma_y$) and ΔT_{100} for weld metals and base metals. Regression analysis indicates about the same ratio between fracture toughness shift and an increase of yield strength for base metals and weld metals. The combined 71 data points (see Fig. 39) for weld and base metals gave the following fit:

$$\Delta T_{100} = 0.70 \Delta\sigma_y \ , \ (°C) \qquad (r^2 = 0.66) \ . \tag{16}$$

The correlations between fracture toughness data and tensile data obtained in the present analysis are in agreement with correlations between Charpy impact data and tensile data published in Refs. [36] and [37] for irradiation in test reactors. In general, the data in Fig. 39 show that the radiation-induced shift of fracture toughness is very likely associated with radiation-hardening mechanisms, but there is a significant scatter in the data for both base metals and weld metals. This scatter is similar to that shown earlier for the ΔT_{41J} and, thus, suggests that the use of radiation hardening is not necessarily better than the Charpy shift correlation for estimation of fracture toughness shift. The other interesting observation is a comparison of the current correlation to the correlation between Charpy T_{41J} shifts and the increase in yield strength from a power reactor surveillance embrittlement database (PR-EDB). There were 232 data points of base metals and weld metals available in the PR-EDB [38] for comparison. The comparison is made in Fig. 40. The vertical axis is the transition temperature shift, ΔT_{100}, for fracture toughness shift from the present study or ΔT_{41J} for the surveillance data. The ΔT_{100} data are, on average, higher than Charpy shifts from the surveillance database at the same level of hardening. Charpy data from the PR-EDB provide the following fit:

$$\Delta T_{41J} = 0.55 \Delta\sigma_Y \ . \tag{17}$$

The other property of interest is the drop-weight nil-ductility temperature (NDT). The NDT was available for a limited number (23) of materials in the unirradiated condition and only for three irradiated steels such that the fluence of the irradiated NDT would match that for the T_{100}. A comparison between these two transition temperatures is given in Fig. 41(a). Five more unirradiated data were added from Ref. [39] to increase the total number of data points. Perhaps, NDT has the least relationship with T_{100} in comparison with Charpy transition temperatures. However, a very limited number of data in Fig. 41(b), for which both fracture toughness and NDT shifts were available, suggest that correlation between shifts of fracture toughness and NDT transition temperatures might be as good as the correlation between fracture toughness and Charpy transition temperatures.

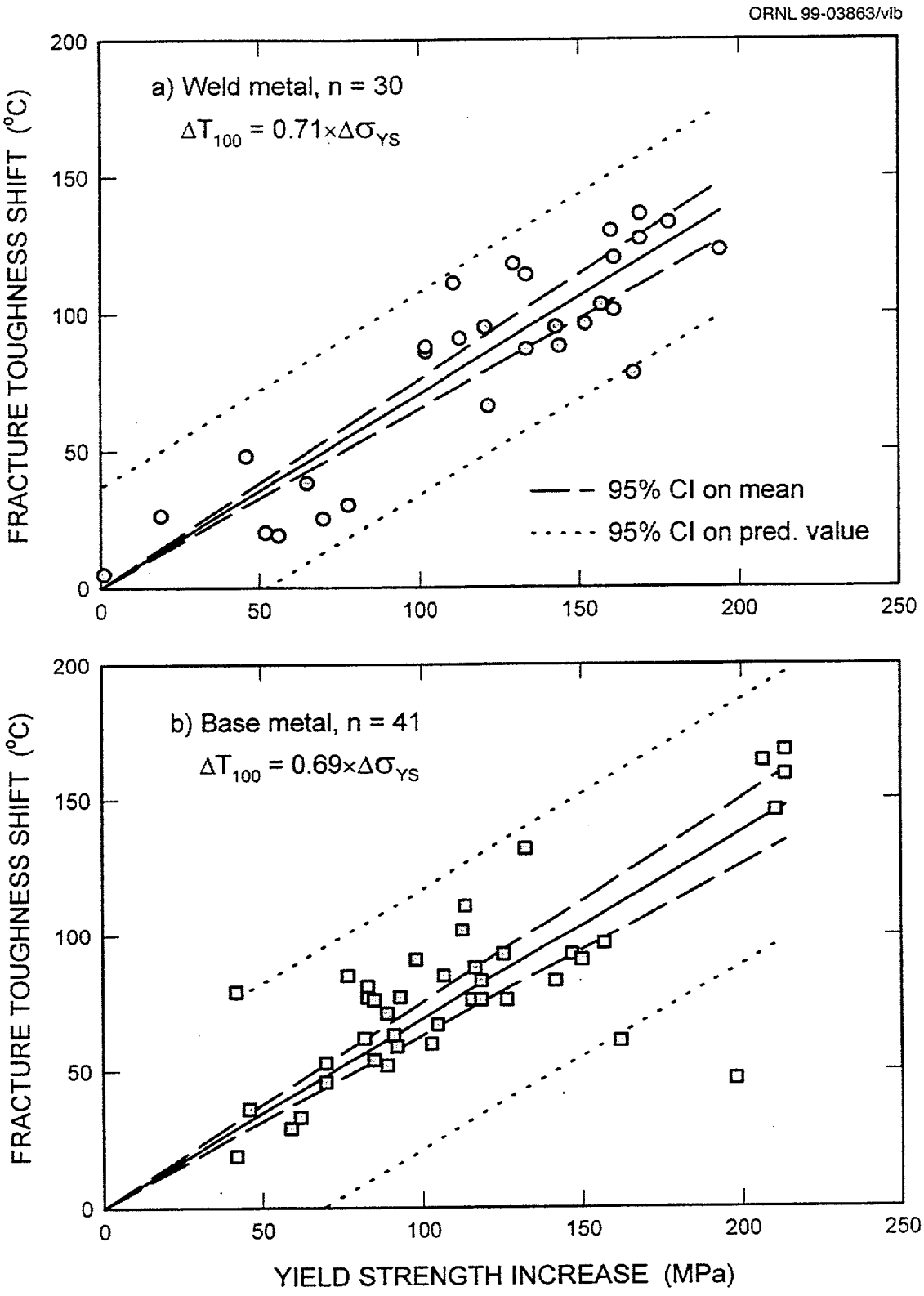

Fig. 38. **Correlation between fracture toughness shift and yield strength increase for (a) weld and (b) base metals.**

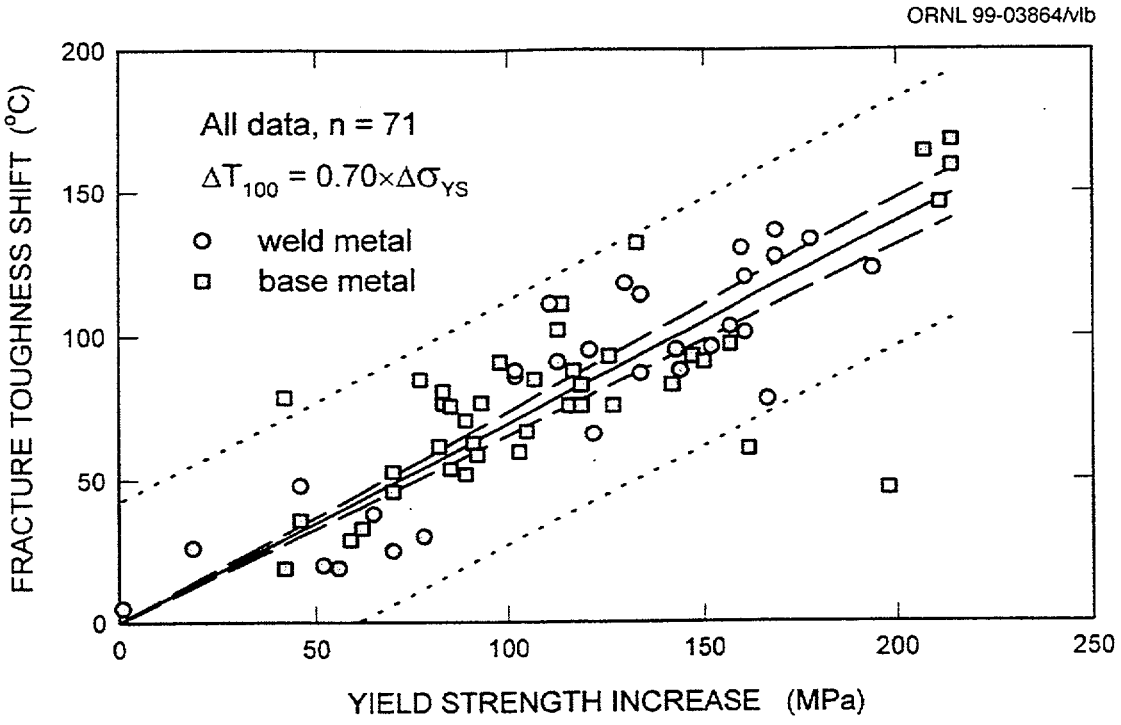

Fig. 39. **Correlation between fracture toughness shift and yield strength increase for both weld and base metals.**

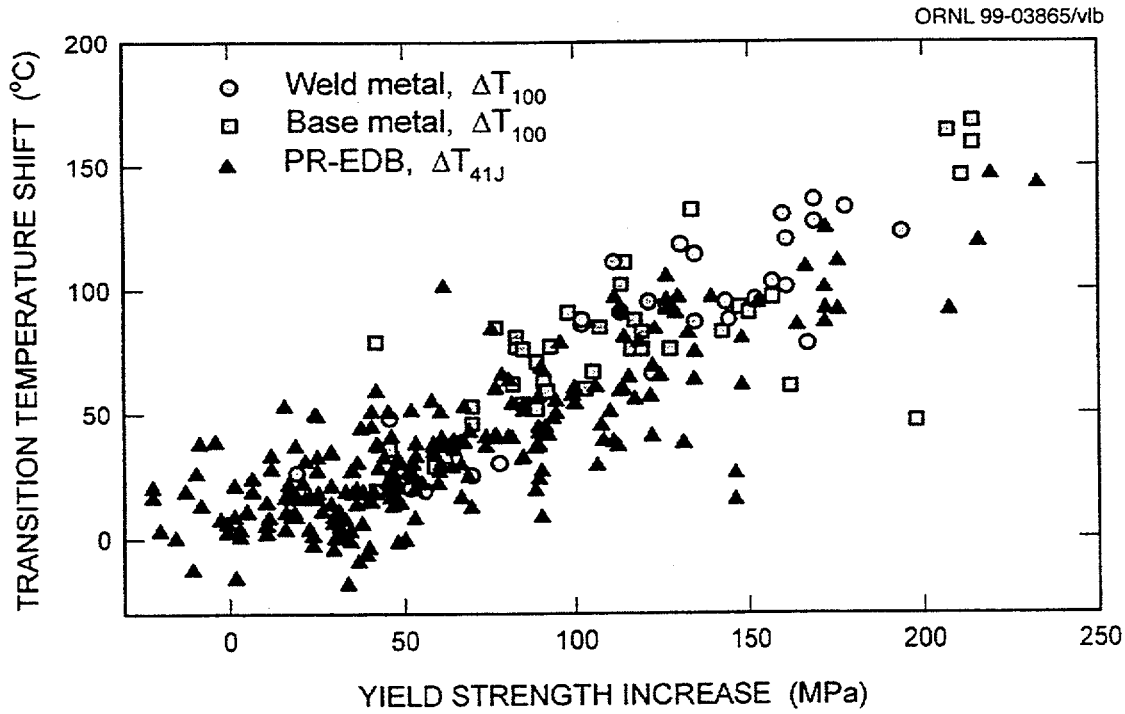

Fig. 40. **Correlation between transition temperature shift and yield-strength increase for all fracture toughness data in the present study and Charpy data in the PR-EDB.**

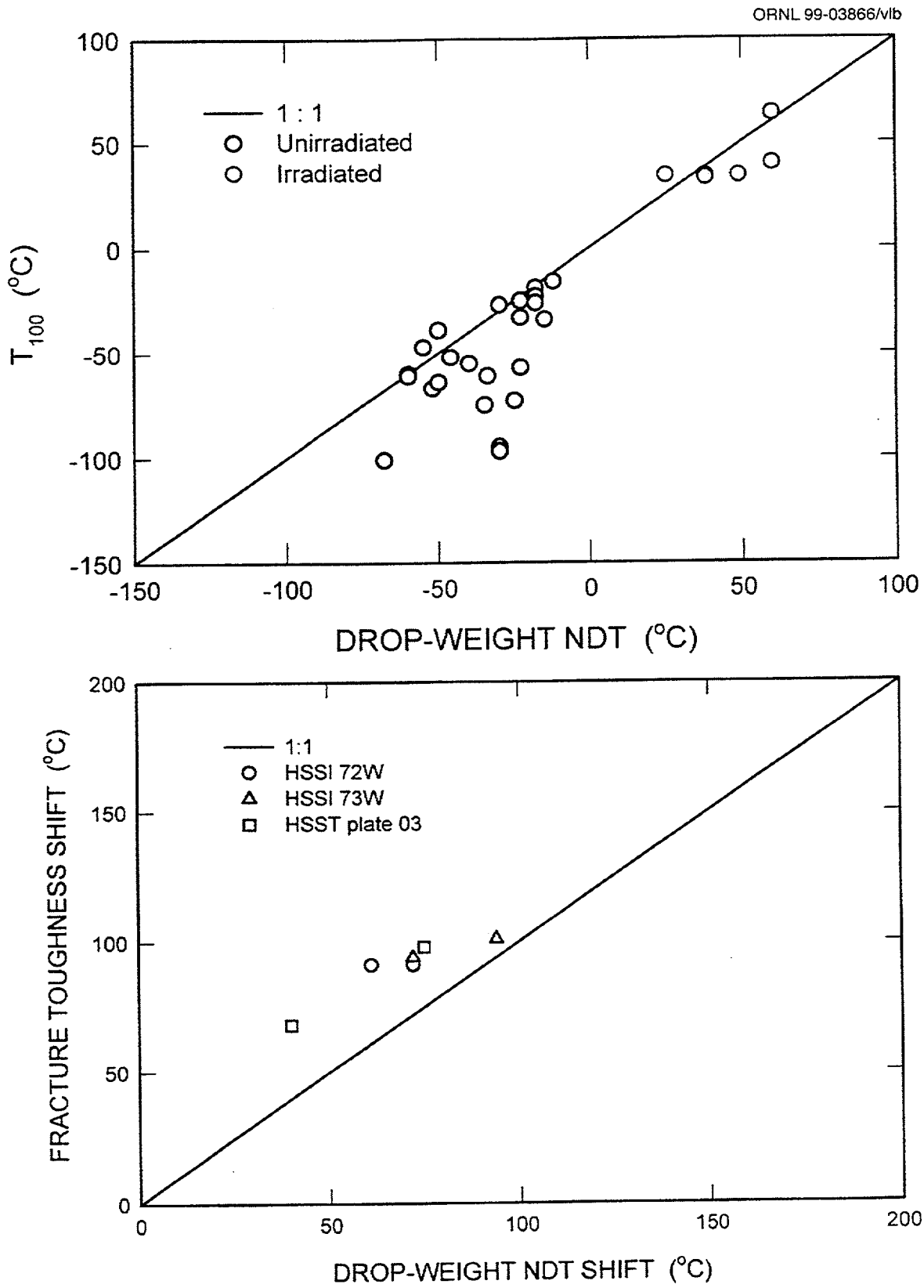

Fig. 41. Comparison of (a) fracture toughness T_{100} and drop-weight NDT temperatures and (b) corresponding radiation-induced shifts.

8. MEASURED FRACTURE TOUGHNESS SHIFT VS PREDICTIONS OF EMBRITTLEMENT

In this chapter fracture toughness shifts from the present study are compared with the predicted radiation-induced shift from the currently available procedures. The main data are summarized in Appendix B, Tables B.3 and B.4. The major procedure of interest is the Nuclear Regulatory Commission (NRC) *Regulatory Guide 1.99* procedure. Revision 1 of RG 1.99 was represented by a single formula for base metals and weld metal:

$$\Delta T\,(°C) = \frac{5}{9}\,[40 + 5000(P - 0.008) + 1000(Cu - 0.08)](\varphi t)^{0.5} \quad , \tag{18}$$

where P and Cu are phosphorus and copper content, respectively, in weight percent; φt is neutron fluence in 10^{19} n/cm^2 (E > 1 MeV). Predictions based on this formula are in Tables B.3 and B.4 under the column designated "RG 1.99.1."

Revision 2 (which is currently in force) has a more complicated relationship but can be simplified in the following:

$$\Delta T = (\text{chemistry factor})\,(\varphi t)^{[0.28 - 0.1\log(\varphi t)]} \quad , \tag{19}$$

where $\log(\varphi t)$ is a logarithm to the base 10.

In Revision 2, the chemistry factor is tabulated and is different for base metals and weld metals. Phosphorus was removed from the chemistry factor while nickel became a part of it. Predictions based on this formula are in Tables B.3 and B.4 under the column designated "RG 1.99.2."

Research is currently under way to develop a new revision of RG 1.99. For this study, a potential equation for that revision has been taken from Draft NUREG/CR-6551 [40]. It is given as

$$\Delta T\,(°F) = A\,\exp\left(\frac{1.843 \times 10^4}{T_c + 460}\right)(1 + 54.3P)f(\varphi t) + B(1 + 2.62Ni^{1.358})h(Cu)g(\varphi t) \quad , \tag{20}$$

where

$$f(\varphi t) = (\varphi t)^{[0.4265 + 0.0761 \log(\varphi t)]}$$

$$g(\varphi t) = \frac{1}{2} + \frac{1}{2}\tanh\left\{\frac{\left[\log\left[\varphi t \cdot 10^{19}\left(1 + \frac{1.77 \cdot 10^{9}}{\varphi}\right)\right]\right] - 18.304}{0.584}\right\}$$

$$h(Cu) = \begin{cases} 0, & Cu \le 0.074\ \text{wt\%} \\ (Cu - 0.074)^{0.673}, & 0.074 < Cu < 0.300\ \text{wt\%} \\ 0.368, & Cu \ge 0.300\ \text{wt\%} \end{cases} \qquad (21)$$

$$A = \begin{cases} 2.18 \times 10^{-7} \text{ for welds} \\ 2.43 \times 10^{-7} \text{ for plates} \\ 1.82 \times 10^{-7} \text{ for forgings} \end{cases}$$

$$B = \begin{cases} 203 \text{ for welds} \\ 167 \text{ for plates} \\ 130 \text{ for forgings} \end{cases}$$

ΔT and T_c are in degrees Fahrenheit. T_c is the inlet coolant temperature. The prediction by this procedure is given in Tables B.3 and B.4 under the column designated "EWO."[1]

In addition to these revisions of RG 1.99, three other national procedures have been considered. One of these procedures is accepted in Germany as the KTA 3203 standard [41]. This standard has a very restricted validity range relative to chemical composition. For example, copper content is basically limited to a maximum of 0.18%, and the prediction is given in a graphical form. Thus, it is not clear how to apply it to materials with higher copper content. For this reason, this procedure has not been used to predict the transition-temperature shift for materials in the present database.

The FIM formula is accepted in France for the evaluation of surveillance results [42]:

$$\Delta T\,(°C) = (17.3 + 1537(P - 0.008) + 238(Cu - 0.08) + 191\,Ni^2\,Cu)(\varphi t)^{0.35} \quad . \qquad (22)$$

The prediction by this procedure is given in Tables B.3 and B.4 under the column designated "FIM."

[1]Note that the final (published) version of this NUREG [40] contains slightly different fitting coefficients.

The fourth predictive procedure is the one accepted recently in Japan and has the following form for base metal:

$$\Delta T\,(°C) = (-16 + 1210\,P + 215\,Cu + 77\sqrt{Ni\,Cu}\,)(\varphi t)^{0.29 - 0.04\log(\varphi t)} \quad . \tag{23}$$

It has the following form for weld metal:

$$\Delta T = (26 - 24\,Si - 61\,Ni + 301\sqrt{Ni\,Cu}\,)(\varphi t)^{0.25 - 0.1\log(\varphi t)} \quad , \tag{24}$$

where Si is silicon content in weight percent. Predictions of transition-temperature shift based on these equations are given in Tables B.3 and B.4 under the column designated "JEPE" [43].

All of these predictive equations are based on analyses of corresponding surveillance databases. However, almost all of these data are Charpy impact energy shifts. Thus, actual fracture toughness shifts from the current analysis could be compared with predictions based on Charpy data. Note that fracture toughness specimens were irradiated in test reactors. The comparison will be made in terms of residuals:

$$\Delta T_{PRED} - \Delta T_{100\ MEASURED} \tag{25}$$

vs neutron fluence (logarithm scale). In this case, any data point below zero would mean that the measured fracture toughness shift is higher than that predicted by an equation or, in other words, the predictive equation underestimates the fracture toughness shift. All of these equations, except the RG 1.99.1, are accompanied by a standard deviation, σ. Thus, 2σ is added to the predicted value as a margin. The comparison is presented in Figs. 42 through 46. A prediction based on an equation only is designated as $\Delta T_{PRED(EQ)}$ and is presented by the left axis. A prediction based on an equation and a margin (+2σ) is designated as $\Delta T_{PRED(EQ+2\sigma)}$ and is presented by the right axis. The first observation is that none of these predictions provides enough conservatism for predicting fracture toughness shifts of base metals at neutron fluence above 1.5×10^{19} n/cm^2, even with 2σ margin. That supports the observation that, on average, the fracture toughness shift is higher than the Charpy shift for base metal data in this database. For the case of weld metal, where, on average, the fracture toughness shift is equal to the Charpy shift, the equation for the new potential revision of RG 1.99 [40] provides the most

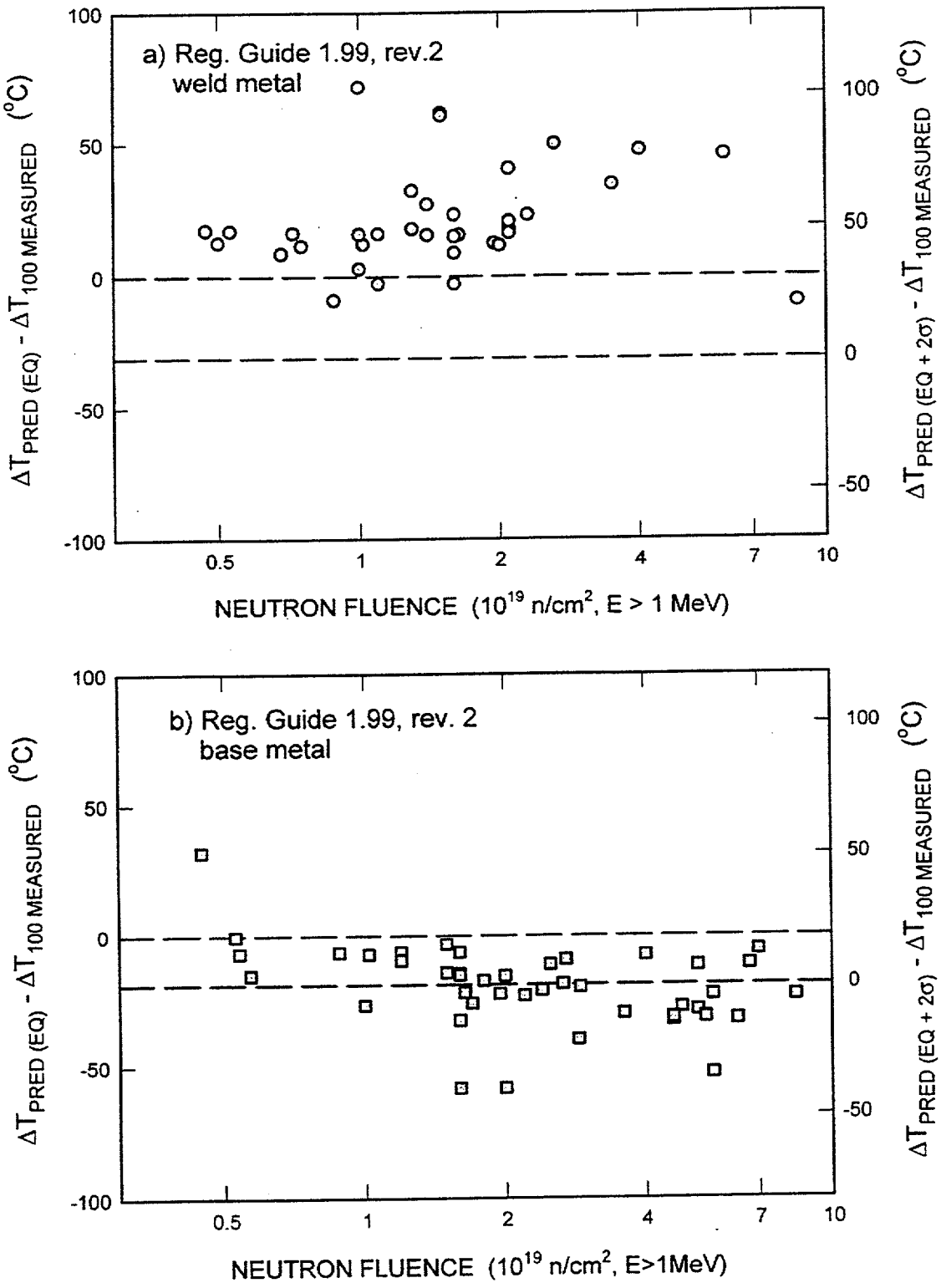

Fig. 42. **Comparison of fracture toughness shifts with prediction of embrittlement based on Regulatory Guide 1.99 Rev. 2 for (a) weld metals and (b) base metals.**

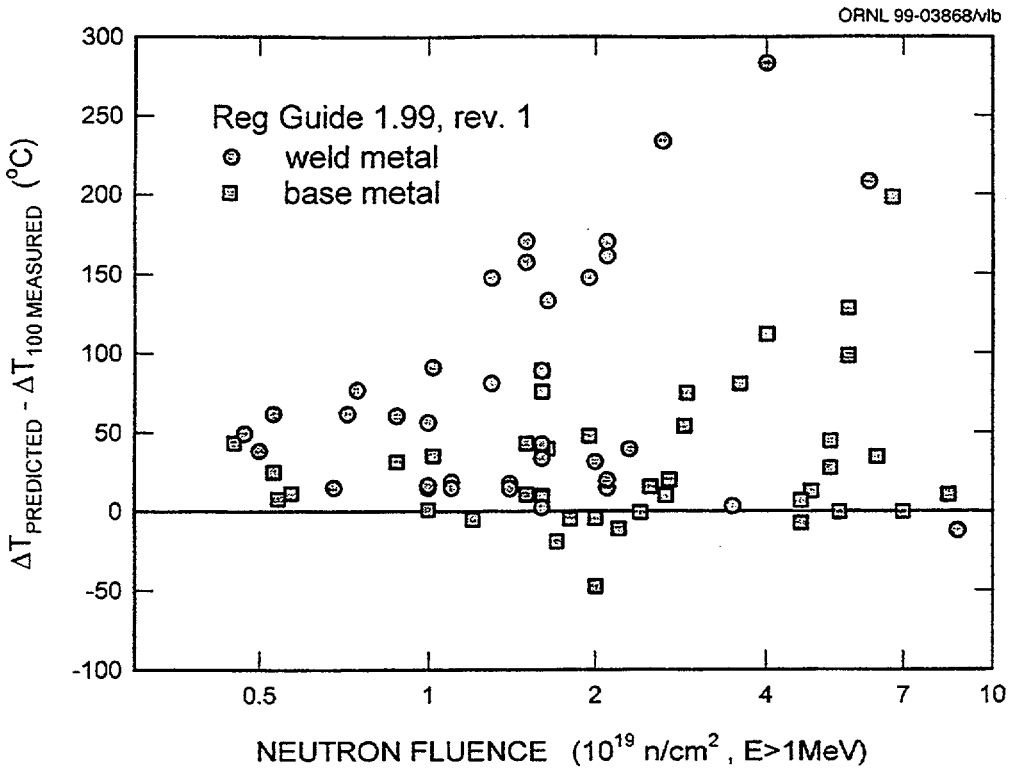

Fig. 43. Comparison of fracture toughness shifts with prediction of embrittlement based on Regulatory Guide 1.99 Rev. 1.

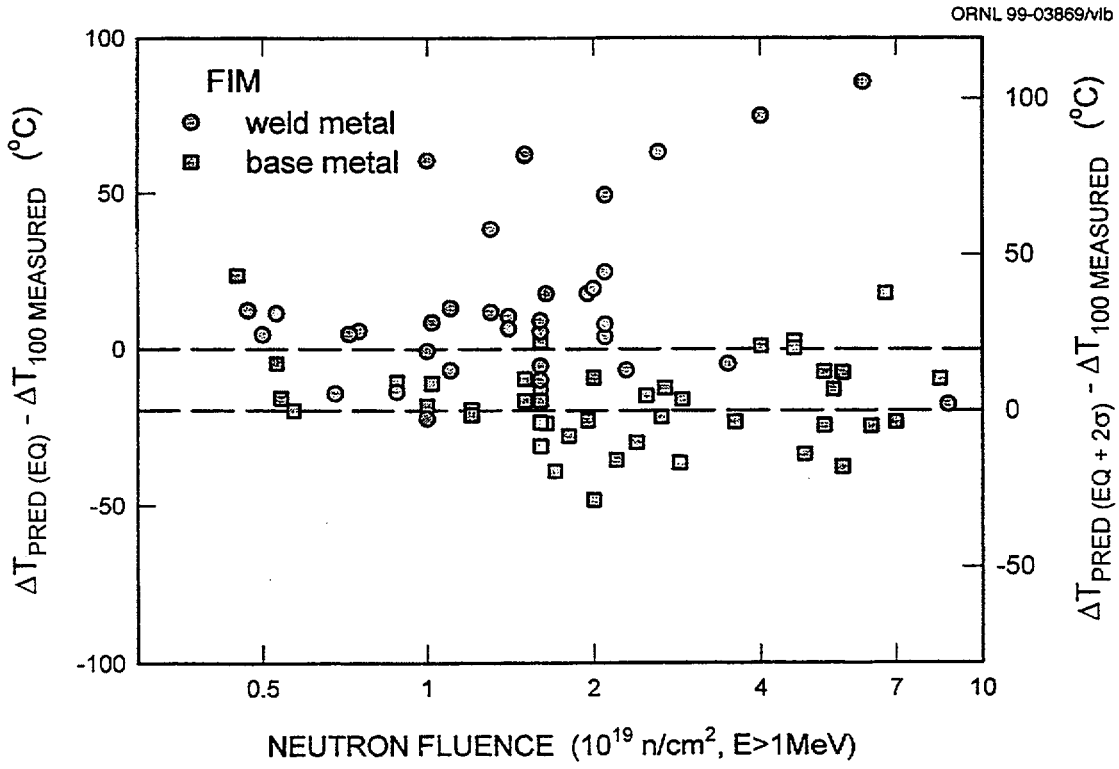

Fig. 44. Comparison of fracture toughness shifts with prediction of embrittlement based on French predictive equation FIM.

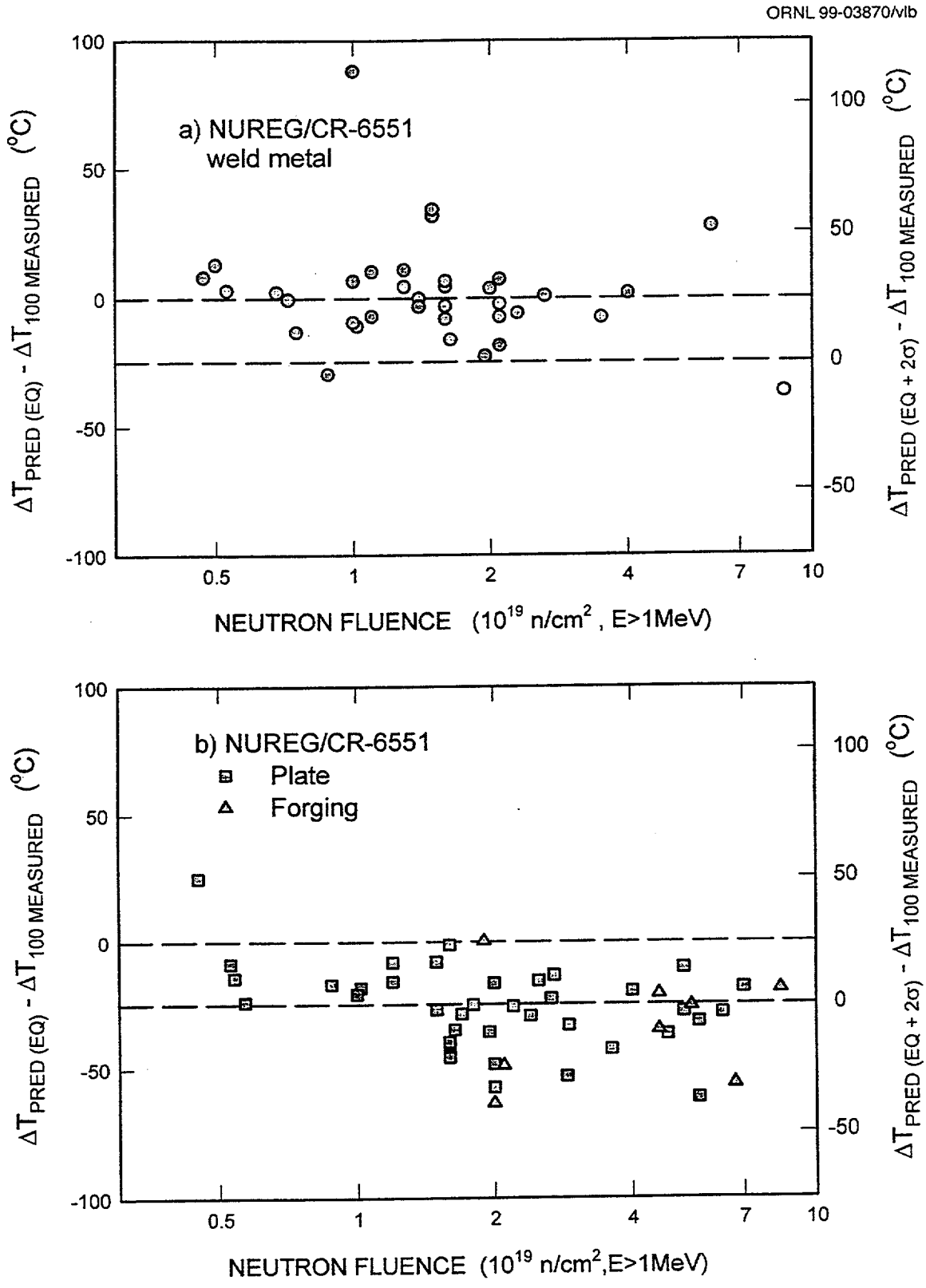

Fig. 45. Comparison of fracture toughness shifts with prediction of embrittlement based on proposed equations in NUREG/CR-6551 for (a) weld metals and (b) plate and forging metals.

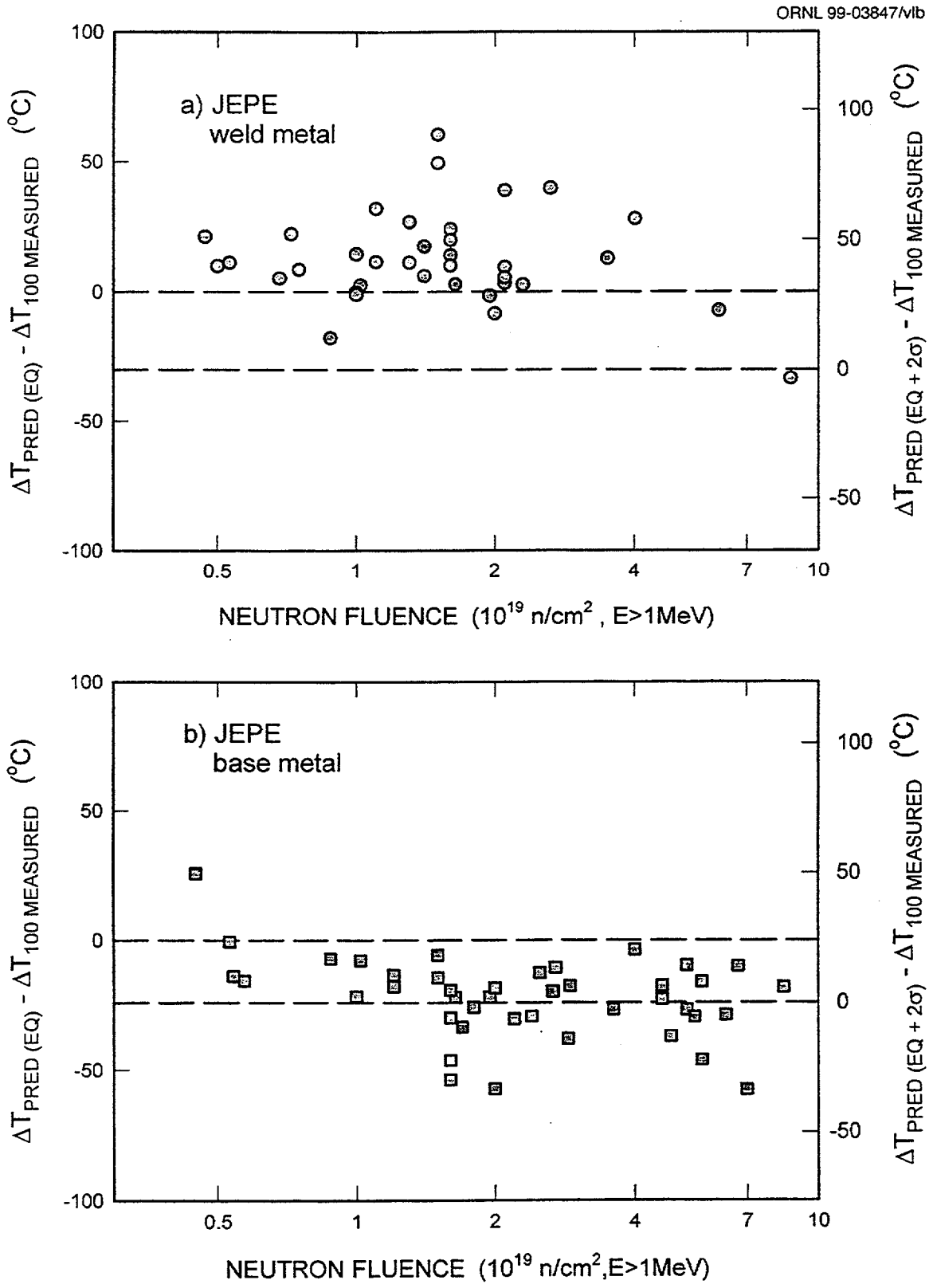

Fig. 46. Comparison of fracture toughness shifts with prediction of embrittlement based on JEPE predictive equation for (a) weld metal and (b) base metal.

accurate prediction of fracture toughness shift in the whole range of neutron fluence. The other equations tend to provide predictions that are conservative with respect to the measured fracture toughness shift.

9. SUMMARY AND CONCLUSIONS

A database was assembled from information reported in the literature regarding radiation-induced shifts of static fracture toughness and Charpy impact toughness. Application of the master curve concept was used to determine shifts of fracture toughness curves; the hyperbolic tangent function was used to fit Charpy data.

Analysis shows that the master curve methodology models very well both the scatter of fracture toughness data and the temperature dependence of fracture toughness in both unirradiated and irradiated conditions. Moreover, it was shown that the master curve concept can easily work on the ASME K_{Ic} database, which has for many years been used as the basis for the deterministic lower-bound approach. The present analysis shows that the same ASME K_{Ic} database can be modeled with the statistical approach of the master curve methodology. T_{100} values for all materials in the ASME K_{Ic} database were determined and reported. No correlation has been found between T_{100} and RT_{NDT} for the materials in the ASME K_{Ic} database. Need for a systematic experimental study of the master curve shape for highly embrittled materials is recognized, especially in light of the absence of any data generated by the HSSI Program at such embrittlement levels.

1. No change in the slope of the master curve was observed for the overall irradiated data. However, separate analysis of a limited number of irradiated materials with a high postirradiation Charpy transition temperature raised a concern that caution needs to be used in applying (extrapolating) the results of this analysis of the current database to end-of-life conditions.

2. Fracture toughness shifts were compared with Charpy impact toughness shifts at various levels of energy, lateral expansion, and percent shear fracture. The following six observations are based on regression analysis.

   a. For weld metals, on average, the Charpy transition temperature shift at 41 J is the same as the shift of fracture toughness, with 95 % confidence intervals of about ±26°C.

b. For base metals, on average, the fracture toughness shift is 16% greater than the Charpy 41-J temperature shift, with 95% confidence intervals of about ±36°C. Using other indices for Charpy transition temperature does not significantly improve the correlation.

c. A power law function tends to provide a better fit than a linear fit to the shift data, acknowledging that, on average, fracture toughness shifts tend to be higher than Charpy shifts at low and intermediate shifts, but become less than Charpy shifts with greater embrittlement. Out of the total 89 data points with both fracture toughness and Charpy shifts, only 16 points are for Charpy shifts above 110°C; most are in the range of Charpy shifts from 40 to 110°C.

d. Regression analysis indicates about the same correlation of fracture toughness shift with increase of yield strength for both base metals and weld metals, with substantial scatter (about ±40°C):

$$\Delta T_{100} = 0.70\,\Delta\sigma_Y \quad . \tag{26}$$

e. The following relationship was established between absolute values of fracture toughness T_{100} and Charpy T_{41J} transition temperatures:

$$T_{100} = T_{41J} - 24\,°C \quad , \qquad \sigma = 20\,°C \quad , \tag{27}$$

which can be recommended as a first estimation for positioning of the fracture toughness master curve based on available Charpy T_{41J} data.

f. Nil-ductility temperature (NDT) did not reveal a clear correlation with T_{100}. However, very limited data, for which both fracture toughness and NDT shifts were available, suggest that a correlation between shifts of fracture toughness and NDT temperatures might be about the same as the correlation between fracture toughness and Charpy transition temperatures.

10. REFERENCES

[1] "Title 10," *Code of Federal Regulations*, Part 50, U.S. Government Printing Office, Washington, D.C., January 1987.

[2] *ASME Boiler and Pressure Vessel Code. An American National Standard*, American Society of Mechanical Engineers, New York, 1986.

[3] U.S. Nuclear Regulatory Commission, *Regulatory Guide 1.99*, Rev. 2, "Radiation Embrittlement of Reactor Vessel Materials," May 1988.

[4] "Standard Practice for Conducting Surveillance Tests for Light-Water Cooled Nuclear Power Reactor Vessels, E 706 (IF)," ASTM E 185-94, *Annual Book of ASTM Standards*, Vol. 03.01, American Society for Testing and Materials, Philadelphia.

[5] A. L. Hiser, *Correlation of C_V and K_{Ic}/K_{Jc} Transition Temperature Increases Due to Irradiation*, NUREG/CR-4395 (MEA-2086), Materials Engineering Associates, Inc., 1985.

[6] J. R. Hawthorne, *Evaluation and Prediction of Neutron Embrittlement in Reactor Pressure Vessel Materials*, EPRI NP-2782, Electric Power Research Institute, 1982.

[7] J. R. Hawthorne, B. H. Menke, and A. L. Hiser, *Light Water Reactor Pressure Vessel Surveillance Dosimetry Improvement Program: Notch Ductility and Fracture Toughness Degradation of A 302-B and A 533-B Reference Plates from PSF Simulated Surveillance and Through-Wall Irradiation Capsules*, NUREG/CR-3295 (MEA-2017), Vol.1, Materials Engineering Associates, Inc., 1983.

[8] A. L. Hiser, *Post-Irradiation Fracture Toughness Characterization of Four Lab-Melt Plates*, NUREG/CR-5216 (MEA-2311), Rev. 1, Materials Engineering Associates, Inc., 1989.

[9] J. R. Hawthorne and A. L. Hiser, *Influence of Fluence Rate on Radiation-Induced Mechanical Property Changes in Reactor Pressure Vessel Steels*, NUREG/CR-5493 (MEA-2376), Materials Engineering Associates, Inc., 1990.

[10] R. J. McElroy, A. J. E. Foreman, G. Gage, W. J. Phythian, P. H. N. Ray, and I. A. Vatter, "Optimization of Reactor Surveillance Programmes and their Analysis," UK Contribution to the IAEA Phase 3 Coordinated Research Programme, AEA-RS-2426, AEA Technology, 1994.

[11] T. Kodaira, S. Miyazono, N. Nakajima, K. Ishimoto, and H. Itami, "Evaluation of Neutron Irradiation Embrittlement of Heavy Section Nuclear Reactor Pressure Vessel Steels in Terms of Elastic-Plastic Fracture Toughness" *Nuclear Engineering and Design*, 85, 1985, 1–13.

[12] M. Valo, K. Wallin, K. Torronen, and R. Ahlstrand, "Irradiation Response of the New IAEA Correlation Monitor Material JRQ Measured by Fracture Mechanical Properties," pp. 203–215 in *Effects of Radiation on Materials: 15th International Symposium, ASTM STP 1125*, ed. R. E. Stoller, A. S. Kumar, and D. S. Gelles, American Society for Testing and Materials, Philadelphia, 1992.

[13] M. Valo, K. Wallin, K. Torronen, and R. Ahlstrand, "Irradiation Response of the IAEA CRP-3 Material FFA Measured by Fracture Toughness Specimens," pp. 238–248 in *Radiation Embrittlement of Nuclear Reactor Pressure Vessel Steels: An International Review* (Fourth Volume), ASTM STP 1170, ed. L. E. Steele, American Society for Testing and Materials, Philadelphia, 1993.

[14] S. Ishino, T. Kawakami, T. Hidaka, and M. Satoh, "The Effect of Chemical Composition on Irradiation Embrittlement," pp. 3.1–13.15 *14th MPA-Seminar on Safety and Reliability of Plant Technology*, Vol. 1, 1988.

[15] J. Ahlf, D. Bellmann, and F. J. Schmitt, "Irradiation Programs to Establish the Safety Margins of German Licensing Rules Related to RPV Steel Embrittlement," pp. 115–129 in *Radiation Embrittlement of Nuclear Reactor Pressure Vessel Steels: An International Review* (Third Volume), ASTM STP 1011, ed. L. E. Steele, American Society for Testing and Materials, Philadelphia, 1989, pp. 115-129.

[16] *Analysis of the Behavior of Advanced Reactor Pressure Vessel Steels under Neutron Irradiation*, Technical Reports Series No. 265, International Atomic Energy Agency, Vienna, 1986.

[17] R. Havel, M. Vacek, and P. Novosad, "Effects of Neutron Irradiation on Advanced CrNiMoV Reactor Pressure Vessel Steel," pp. 227–237 in *Transactions of the 10th International Conference on Structural Mechanics in Reactor Technology*, Vol. G, 1989.

[18] K. Wallin, "Summary of the IAEA/CRP3 Fracture Mechanical Results," in *Proceedings of a Specialists Meeting on Irradiation Embrittlement and Mitigation*, IAEA, Espoo, Finland, Vol. 2, 1995.

[19] J. J. McGowan, R. K. Nanstad, and K. R. Thoms, *Characterization of Irradiated Current-Practice Welds and A533 Grade B Class 1 Plate for Nuclear Pressure Vessel Service*, NUREG/CR-4880, Vol. 1 (ORNL-6484/V1), Oak Ridge National Laboratory, 1988.

[20] R. K. Nanstad, F. M. Haggag, D. E. McCabe, S. K. Iskander, K. O. Bowman, and B. H. Menke, *Irradiation Effects on Fracture Toughness of Two High-Copper Submerged-Arc Welds, HSSI Series 5*, NUREG/CR-5913, Vol. 1 (ORNL/TM-12156/V1), Oak Ridge National Laboratory, 1992.

[21] D. E. McCabe, R. K. Nanstad, S. K. Iskander, and R. L. Swain, *Unirradiated Material Properties of Midland Weld WF-70*, NUREG/CR-6249 (ORNL/TM-12777), Oak Ridge National Laboratory, 1994.

[22] D. E. McCabe, M. A. Sokolov, R. K. Nanstad, and R. L. Swain, *Effects of Irradiation to 0.5 and 1.0 x 10^{19} neutron/cm^2 (E>1 MeV) on the Midland Reactor Low Upper-Shelf Weld: Capsules 10.01, 10.02, and 10.05 in the Heavy-Section Steel Irradiation Program Tenth Irradiation Series*, ORNL/NRC/LTR-95/18, Oak Ridge National Laboratory, 1995.

[23] M. A. Sokolov and D. E. McCabe, *Comparison of Irradiation-Induced Shifts of K_{Jc} and Charpy Curves: Analysis of Heavy-Section Steel Irradiation Program Data*, ORNL/NRC/LTR-95/4, Oak Ridge National Laboratory, 1995.

[24] M. A. Sokolov, D. E. McCabe, S. K. Iskander, and R. K. Nanstad, "Comparison of Fracture Toughness and Charpy Impact Properties Recovery by Thermal Annealing of Irradiated Reactor Pressure Vessel Steels," pp. 771–782 in *7th International Symposium on Environmental Degradation of Materials in Nuclear Power Systems—Water Reactors*, Vol. 2, NACE International.

[25] R. K. Nanstad, D. E. McCabe, R. L. Swain, and M. K. Miller, *Chemical Composition and RT_{NDT} Determination for Midland Weld WF-70*, NUREG/CR-5914 (ORNL-6740), Oak Ridge National Laboratory, 1992.

[26] *Flaw Evaluation Procedures: ASME Section XI, EPRI Special Report*, EPRI NP-719-SR, Electric Power Research Institute, Palo Alto, Calif., 1978.

[27] "Standard Test for Plane-Strain Fracture Toughness of Metallic Materials," ASTM E-399, American Society for Testing and Materials, Philadelphia.

[28] "Test Method for the Determination of Reference Temperature, T_o, for Ferritic Steels in the Transition Range," ASTM E-1921-97, American Society for Testing and Materials, Philadelphia.

[29] K. Wallin, "The Scatter in K_{Ic}-Results," *Engineering Fracture Mechanics* 19(6), 1984, 1085–93.

[30] K. Wallin, "The Size Effect in K_{Ic}-Results," *Engineering Fracture Mechanics* 22(1), 1985, 149–163.

[31] K. Wallin, "Validity of Small Specimen Fracture Toughness Estimates Neglecting Constraint Corrections," pp. 519–537 in *Constraint Effects in Fracture: Theory and Applications, ASTM STP 1244*, ed. M. Kirk and A. Bakker, American Society for Testing and Materials, Philadelphia, 1995.

[32] D. I. A. Steinstra, "Stochastic Micromechanical Modeling of Cleavage Fracture in the Ductile-Brittle Transition Region," MM6013-90-11, Ph.D. Thesis, Texas A&M University, College Station, Texas, August 1990.

[33] K. Wallin, "A Simple Theoretical Charpy-V-K_{Ic} Correlation for Irradiation Embrittlement," pp. 93–100 in *Proc. ASME Pressure Vessels and Piping Conference, Innovative Approaches to Irradiation Damage and Fracture Analysis*, PVP-Vol. 170, American Society of Mechanical Engineers, New York, 1989.

[34] R. K. Nanstad, J. A. Keeney, and D. E. McCabe, *Preliminary Review of the Bases of the K_{Ic} Curve in the ASME Code*, ORNL/NRC/LTR-93/15, 1993.

[35] M. A. Sokolov "Statistical Analysis of the ASME K_{Ic} Database," *Journal of Pressure Vessel Technology* 120, February 1998, 24–28.

[36] G. R. Odette, P. M. Lombrozo, and R. A. Wullaert, "Relationship Between Irradiation Hardening and Embrittlement of Pressure Vessel Steels," pp. 840–860 in *Effects of Radiation on Materials: 12th International Symposium, ASTM STP 870*, ed. F. A. Garner and J. S. Perrin, American Society for Testing and Materials, Philadelphia, 1985.

[37] R. K. Nanstad and R. G. Berggren, *Irradiation Effects on Charpy Impact and Tensile Properties of Low Upper-Shelf Welds, HSSI Series 2 and 3*, NUREG/CR-5696 (ORNL/TM-11804), Oak Ridge National Laboratory, 1991.

[38] F. W. Stallmann, J. A. Wang, and F. B. K. Kam, *PR-EDB: Power Reactor Embrittlement Data Base, Version 2*, NUREG/CR-4816, U.S. Nuclear Regulatory Commission, 1994.

[39] J. G. Merkle, K. Wallin, and D. E. McCabe, *Technical Basis for an ASTM Standard on Determining the Reference Temperature, T_o, for Ferritic Steels in the Transition Range*, NUREG/CR-5504 (ORNL/TM-13631), Oak Ridge National Laboratory, 1998.

[40] E. D. Eason, J. E. Wright, and G. R. Odette, *Improved Embrittlement Correlations for Reactor Pressure Vessel Steels*, NUREG/CR-6551, Modeling and Computing Services, 1998

[41] KTA Kerntechnischer Ausschuß (Nuclear Safety Standard Commission), KTA 3203, Germany, 1984.

[42] C. Brillaud, F. Hedin, and B. Houssin, "A Comparison Between French Surveillance Program Results and Predictions of Irradiation Embrittlement," pp. 420–47 in *Influence of Radiation on Material Properties: 13th International Symposium, ASTM STP 956*, ed. F. A. Garner, C. H. Henager, and N. Igata, American Society for Testing and Materials, Philadelphia, 1987.

[43] "Surveillance Tests of Structural Materials for Nuclear Reactors," *Japanese Electric Association Codes (JEAC) 4201-1991*, Japanese Electric Association, 1991 (in Japanese).

APPENDIX A

WEIBULL STATISTICS AND THE MASTER CURVE

K. Bowman

This section presents a comparison of and discussion regarding the two methods used to estimate the mean value of a data set. In comparison of the method of moment and the method of maximum likelihood, one may conclude that the moment estimator is better because it is unbiased and the variance is exact. However, for a censored sample it is difficult to estimate K_o. The maximum likelihood estimate, on the other hand, is biased, but, for a censored sample, K_o is estimated easily. To find out properties of the maximum likelihood estimator, one can conduct an extensive Monte Carlo experiment with specified sample size and find its bias and variance of the estimators.

Weibull Distribution

Let's define $X = K_{Jc}$ and consider that a random variable X has a Weibull distribution with parameter $b(>0)$, $\alpha = K_0 - K_{min}$ (>0), and $\zeta_0 = K_{min}$. Then

$$Y = \left(\frac{X - \zeta_0}{\alpha} \right)^b , \tag{A.1}$$

$$P_Y(y) = e^{-y} \qquad (y > 0) , \tag{A.2}$$

$$P_X(x) = \frac{b}{\alpha} \left(\frac{x - \zeta_0}{\alpha} \right)^{b-1} e^{-[(x - \zeta_0)/\alpha]^b} \qquad (x > \zeta_0) . \tag{A.3}$$

The cumulative probability function is

$$F_X(x) = 1 - e^{-[(x-\zeta_0)/\alpha]^b} . \tag{A.4}$$

The mode will be

$$x = \alpha\left(\frac{b-1}{b}\right)^{1/b} + \zeta_o \quad . \tag{A.5}$$

If $b \to \infty$, then $x = \alpha + \zeta_o$.

The median will be

$$\text{median} = \alpha(\log 2)^{1/b} + \zeta_o \quad . \tag{A.6}$$

Then, for all values of b,

$$F_X(\zeta_o + \alpha) = 1 - e^{-1} \sim 0.63 \quad . \tag{A.7}$$

The rth moments of Weibull distribution are

$$\mu_r' = E[X' - \zeta_o]^r = \alpha^r \Gamma\left(\frac{r}{b} + 1\right) \qquad (r = 1, 2, 3, 4) \quad , \tag{A.8}$$

from which we get

$$E[X] = \alpha\Gamma\left(\frac{1}{b} + 1\right) + \zeta_o \quad , \tag{A.9}$$

where E[X] is the mean value at the variate X. For the variance,

$$\text{Var}(X) = \alpha^2\left\{\Gamma\left(\frac{2}{b} + 1\right) - \left[\Gamma\left(\frac{1}{b} + 1\right)\right]^2\right\} \quad . \tag{A.10}$$

If b = 4, the mean is 0.9064, the standard deviation is 0.2543, the skewness is –0.09, and the kurtosis is 2.75 for a standardized Weibull distribution ($\zeta_o = 0$, $\alpha = 1$).

The population skewness and kurtosis are defined as $\mu_3/\mu_2^{3/2}$, and μ_4/μ_2^2, where μ_2, μ_3, and μ_4 are central moments and assumed to exist. Skewness and kurtosis are shape parameters; the normal distribution is symmetric and "bell" shaped with $\mu_3 = 0$ and $\mu_4/\mu_2^2 = 3$. All normal distributions have this characteristic so that shape parameters are independent of location and scale parameters. The exponential density e^{-x}, $x > 0$, has positive skewness and is sometimes described as having a long "tail" to the right. Positive skewness, roughly speaking, has high density to the left and low density to the right for positive valued random variables; for example, the density $x^3 e^{-x}/6$, $x > 0$ has skewness $\mu_3/\mu_2^{3/2} = 2$ with a long "tail" to the right ($x >> 0$). Negative skewness, similarly, has more densities to the right and a long "tail" to the left.

There are other measures of shape, some of which refer to the range. Care must be taken in interpreting zero skewness; it does not in general imply symmetry.

The kurtosis measure shows whether density itself is platikurtic or leptokurtic. The first four standardized moments of the distribution may describe the properties of the model assumed. First moment (mean) shows location, and second moment (variance) represents the scale; the third moment (skewness) and fourth moment (peakedness) complete the picture of the distribution.

The skewness and kurtosis are often used in comparison to the normal density. Standard Weibull distribution with values (–0.09, 2.75) is not so distinctively different from normal value of (0, 3).

Estimation Method

For the maximum likelihood estimator, when b and ζ_o are known, the likelihood function of sample n is

$$L(x_1,\ldots x_n;\alpha) = \prod_{i=1}^{n} \frac{b}{\alpha}\left(\frac{x_i - \zeta_o}{\alpha}\right)^{b-1} e^{-[(x_i-\zeta_o)/\alpha]^b}, \qquad \text{(A.11)}$$

$$\hat{\alpha} = \left[\frac{1}{n}\sum_{i=1}^{n}(X_i - \zeta_o)^b\right]^{1/b}, \qquad \text{(A.12)}$$

$$n\mathrm{Var}(\hat{\alpha}) \sim \left\{1 + \frac{[\psi(2)]^2}{\psi'(1)}\right\}\left(\frac{\alpha}{b}\right)^2 - 1.109\left(\frac{\alpha}{b}\right)^2 \quad . \tag{A.13}$$

In Eq. (A.13) $\psi(x)$ is the Psi function and belongs to the class of polygamma functions, these referring to derivatives. Thus, as is well-known in terms of the gamma function,

$$\psi(x) = \psi_0(x) = \frac{d \ln \Gamma(x)}{dx} \quad , \tag{A.14}$$

$$\psi_1(x) = \frac{d\psi(x)}{dx} = \frac{d^2 \ln \Gamma(x)}{dx^2} \quad , \tag{A.15}$$

$$\psi_s(x) = \frac{d^s \ln \Gamma(x)}{dx^s} \qquad (s = 0, 1, \cdots) \quad . \tag{A.16}$$

Asymptotic series and definite integrals are available for the polygamma functions (see *Handbook of Mathematical Functions*, N.B.S. 55, 1964).

The maximum likelihood estimator is biased, and its variance is valid only for the asymptotic situation ($n \to \infty$). To determine what sample size is necessary to use this formula requires considerable study.

Note that it is slightly different from the estimator of Wallin [31]; he uses $n - [1 - \ln(2)]$ for n. The origin of "$1 - \ln(2)$" in his formulation is used as a bias correction with respect to the median [39].

If $n - k$ observations are censored and their values are replaced by X_k^*, then n^{-1} is replaced by k^{-1}, and $\sum_{i=1}^{n}(X_i - \zeta_o)^b$ is replaced by $\sum_{i=1}^{k}(X_i - \zeta_o)^b + (n - k)\left(X_k^* - \zeta_o\right)^b$.

For the moment estimator, when b and ζ_o are known,

$$\alpha^* = \frac{\frac{1}{n}\sum_{j=1}^{n}(X_j - \zeta_o)}{\Gamma\left(\frac{1}{b}+1\right)} \tag{A.17}$$

$$n\mathrm{Var}\left(\frac{\alpha^*}{\alpha}\right) = \frac{\Gamma\left(\frac{2}{b}+1\right) - \left[\Gamma\left(\frac{1}{b}+1\right)\right]^2}{\left[\Gamma\left(\frac{1}{b}+1\right)\right]^2} \tag{A.18}$$

When b and ζ_o are known, the moment estimator of α is unbiased and the variance is exact. In this case if n – k observations are censored, the statistics become order statistics and will be much more complicated.

Discussion of an Example Problem

When b, ζ_o, and α, or b and α are unknown, the problem becomes very difficult in that no properties of these estimators are known except the asymptotic properties, which leads to a question of sample size without answer.

In the present case, however, b and ζ_o are known and the problem is the sample size. If the sample size is less than 10, it is impossible to say which method is better than the other (note the shape parameter b is set to be 4 arbitrarily).

For example, take the case in Table A1 of Appendix A of ASTM E 1921-98 [28]. Six 4T compact specimens of A533 grade B (–75°C) are given:

Rank	K_{jc}
1	59.1
2	68.3
3	77.9
4	97.9
5	100.9
6	112.4

Then:

Parameter	Maximum likelihood estimate	Moment estimate
K_o	93.1	92.9 (unbiased)
σ	8.25 (asymptotic)	8.4 (exact)
$K_{Jc\ (med)}$	86.7	86.5

Statistical Analysis of a Data Set with Invalid Data

In this case an appeal could be made to pure scientific method. Censoring is defined as "a data sample is said to be censored when, either by accident or design, the value of the random variable under investigation is unobserved for some of the items in the sample." A censored observation is distinct from a "missing" observation in that the order of the censored observation relative to some of the uncensored observations is known and conveys information regarding the distribution being sampled.

There are two types of censoring, for example, for life or survival. In type I censoring on the right, testing is suspended when a preestablished life is reached. In type II censoring on the right, testing ceases at the occurrence of the r^{th} order failure time in a sample of n items.

The maximum likelihood method is the most widely used method for censored samples. Therefore, the reason for censoring is valid and one can then use the statistical method accordingly.

APPENDIX B

SUMMARY TABLES

APPENDIX B

GLOSSARY

CH	Average fluence of Charpy specimens in 10^{19} n/cm^2 (E > 1 MeV)
CONDIT	"Condition," either unirradiated (UNIRR) or, if a value is given, the average value of fluence for Charpy specimens in 10^{19} n/cm^2 (E > 1 MeV)
ENERGY	Value of the Charpy absorbed energy at temperature T = T_{100}
EWO	Transition temperature shift predicted from Eq. (21)
FIM	Transition temperature shift predicted from Eq. (22)
FT	Average fluence of fracture-toughness specimens in 10^{19} n/cm^2 (E > 1 MeV)
JEPE	Transition temperature shift predicted from Eq. (23) for base metal and/or Eq. (24) for weld metal
NDT	Nil-ductility temperature
ORIENT	Specimen orientation: CL, LT, or TL
REF	Reference
RG 1.99.1	Transition temperature shift predicted from Nuclear Regulatory Commission (NRC) *Regulatory Guide 1.99*, rev. 1
RG 1.99.2	Transition temperature shift predicted from Nuclear Regulatory Commission (NRC) *Regulatory Guide 1.99*, rev. 2
SLOPE	Fitting coefficient C in Eq. (6) when E is the absorbed energy and is one-half of the transition zone temperature width
SLOPEXP	Fitting coefficient C in Eq. (6) when E is the lateral expansion and is one-half of the transition zone temperature width
$T_{0.9mm}$	Charpy transition temperature at the lateral expansion = 0.9 mm
T_{100}	Reference fracture-toughness temperature at $K_{Jc(med)}$ = 100 MPa$\sqrt{m}$
T_{20J}	Charpy transition temperature at absorbed energy = 20 J
T_{28^*J}	Charpy transition temperature at absorbed energy = 28 J times the ratio of unirradiated to irradiated upper-shelf energies
T_{28J}	Charpy transition temperature at absorbed energy = 28 J
T_{41J}	Charpy transition temperature at absorbed energy = 41 J

$T_{50\%}$	Charpy transition temperature at shear fracture = 50%
T_{68J}	Charpy transition temperature at absorbed energy = 68 J
T_{MT}	Charpy transition temperature at the middle of the transition range. Fitting coefficient in Eq. (6) when E is the absorbed energy
T_{MT}XP	Charpy transition temperature at the middle of the transition range. Fitting coefficient in Eq. 6 when E is the lateral expansion
UNIRR	Unirradiated condition
USE	Upper-shelf energy
USE_DRP	Ratio of the unirradiated to irradiated upper-shelf energies
USE_{IRR}	Upper-shelf energy in the irradiated condition
USEXP	Upper-shelf lateral expansion
UTS	Ultimate tensile strength
UTS/YIEL	Ratio of ultimate tensile strength to yield strength
YIELD	Yield strength
ΔYIELD	Change in yield strength

Table B.1. Summary of analysis for base metal data[a]

CODE	CONDIT	T_{100} (°C)	ENERGY (J)	USE (J)	SLOPE (°C)	T_{MT} (°C)	T_{68J} (°C)	T_{41J} (°C)	T_{28J} (°C)	T_{28^*J} (°C)	T_{20J} (°C)	YIELD (MPa)	UTS (MPa)	USEXP (mm)	SLOPEXP (°C)	T_{MT}XP (°C)	$T_{0.9mm}$ (°C)	$T_{50\%}$ (°C)	NDT (°C)	Cu (wt %)	Ni (wt %)	P (wt %)	Si (wt %)	Mn (wt %)	Cr (wt %)	ORIENT	REF.
3P	UNIRR	–16	27	150	58	31	25	1	–15	N/A	–28	454	641	2.15	68.1	17	6	–	–12	0.12	0.56	0.011	0.25	1.26	0.1	TL	[7]
3P-SSC1	2.7	60	30	122	42	85	89	70	58	64	48	570	713	1.77	46.7	85	85	–	–								
3P-SSC2	5.2	77	37	110	52	97	108	82	66	79	54	601	732	1.829	53	96	96	–	–								
3P-W1	5.2	60	33	112	57	88	99	70	54	66	40	581	730	1.67	51.1	85	89	–	–								
3P-W2	2.7	51	30	112	55	81	92	64	48	60	35	559	710	1.73	53.8	76	78	–	–								
3P-W3	1.5	38	29	128	53	73	76	52	37	43	25	539	689	1.98	51.4	67	62	–	–								
F23-1/4	UNIRR	–46	10	109	42	9	19	–3	–16	N/A	–26	482	660	1.62	40.4	3	7	–	–	0.2	0.18	0.011	0.23	1.34	0.11	LT	[9] [17]
F23-SSC1	2.9	65	35	86	34	73	94	70	59	66	50	596	733	1.34	36	73	86	–	–								
F23-SSC2	5.6	86	39	75	22	86	110	87	79	87	73	615	741	1.27	29	82	95	–	–								
F23-W1	5.6	56	28	84	42	73	102	70	56	65	46	595	737	1.35	46.7	68	84	–	–								
F23-W2	2.9	45	35	79	47	53	94	53	36	50	24	580	720	1.38	49	56	72	–	–								
F23-W3	1.5	30	27	82	42	47	79	46	31	42	20	567	714	1.42	48.6	49	63	–	–								
F23-UBR	3.6	58	10	82	25	88	107	87	78	84	72	–	–	–	–	–	–	–	–								
F23-1/2	UNIRR	–35	21	127	43	2	5	–15	–27	N/A	–36	447	589	1.93	47.6	–5	–8	–	–								
F23-IP1	0.55	27	29	117	39	50	56	37	26	28	17	529	661	1.91	50	49	46	–	–								
F23-CE1	0.8	25	25	110	50	59	70	44	29	34	17	550	680	2.14	71	69	58	–	–								
F23-CE2	1.5	50	43	108	51	62	75	48	33	39	21	554	683	1.67	55.7	55	60	–	–								
F23-CE3	3.9	48	32	99	40	64	79	56	44	51	34	566	696	1.7	51.8	60	63	–	–								
F23-IC1	0.5	11	22	110	40	41	50	30	18	22	9	517	647	1.85	49.5	34	33	–	–								
F23-IC2	1.1	28	27	110	47	57	67	43	29	34	18	538	668	1.86	53	53	51	–	–								
F23-IC3	2	53	39	102	39	64	76	55	43	49	34	564	691	1.98	55.6	68	63	–	–								
23G	UNIRR	–62	12	149	40	–8	–12	–29	–39	N/A	–48	431	581	1.84	40	–17	–18	–	–	0.2	0.63	0.017	0.19	1.4	0.19	TL	[9]
23G-IP1	0.5	14	35	145	75	60	54	22	2	4	–14	550	699	2.16	83	57	43	–	–								
23G-IP4	0.5	–31	13	134	44	25	25	5	–7	–5	–17	493	641	2.17	51	22	13	–	–								
CAB	UNIRR	–33	16	133	57	30	29	4	–11	N/A	–25	443	599	2.06	–	–	10	–	–23	0.12	0.46	0.008	0.26	1.41	0.11	TL	[6]
CAB-1.2	1.2	20	29	127	72	68	71	39	19	21	3	513	651	1.52	–	–	74	–	–								
CAB-1.6	1.6	44	27	134	62	90	90	63	46	46	32	526	655	1.55	–	–	102	–	–								
CAB-2.1	2.1	44	27	138	58	88	86	61	45	43	32	536	670	1.63	–	–	81	–	–								
CBB	UNIRR	–52	8	139	42	17	15	–3	–14	N/A	–24	450	594	2.13	–	–	4	–	–46	0.13	0.55	0.006	0.23	1.45	0.05	TL	[6]
CBB-4.4	4.4	45	4	124	22	99	100	90	84	86	79	607	724	1.65	–	–	104	–	–								
JP	UNIRR	–75	13	235	39	–15	–33	–47	–56	N/A	64	478	608	2.3	–	–	–36	–	–35	0.01	0.66	0.007	0.22	1.48	0.2	TL	[11]
JP-7	6.7	–16	24	181	45	29	16	–1	–12	–4	–22	570	673	2.35	–	–	6	–	–								
68C	UNIRR	–19	33	147	61	21	15	–10	–26	N/A	–39	463	625	2.17	70	21	9	–	–18	0.3	0.7	0.028	0.22	1.31	0.003	LT	[8]
68C-1.6	1.6	145	51	86	52	136	170	132	115	141	101	670	790	1.3	55	130	153	–	–								
68A	UNIRR	–25	33	154	72	25	15	–14	–33	N/A	–48	459	628	2.26	73.8	19	3	–	–23	0.3	0.7	0.003	0.22	1.31	0.003	LT	[8]
68A-1.6	1.6	121	41	103	63	136	155	121	102	122	87	670	789	1.33	60	117	139	–	–								
67C	UNIRR	–23	32	154	58	18	10	–13	–28	N/A	–41	437	607	2.13	54.7	10	2	–	–18	0.002	0.7	0.023	0.2	1.31	0.003	LT	[8]
67C-1.6	1.6	48	37	121	63	76	83	53	36	46	21	526	674	1.89	55.3	65	62	–	–								
6A	UNIRR	–14	18	147	52	41	36	14	1	N/A	–11	542	679	1.95	49.8	31.7	28	–	–	0.28	0.045	0.002	0.22	1.29	–	LT	[8]
6A-1.6	1.6	79	32	118	61	112	120	91	73	83	59	668	779	1.59	55	100	107	–	–								
JRQV-70	UNIRR	–54	7	212	32	8	–4	–15	–23	N/A	–30	482	610	2.35	30.1	–3	–10	14	–15	0.14	0.83	0.019	0.25	1.4	0.12	LT	[12]
JRQV-70	2	105	31	129	42	130	132	113	102	117	92	696	820	1.9	49.5	132	126	119	–								
JRQV-45	UNIRR	–74	3	212	19	–8	–15	–22	–27	N/A	–31	482	610	2.3	14.4	–14	–17	13	–15							LT	[12]
JRQV-45	2	94	23	129	33	121	122	107	98	110	91	696	820	1.9	49.5	132	126	122	–								
JRQA	UNIRR	–55	10	200	35	2	–10	–22	–31	N/A	–39	482	625	2.04	30	–10	–14	–1	–15							TL	[10]
JRQA	1	30	47	160	64	60	49	24	7	17	–7	559	697	2.1	61.7	51	42	74	-								

Table B.1 (continued)

CODE	CONDIT	T_{100} (°C)	ENERGY (J)	USE (J)	SLOPE (°C)	T_{MT} (°C)	T_{68J} (°C)	T_{41J} (°C)	T_{28J} (°C)	$T_{28°J}$ (°C)	T_{20J} (°C)	YIELD (MPa)	UTS (MPa)	USEXP (mm)	SLOPEXP (°C)	T_{MT}XP (°C)	$T_{0.9mm}$ (°C)	$T_{50\%}$ (°C)	NDT (°C)	Cu (wt %)	Ni (wt %)	P (wt %)	Si (wt %)	Mn (wt %)	Cr (wt %)	ORIENT	REF.
02G	UNIRR	–26	17	141	49	27	24	3	–10	N/A	–21	467	622	1.892	49.3	25	20	29	–18	0.14	0.67	0.009	0.2	1.55	0.04	TL	[19]
02G-1.1	1.1	43	30	128	63	83	86	57	40	44	25	–	–	1.361	22.7	86	92	77	–								[23]
02G-1.5	1.5	57	26	119	38	83	87	69	59	63	50	609	749	1.345	20.6	82	88	90	–								
02G-2.1	2.1	65	28	121	46	96	101	79	66	71	55	617	753	1.423	34.2	108	116	93	–								
JPJ-RG	UNIRR	–27	41	203	51	10	–9	–27	–39	N/A	–50	438	578	2.4	35.4	–9	–17	10	–30	0.05	0.63	0.005	–	–	–	TL	[18]
JPJ-RG	2	9	67	225	34	34	9	–2	–10	–13	–17	484	614	2	35.9	12	7	22	–								
JPI-JA	UNIRR	–154	8	220	63	–37	–64	–86	–101	N/A	–114	485	628	2.6	41.8	–49	–60	–41	–40	0.01	0.69	0.006	–	–	–	TL	[18]
JPI-JA	1.6	–135	6	220	54	–18	–41	–60	–73	–73	–84	527	638	–	–	–	–	–21	–								
O3	UNIRR	–34	–	129	–	–	–	0	–	N/A	–	–	–	2.03	–	–	17	26	–15	0.12	0.56	0.011	0.25	1.26	0.45	TL	[15]
O3-2.5	2.5	34	–	127	–	–	–	52	–	–	–	–	–	2	–	–	74	73	25								
O3-6.3	6.3	64	–	102	–	–	–	93	–	–	–	–	–	1.6	–	–	134	121	60								
JF	UNIRR	–67	13	219	46	0	–19	–35	–46	N/A	–55	483	618	2.3	–	–	–26	–	–52	0.04	0.76	0.007	0.27	1.35	0.11	TL	[11]
JF-5	5.1	–15	8	171	30	36	29	18	10	15	4	572	691	2.4	–	–	16	–	–								
FFA	UNIRR	–106	4	204	29	–38	–49	–59	–66	N/A	–72	427	569	2.4	22.6	–44	–50	–28	–	0.061	0.713	0.0053	0.194	1.33	0.169	LT	[13]
FFA	1.8	–34	17	200	40	17	3	–12	–22	–21	–30	510	635	2.45	42.7	6	–6	27	–								
5B	UNIRR	–73	21	144	69	–9	–14	–42	–61	N/A	–76	–	–	–	–	–	–10	5	–25	0.23	0.61	0.018	0.26	–	–	–	[14]
5B-5.6	5.6	74	21	96	77	127	160	114	90	116	71	–	–	–	–	–	143	134	–								
1B	UNIRR	–95	13	145	58	–20	–25	–49	–64	N/A	–77	–	–	–	–	–	–23	–8	–30	0.06	0.58	0.008	0.21	–	–	–	[14]
1B-6.7	6.7	–41	13	133	59	31	31	5	–11	–7	–24	–	–	–	–	–	26	33	–								
GFB-LT	UNIRR	–122	4	183	36	–39	–49	–62	–71	N/A	–79	497	632	2.2	29.5	–47	–51	–25	–	0.05	0.85	0.006	–	–	–	LT	[18]
GFB-LT	2	–43	40	204	33	–19	–31	–43	–51	–53	–58	539	658	2.1	32.6	–29	–35	–17	–								
JFL	UNIRR	–97	7	210	42	–17	–34	–49	–59	N/A	–68	451	593	2.4	38.9	–29	–38	–10	–30	0.01	0.74	0.004	0.25	1.4	0.15	LT	[18]
JFL	1.9	–68	4	210	30	6	–5	–16	–23	–23	–30	510	642	2.4	29	1	–7	6	–								
V-1000A	UNIRR	–152	16	221	59	–72	–97	–118	–132	N/A	–144	632	744	2.34	54.8	–75	–88	–71	–	0.06	1.27	0.009	0.29	0.41	2.05	CL	[17]
V-1000A	4.4	–91	3	201	24	–17	–25	–34	–40	–39	–45	794	852	2.29	21.8	–17	–22	–2	–								
V-1000B	UNIRR	–147	5	221	27	–85	–97	–107	–113	N/A	–119	528	641	2.27	24	–91	–96	–67	–	0.03	1.25	0.009	0.27	0.51	2.1	CL	[17]
V-1000B	4.6	–100	3	193	15	–13	–18	–23	–27	–26	–30	726	779	2.16	13	–14	–16	–11	–								

[a]N/A = not applicable. – = Not available.

Table B.2. Summary of analysis for weld metal data[a]

CODE	CONDIT	T_{100} (°C)	ENERGY (J)	USE (J)	SLOPE (°C)	T_{MT} (°C)	T_{68J} (°C)	T_{41J} (°C)	T_{28J} (°C)	T_{28^*J} (°C)	T_{20J} (°C)	YIELD (MPa)	UTS (MPa)	USEXP (mm)	SLOPEXP (°C)	T_{MT}XP (°C)	$T_{0.9mm}$ (°C)	$T_{50\%}$ (°C)	NDT (°C)	Cu (w %t)	Ni (wt %)	P (wt %)	Si (wt %)	Mn (wt %)	Cr (wt %)	REF.
W8A	UNIRR	–47	26	81	84	–12	58	–13	–42	N/A	–64	490	611	1.645	86.1	6	14	–	–	0.39	0.59	0.011	0.77	1.33	0.12	[9]
W8A-2	2	86	22	52	43	96	N/A	123	97	129	83	668	750	0.872	45.1	97	N/A	–	–							
W8A-IAR	2.2	49	10	59	37	85	N/A	99	82	95	70	642	734	0.988	35.11	82.5	123	–	–							
W8A-1.5	1.5	31	29	80	49	48	89	47	30	30	17	657	744	1.09	37.87	32	61	–	–							
W8A-CE1	0.79	83	28	53	35	83	N/A	102	83	105	71	650	741	0.927	36.7	83	147	–	–							
W8A-CE3	3.85	76	14	46	37	95	N/A	139	102	N/A	88	684	767	0.804	44.2	92	N/A	–	–							
W8A-CE2	1.5	80	24	49	38	84	N/A	112	87	129	73	659	751	1.133	57.8	94	133	–	–							
W8A-IC1	0.56	39	24	61	61	55	N/A	75	47	67	29	592	699	1.22	74.5	51	90	–	–							
W8A-IC2	1.22	67	29.5	56	69	66	N/A	99	63	97	41	624	726	1.096	85.3	69	134	–	–							
W8A-IC3	2.2	89	32	53	58	79	N/A	112	79	116	60	659	747	0.98	61.7	144	N/A	–	–							
W9A	UNIRR	–75	34	167	64	–29	–42	–67	–83	N/A	–97	565	638	2.19	62.3	–41	–52	–	–	0.39	0.7	0.01	0.23	1.24	0.1	[9]
W9A-2	2	45	40	107	59	62	77	46	29	50	15	726	799	1.7	75.7	70	74	–	–							
W9A-IAR	2.2	20	35	112	56	44	55	27	11	28	–2	686	771	1.61	56.7	40	47	–	–							
W9A-1.5	1.5	13	27	117	69	58	68	34	14	33	–2	709	785	1.58	63	54	63	–	–							
W9A-IC4	0.5	13	51	124	52	24	28	4	–11	0	–23	667	740	1.96	57.8	20	15	–	–							
E23	UNIRR	–52	20	93	61	–9	20	–18	–37	N/A	–53	456	583	1.75	–	–	–9	–	–46	0.24	0.6	0.008	0.52	1.36	0.04	[6]
E23-7	0.69	25	21	76	69	62	135	65	40	52	22	–	–	0.99	–	–	99	–	–							
E19	UNIRR	–55	24	89	86	–8	41	–18	–46	N/A	–67	492	614	1.32	–	–	27	–	–40	0.43	0.59	0.007	0.53	1.37	0.04	[6]
E19-0.1	0.1	–7	18	82	67	41	92	38	15	20	–2	538	632	1.12	–	–	71	–	–							
E19-0.7	0.7	56	32	64	71	59	N/A	78	47	73	26	603	698	–	–	–	–	–	–							
E19-2.5	2.5	63	23	60	78	86	N/A	113	77	116	53	622	670	–	–	–	–	–	–							
5W	UNIRR	–39	52	220	56	–5	–28	–48	–62	N/A	–73	–	–	–	–	–	–25	–18	–50	0.25	1.06	0.019	0.3	–	–	[14]
5W-5	4.6	117	42	127	68	143	146	115	96	124	81	–	–	–	–	–	155	133	–							
1W	UNIRR	–60	57	213	62	–27	–52	–74	–89	N/A	–102	–	–	–	–	–	–49	–38	–60	0.06	0.98	0.007	0.31	–	–	[14]
1W-8	8.8	18	48	168	45	40	30	13	1	8	–8	–	–	–	–	–	40	29	–							
68W	UNIRR	–92	18	205	40	–43	–57	–71	–81	N/A	–89	554	647	–	–	–	–	–	–	0.04	0.13	0.008	0.16	1.38	0.04	[19]
68W-1	1	–87	14	219	45	–21	–40	–56	–67	–69	–76	554	634	–	–	–	–	–	–							[23]
68W-1.6	1.6	–66	12	203	28	–23	–33	–43	–50	–50	–57	573	656	–	–	–	–	–	–							
69W	UNIRR	–15	49	148	35	–2	–6	–20	–30	N/A	–37	639	722	1.769	32.7	–2	–3	–12	–	0.12	0.1	0.01	0.19	1.19	0.09	[19]
69W-1.2	1.2	23	68	146	40	27	23	6	–4	–4	–13	704	776	1.366	29.8	33.1	41	18	–							[23]
69W-1.5	1.5	15	50	148	74	42	35	4	–15	–15	–32	717	792	1.309	38.7	43.6	57	13	–							

Table B.2 (continued)

CODE	CONDIT	T_{100} (°C)	ENERGY (J)	USE (J)	SLOPE (°C)	T_{MT} (°C)	T_{68J} (°C)	T_{41J} (°C)	T_{28J} (°C)	$T_{28°J}$ (°C)	T_{20J} (°C)	YIELD (MPa)	UTS (MPa)	USEXP (mm)	SLOPEXP (°C)	T_{MT}XP (°C)	$T_{0.9mm}$ (°C)	$T_{50\%}$ (°C)	NDT (°C)	Cu (wt %)	Ni (wt %)	P (wt %)	Si (wt %)	Mn (wt %)	Cr (wt %)	REF.
70W	UNIRR	–61	22	135	42	–23	–24	–42	–54	N/A	–63	478	593	1.998	44	–17	–23	–31	–	0.056	0.63	0.011	0.44	1.48	0.13	[19]
70W-1.6	1.6	–42	22	132	45	–3	–3	–23	–35	–34	–46	534	649	1.433	49.2	13.2	24	–11	–							[23]
70W-2	2	–31	25	132	63	17	18	–10	–27	–26	–41	–	–	1.347	34.7	25.5	36	17	–							
71W	UNIRR	–40	14	105	43	4	16	–7	–20	N/A	–30	469	599	1.65	35.2	8.5	10	3	–	0.046	0.63	0.011	0.54	1.58	0.12	[19]
71W-1.6	1.6	–18	23	123	82	48	54	16	–7	–17	–26	539	649	1.224	19.6	35.4	44	38	–							[23]
71W-2	2	–15	17	114	51	33	42	17	2	–1	–10	–	–	1.262	28.9	39.6	51	26	–							
72W	UNIRR	–57	18	136	52	–4	–5	–28	–42	N/A	–53	500	609	2.12	49.2	–6	–15	–1	–23	0.23	0.6	0.006	0.44	1.6	0.27	[20]
72W-1	1	34	30	109	62	66	81	49	30	40	16	–	–	1.24	63	53	84	80	38							[23]
72W-1.6	1.6	34	33	96	55	54	77	44	27	42	13	613	715	1.25	52.7	70	92	61	49							
73W	UNIRR	–61	22	135	50	–17	–18	–40	–53	N/A	–65	494	604	2.08	48.6	–18	–27	–15	–34	0.31	0.6	0.005	0.45	1.56	0.25	[20]
73W-1	1	33	34	99	42	48	64	40	26	37	16	–	–	1.313	42.3	46	60	57	38							[23]
73W-1.6	1.6	40	40	91	68	51	86	42	20	43	3	655	743	1.29	74.6	79	106	57	60							
NOZ	UNIRR	–47	17	88	65	5	44	–1	–23	N/A	–39	545	645	1.483	56.4	9	18	19	–55	0.4	0.57	0.015	0.55	1.59	–	[21]
NOZ-1	1	56	26	68	71	78	N/A	90	61	79	41	702	792	0.892	58	80	N/A	73	–							[22]
NOZ-IA	1–454[b]	–11	17	105	62	47	64	31	12	4	–3	–	–	1.227	50.4	40	63	37	–							[23] [24]
MW	UNIRR	–61	12	89	55	–3	28	–9	–27	N/A	–41	512	613	1.69	63.1	1	2	–2	–60	0.26	0.57	0.017	0.622	1.61	–	[21]
MW-0.5	0.5	5	23	81	62	37	88	36	14	19	–2	634	718	1.152	55.2	38	73	55	–							[22]
MW-1	1	26	16	80	90	96	171	95	64	71	40	646	747	0.977	91.5	102	N/A	93	–							[23]
MW-454	1–454[b]	–48	9	106	58	30	46	15	–2	–10	–16	–	–	1.226	65.8	33	62	20	–							[24]
MW-343	1–343[b]	10	18	92	53	51	79	44	27	26	14	–	–	0.885	44.3	79.4	N/A	63	–							
GWA	UNIRR	–69	40	185	38	–43	–54	–68	–78	N/A	86	617	693	2.1	24.3	–42	–49	–37	–	0.035	0.93	0.013	0.17	1.45	0.02	[18]
GWA-2	2	–49	13	209	30	–4	–16	–27	–34	–36	–41	669	747	1.9	25.5	–13	–15	–14	–							
E4	UNIRR	–68	8	132	33	–17	–16	–31	–40	N/A	–47	–	–	2.06	40.1	–22	–27	–	–	0.16	0.65	0.013	0.49	1.38	0.1	[6]
E4-2	2.3	15	15	104	60	75	93	60	42	53	28	–	–	1.58	64	71	80	–	–							
JW	UNIRR	–64	33	217	35	–32	–47	–59	–67	N/A	–75	540	634	–	–	–	–	–58	–50	0.084	0.71	0.009	0.36	1.24	0.07	[11]
JW	3	–16	61	186	33	–4	–13	–25	–33	–30	–40	644	703	–	–	–	–	–	–							
E24	UNIRR	–101	13	180	44	–40	–51	–68	–79	N/A	–89	549	638	2.21	–	–	–54	–	–68	0.37	0.59	0.005	0.17	1.25	0.04	[6]
E24-.75	0.75	–7	33	144	73	40	34	4	–16	–5	–32	–	–	1.5	–	–	32	–	–							
BW	UNIRR	–67	16	162	61	5	–6	–30	–45	N/A	–59	405	–	2.4	60	–2	–17	3	–	0.22	1.58	0.012	0.55	1.33	0.06	[10]
BW-1	1	16	10	99	42	82	98	73	60	77	50	548	–	1.67	51	80	84	83	–							

[a]N/A = not applicable. – = Not available.

[b]1–454 means annealing at 454°C for 168 h after irradiation to 1.10^{19} n/cm^2, and 1–343 means annealing at 343°C for 168 h after irradiation to 1.10^{19} n/cm^2.

Table B.3. Summary of fracture toughness and Charpy shifts for base metal data[a]

CODE	CH	FT	Shift at 100 MPa√m (°C)	Shift at 68 J (°C)	Shift at 41 J (°C)	Shift at 28 J (°C)	Shift at 28* J (°C)	Shift at 20 J (°C)	Shift at T_{MT} (°C)	Shift at 0.9 mm (°C)	Shift at 50% (°C)	Δ YIELD (MPa)	YIELD (MPa)	UTS/YIEL	USE DRP	USE_{IRR} (J)	ΔT_{100}-ΔT_{41} (°C)	RG 1.99.1 (°C)	RG 1.99.2 (°C)	EWO (°C)	FIM (°C)	JEPE (°C)
3P-SSC1	2.66	2.66	76	64	69	73	79	76	54	79	–	116	570	1.25	1.23	122	7	86	57	53	54	56
3P-SSC2	5.2	5.2	93	83	81	81	94	82	66	90	–	147	601	1.22	1.36	110	12	120	64	65	69	66
3P-W1	5.2	5.2	76	74	69	69	81	68	57	83	–	127	581	1.26	1.34	112	7	120	64	65	69	66
3P-W2	2.7	2.7	67	67	63	63	75	63	50	72	–	105	559	1.27	1.34	112	4	87	58	54	55	56
3P-W3	1.5	1.5	54	51	51	52	58	53	42	56	–	85	539	1.28	1.17	128	3	65	51	46	45	48
F23-SSC1	2.87	2.87	111	75	73	74	81	76	64	79	–	114	596	1.23	1.27	86	38	165	71	58	75	73
F23-SSC2	5.6	5.6	132	91	90	94	102	99	77	88	–	133	615	1.20	1.45	75	42	230	79	70	94	86
F23-W1	5.6	5.6	102	83	73	71	80	72	64	77	–	113	595	1.24	1.3	84	29	230	79	70	94	86
F23-W2	2.9	2.9	91	75	56	51	65	50	44	65	–	98	580	1.24	1.38	79	35	166	71	58	75	73
F23-W3	1.5	1.5	76	60	49	46	57	46	38	56	–	85	567	1.26	1.33	82	27	119	62	49	60	62
F23-UBR	3.6	3.6	104	88	90	93	99	98	79	N/A	–	–	–	–	1.33	82	14	184	74	62	81	77
F23-IP1	0.54	0.57	62	51	52	53	55	53	48	54	–	82	529	1.25	1.09	117	10	73	47	38	42	46
F23-CE1	0.79	0.88	60	65	59	56	61	53	57	66	–	103	550	1.24	1.15	110	1	91	54	43	49	53
F23-CE2	1.5	1.64	85	70	63	60	66	57	60	68	–	107	554	1.23	1.18	108	22	125	63	50	61	63
F23-CE3	3.85	4.01	83	74	71	71	78	70	62	71	–	119	566	1.23	1.28	99	12	195	75	64	84	79
F23-IC1	0.56	0.53	46	45	45	45	49	45	39	41	–	70	517	1.25	1.15	110	1	71	46	37	41	45
F23-IC2	1.22	1.02	63	62	58	56	61	54	55	59	–	91	538	1.24	1.15	110	5	98	56	45	52	55
F23-IC3	2.23	1.95	88	71	70	70	76	70	62	71	–	117	564	1.23	1.25	102	18	136	66	52	65	66
23G-IP1	0.54	0.54	76	66	51	41	43	33	68	61	–	119	550	1.27	1.03	145	25	84	69	62	60	62
23G-IC4	0.45	0.45	31	37	34	32	34	31	33	31	–	62	493	1.3	1.11	134	–3	76	65	58	57	59
CAB-1.2	1.2	1.2	53	42	35	30	32	28	38	64	–	70	513	1.27	1.05	127	18	49	47	45	34	40
CAB-1.6	1.6	1.7	77	61	59	57	57	57	60	92	–	83	526	1.25	0.99	134	18	58	51	49	38	44
CAB-2.1	2.1	2.2	77	57	57	56	54	57	58	71	–	93	536	1.25	0.96	138	20	66	54	52	42	47
CBB-4.4	4.4	4.8	97	85	93	97	100	103	82	100	–	157	607	1.19	1.12	124	4	110	69	60	64	60
JP-6.7	6.7	7	59	49	46	44	52	42	44	42	–	92	570	1.18	1.3	181	13	59	53	41	36	1
68C-1.6	1.6	1.6	164	155	142	141	167	140	115	144	–	207	670	1.18	1.71	86	22	253	131	120	151	134
68A-1.6	1.6	1.6	146	140	135	135	155	135	111	136	–	211	670	1.18	1.5	103	11	183	131	101	115	100
67C-1.6	1.6	1.6	71	73	66	64	74	62	58	60	–	89	526	1.28	1.27	121	5	81	13	31	48	17
6A-1.6	1.6	1.6	93	84	77	72	82	70	71	79	–	126	668	1.17	1.25	118	16	169	78	47	77	63
JRQV-40	2	2	168	137	129	125	137	122	129	136	105	214	696	1.18	1.64	129	39	N/A	N/A	111	N/A	N/A
JRQV-70	2	2	159	136	128	125	140	122	122	143	109	214	696	1.18	1.64	129	31	N/A	N/A	111	N/A	N/A
JRQA-1	1	1	85	59	46	38	48	32	58	56	75	77	559	1.25	1.25	160	39	86	58	64	67	63
02G-1.1	1.1	1.2	69	62	54	50	54	46	56	72	48	–	–	–	1.1	128	15	64	60	53	48	51
02G-1.5	1.5	1.8	83	63	66	69	73	71	56	68	61	142	609	1.23	1.18	119	17	78	66	58	55	57
02G-2.1	2.1	2.4	91	77	76	76	81	76	69	96	64	150	617	1.22	1.17	121	15	90	70	62	61	62
JPJ-2	2	2	36	18	25	29	26	33	14	24	12	46	484	1.27	0.9	225	11	31	20	20	27	18
JPI-1.6	1.6	1.6	19	23	26	28	28	30	19	–	20	42	527	1.21	1	220	–7	28	13	18	21	0
O3-2	2.5	2.5	68	–	52	–	–	–	–	57	47	–	–	–	1.02	127	16	83	57	53	53	55
O3-5.1	6.3	6.3	98	–	93	–	–	–	–	117	95	–	–	–	1.26	102	5	132	66	70	74	69
JF-5.1	5.1	5.4	52	48	53	56	61	59	36	42	–	89	572	1.21	1.28	171	–1	52	20	26	39	22
FFA-1.8	1.8	1.9	72	52	47	44	45	42	55	44	55	83	510	1.25	1.02	200	25	31	24	31	29	23
5B-5.6	5.6	6.7	147	174	156	151	177	147	136	153	129	–	–	–	1.5	96	–9	345	136	91	165	137
1B-6.7	6.7	8.4	54	56	54	53	57	53	51	49	41	–	–	–	1.09	133	0	64	31	35	45	36
GFB-2	2	2	79	18	19	20	18	21	20	16	8	42	539	1.22	0.9	204	60	31	20	15	31	22
JFL-1.9	1.9	1.9	29	29	33	36	36	38	23	31	16	59	510	1.26	1	210	–4	31	13	29	23	–3
V-1000A	4.4	4.6	61	72	84	92	93	99	55	66	69	162	794	1.07	1.1	201	–23	54	28	26	64	43
V-1000B	4.3	4.6	47	79	84	86	87	89	72	80	56	198	726	1.07	1.15	193	–37	56	15	25	47	24

[a]N/A = Not applicable. – = Not available.

Table B.4. Summary of fracture toughness and Charpy shifts for weld metal data[a]

CODE	CH	FT	Shift at 100 MP (°C)	Shift at 68 J (°C)	Shift at 41 J (°C)	Shift at 28 J (°C)	Shift at 28* J (°C)	Shift at 20 J (°C)	Shift at T_{MT} (°C)	Shift at 0.9 mm (°C)	Shift at 50% (°C)	Δ YIELD (MPa)	YIELD (MPa)	UTS/YIEL	USE_DRP	USE_{IRR} (J)	ΔT_{100}-ΔT_{41} (°C)	RG 1.99.1 (°C)	RG 1.99.2 (°C)	EWO (°C)	FIM (°C)	JEPE (°C)
W8-2	2.03	2.1	133	N/A	136	139	171	147	108	N/A	–	178	668	1.12	1.56	52	–3	294	151	115	158	136
W8-IAR	2.19	2.2	96	N/A	112	124	137	134	97	109	–	152	642	1.14	1.37	59	–16	N/A	N/A	N/A	N/A	N/A
W8-1.3	1.34	1.5	78	N/A	60	72	72	81	60	47	–	167	657	1.13	1.01	80	18	248	140	110	140	127
W8-CE1	0.79	0.88	130	N/A	115	125	147	135	95	133	–	160	650	1.14	1.53	53	15	190	121	101	116	112
W8-CE3	3.85	4.01	123	N/A	152	144	N/A	152	107	N/A	–	194	684	1.12	1.76	46	–29	406	170	125	198	151
W8-CE2	1.5	1.64	127	N/A	125	129	171	137	96	119	–	169	659	1.14	1.65	49	2	260	143	111	145	130
W8-IC1	0.56	0.53	86	N/A	88	89	109	93	67	76	–	102	592	1.18	1.33	61	–2	148	103	89	97	97
W8-IC2	1.22	1.02	114	N/A	112	105	139	105	78	120	–	134	624	1.16	1.45	56	2	205	126	103	122	116
W8-IC3	2.23	1.95	136	N/A	125	121	158	124	91	N/A	–	169	659	1.13	1.53	53	11	283	148	113	154	134
W9-2	2.03	2.1	120	119	113	112	133	112	91	126	–	161	726	1.10	1.56	107	7	290	161	127	169	159
W9-IAR	2.19	2.2	95	97	94	94	111	95	73	99	–	121	686	1.12	1.49	112	1	N/A	N/A	N/A	N/A	N/A
W9-1.3	1.34	1.5	88	110	101	97	116	95	87	115	–	144	709	1.11	1.43	117	–13	245	149	122	151	148
W9-IC4	0.45	0.47	88	70	71	72	83	74	53	67	–	102	667	1.11	1.35	124	17	137	106	96	100	109
E23-0.7	0.69	0.68	77	115	83	78	90	75	71	108	–	–	–	–	1.22	76	–6	92	86	79	63	82
E19-0.1	0.1	0.1	48	51	56	86	66	87	46	44	–	46	538	1.17	1.09	82	–8	69	56	31	58	58
E19-0.7	0.73	0.75	111	N/A	96	93	119	93	67	N/A	–	111	603	1.16	1.39	64	15	188	123	98	117	120
E19-2.5	2.5	2.63	118	N/A	131	123	162	120	94	N/A	–	130	622	1.08	1.48	60	–13	351	168	119	181	158
5W-4.6	4.6	6.1	156	174	163	158	186	154	148	180	151	–	–	–	1.73	127	–7	364	202	183	242	149
1W-8.8	8.8	8.7	78	82	87	90	97	94	67	89	67	–	–	–	1.27	168	–9	66	68	41	60	45
68W-1	1	1.1	5	17	15	14	14	13	22	–	–	1	554	1.14	0.94	219	–10	23	21	15	18	37
68W-1.6	1.6	1.6	26	24	28	31	31	32	20	–	–	19	573	1.14	1.01	203	–2	28	23	18	21	40
69W-1.2	1.2	1.1	38	29	26	26	26	24	29	44	30	65	704	1.10	1.01	146	12	52	35	31	31	49
69W-1.5	1.5	1.6	30	46	24	56	56	58	44	60	25	78	717	1.10	1	148	6	63	39	34	36	54
70W-1.6	1.6	1.4	19	21	19	19	20	17	20	47	20	56	534	1.22	1.02	132	0	36	46	19	29	36
70W-2	2	2.1	30	42	32	27	28	22	40	59	48	–	–	–	1.02	132	–2	44	51	23	34	39
71W-2	2	2.1	25	26	24	22	19	20	29	34	35	–	–	–	0.92	123	1	44	41	23	33	30
71W-1.6	1.6	1.4	22	38	23	13	3	4	44	41	23	70	539	1.20	0.85	114	–1	36	38	19	29	28
72W-1	1	1	91	86	77	72	82	69	70	99	81	–	–	–	1.25	109	14	106	94	82	69	91
72W-1.6	1.5	1.6	91	82	72	69	84	66	58	107	62	113	613	1.17	1.42	96	19	134	106	88	81	101
73W-1	1	1	94	82	80	79	90	81	65	87	72	–	–	–	1.36	99	14	150	110	101	93	108
73W-1.6	1.5	1.6	101	104	82	73	96	68	68	133	72	161	655	1.13	1.48	91	19	190	124	108	110	121
NOZ-1	1.3	1.3	103	N/A	91	84	102	80	72	N/A	54	157	702	1.13	1.29	68	12	250	135	107	141	130
NOZ-1A	1	1.3	36	20	32	35	27	36	42	45	18	–	–	–	0.84	105	4	N/A	N/A	N/A	N/A	N/A
BL-0.5	0.5	0.5	66	60	45	41	46	39	40	71	57	122	634	1.13	1.1	81	21	104	79	79	71	76
BL-1	1.3	1.3	87	143	104	91	98	81	99	N/A	95	134	646	1.16	1.11	80	–17	168	105	98	99	98
BL-1/454	1	1.3	13	18	24	25	17	25	33	60	22	–	–	–	0.84	106	–11	N/A	N/A	N/A	N/A	N/A
BL-1/343	1	1	71	51	53	41	53	55	54	N/A	65	–	–	–	0.97	92	18	N/A	N/A	N/A	N/A	N/A
GWA-2	2	2	20	38	41	44	42	45	39	34	23	52	669	1.12	0.89	209	–21	51	32	24	39	12
E4	2.3	2.3	83	109	91	82	93	75	92	107	–	–	–	–	1.27	104	–8	122	106	77	76	86
JW-2.9	2.9	3.5	48	34	34	34	37	35	29	–	–	46	644	1.09	1.17	186	14	51	83	41	43	61
E24	0.72	0.72	94	86	72	63	74	57	80	86	–	–	–	–	1.25	144	22	156	110	94	99	116
BW-1	1	1	83	104	103	105	122	109	77	101	80	143	548	–	1.64	99	–20	111	167	183	156	94

[a]N/A = Not applicable. – = Not available.

NRC FORM 335 (2-89) NRCM 1102, 3201, 3202

U.S. NUCLEAR REGULATORY COMMISSION

BIBLIOGRAPHIC DATA SHEET

(See instructions on the reverse)

1. REPORT NUMBER (Assigned by NRC, Add Vol., Supp., Rev., and Addendum Numbers, If any.)

NUREG/CR-6609
ORNL/TM-13755

2. TITLE AND SUBTITLE

Comparison of Irradiation-Induced Shifts of K_{Jc} and Charpy Impact Toughness for Reactor Pressure Vessel Steels

3. DATE REPORT PUBLISHED

MONTH: November | YEAR: 2000

4. FIN OR GRANT NUMBER

5. AUTHOR(S)

Mikhail A. Sokolov and Randy K. Nanstad

6. TYPE OF REPORT

W6953

7. PERIOD COVERED *(Inclusive Dates)*

Technical

8. PERFORMING ORGANIZATION – NAME AND ADDRESS *(If NRC, provide Division, Office or Region, U.S. Nuclear Regulatory Commission, and mailing address; if contractor, provide name and mailing address.)*

Oak Ridge National Laboratory
Oak Ridge, TN 37831-6285

9. SPONSORING ORGANIZATION – NAME AND ADDRESS *(If NRC, type "Same as above", if contractor, provide NRC Division, Office or Region, U.S. Nuclear Regulatory Commission, and mailing address.)*

Division of Engineering Technology
Office of Nuclear Regulatory Research
U.S. Nuclear Regulatory Commission
Washington, DC 20555-0001

10. SUPPLEMENTARY NOTES

C. J. Fairbanks, NRC Project Manager

11. ABSTRACT *(200 words or less)*

The current provisions for determination of the upward temperature shift of the lower-bound static fracture toughness curve due to irradiation of reactor pressure vessel steels are based on the assumption that they are the same as for the Charpy 41-J shifts as a consequence of irradiation. The objective of this report by the Heavy-Section Steel Irradiation Program is to evaluate this assumption relative to data reported in open literature. Depending on the specific source, different sizes of fracture toughness specimens, procedures for the determination of K_{Jc}, and fitting functions were used. It was anticipated that data scatter might be reduced by using a consistent approach to analyze the published data. A method employing Weibull statistics was applied to analyze original fracture toughness data of unirradiated and irradiated pressure vessel steels. The master curve concept was used to determine shifts of fracture toughness transition curves. A hyperbolic tangent function was used to fit Charpy absorbed-energy data. The fracture toughness shifts were compared with Charpy impact shifts evaluated with various criteria. Linear regression analysis showed that for weld metals, on average, the fracture toughness shift is the same as the Charpy 41-J temperature shift, while for base metals, on average, the fracture toughness shift at 41-J is 16% greater than the shift of the Charpy 41-J transition temperature, with both correlations having relatively large (95%) confidence intervals of ±26°C and ±36°C, respectively.

12. KEY WORDS/DESCRIPTORS *(List words or phrases that will assist researchers in locating the report.)*

reactor pressure vessel
fracture toughness
master curve
charpy correlation
irradiation
base metals
weld metals
statistics
embrittlement

13. AVAILABILITY STATEMENT

Unlimited

14. SECURITY CLASSIFICATION

(This Page)

(This Report)

Unclassified

15. NUMBER OF PAGES

Unclassified

16. PRICE

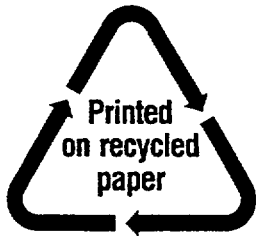

Federal Recycling Program

UNITED STATES
NUCLEAR REGULATORY COMMISSION
WASHINGTON, D.C. 20555-0001